EFFICIENT METHODS FOR UNAMBIGUOUS DIRECTION-OF-ARRIVAL ESTIMATION WITH CO-PRIME LINEAR ARRAYS

A THESIS

Submitted by

ASHOK C

in partial fulfillment of the requirements for the degree of

DOCTOR OF PHILOSOPHY

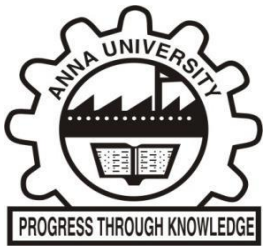

FACULTY OF INFORMATION AND COMMUNICATION ENGINEERING

ANNA UNIVERSITY

CHENNAI 600 025

DECEMBER 2022

ANNA UNIVERSITY

CHENNAI 600 025

BONAFIDE CERTIFICATE

The research work embodied in the present Thesis entitled "**EFFICIENT METHODS FOR UNAMBIGUOUS DIRECTION-OF-ARRIVAL ESTIMATION WITH CO-PRIME LINEAR ARRAYS**" has been carried out in the Department of Biomedical Engineering, Sri Sivasubramaniya Nadar College of Engineering, Chennai. The work reported herein is original and does not form part of any other thesis or dissertation on the basis of which a degree or award was conferred on an earlier occasion or to any other scholar.

I understand the University's policy on plagiarism and declare that the thesis and publications are my own work, except where specifically acknowledged and has not been copied from other sources or been previously submitted for award or assessment.

ASHOK C
RESEARCH SCHOLAR

Dr. N.VENKATESWARAN
SUPERVISOR
Professor
Department of Biomedical Engineering
Sri Sivasubramaniya Nadar
College of Engineering
Chennai - 603 110.

ABSTRACT

In the array signal processing research, estimation of the direction-of-arrival (DOA) of the transmitted source signal has long been of great interest and plays an important role in both civilian and military applications such as radar, sonar, geophysics, acoustics, bioengineering, seismology, multimedia, radio astronomy and wireless communication. Non-uniform linear array (NULA) design, also known as the sparse linear array (SLA) design has been developed for DOA estimation considering the limitations seen in the uniform linear array (ULA) design. The SLA design can attain a large effective array aperture with fewer array elements and also mitigates the influence of mutual coupling effects between array elements. Recently, the co-prime linear array (CLA) design has gained considerable research interest among several SLA designs such as minimal redundant array (MRA), minimum-hole array (MHA) and nested linear array (NLA). However, CLA designs such as general co-prime linear array (GCLA) and unfolded co-prime linear array (UCLA) face the critical problem of ambiguity resulting in an ambiguous estimate of true DOAs. Specifically, GCLA suffers from the problem of pair-matching ambiguity in subarray domain processing but both GCLA and UCLA suffer from the problem of grating-angle ambiguity.

This thesis focuses on the key objectives as follows (i) To resolve the ambiguity problem such as pair-matching and grating-angle ambiguity in estimating the DOA of the incoming source signals using the GCLA and UCLA (ii) To achieve a reliable estimation of true DOAs with superior estimation performances in terms of accuracy, angular resolution and degrees-of-freedom (DOF) compared to the existing methods (ii) To offer good generalization and robustness in estimation performance with less

computational complexity and execution time compared to the existing methods.

In the first proposed solution, the true DOAs are distinguished from ambiguous estimates obtained from UCLA-MUSIC using the estimated power of the transmitted source signals. Here, the source power function derived is based on the signal subspace eigenvalues and its associated eigenvectors to estimate the power of the transmitted source signals. In the second proposed solution, an improved polynomial rooting-based method for high-resolution unambiguous DOA estimation is performed. A polynomial function is derived based on the orthogonality between the noise subspace eigenvectors and array directional vectors. A maximum signal power function is proposed based on the spatial filtering and second-order differential counterparts for the selection of the signal roots associated with the true DOAs over the ambiguous roots. In the third proposed solution, a computationally efficient DOA estimation method based on support vector regression (SVR) is proposed. The ambiguity problem is resolved by treating DOA estimation as approximating the unknown regression function that maps the signal subspace eigenvectors with the DOA of the incoming source signals.

The effectiveness and superiority of the aforementioned proposed solutions are supported by several standard simulation studies in terms of estimation reliability, estimation accuracy, angular resolution, computational complexity, execution time and DOF.

ACKNOWLEDGEMENT

First and foremost, I would like to thank my supervisor, **Dr.N.Venkateswaran**, Professor, Department of Biomedical Engineering, Sri Sivasubramaniya Nadar College of Engineering, Chennai, for always encouraging, motivating, and mentoring me. This thesis would not have been a reality without his consistent support and accommodating demeanor. His affiliation has taught me many great values that I will cherish throughout my life.

I extend my sincere thanks to the doctoral committee members **Dr.Y.V.Ramana Rao**, Professor, Department of Electronics and Communication Engineering, College of Engineering Guindy Campus, Anna University, Chennai, and **Dr.Arun Pachai Kannu**, Associate Professor, Department of Electrical Engineering, Indian Institute of Technology Madras, Chennai, for their helpful suggestions, comments, and encouragement.

I would like to thank the management of St.Joseph's College of Engineering, Chennai and Sri Sivasubramaniya Nadar College of Engineering, Chennai for their support to carry out my research work.

I would like to acknowledge **Ms.Vaddi Lakshmi Satya Sai Sarojnii** and **Ms.Sneha Rajan** for their support on validation.

I would like to thank my friends and well-wishers for their support, motivation and encouragement. Finally, I owe my father **Dr.M.Chandrasekaran,** my mother **C.Usha** and my sister **C.Arthi** for their unwavering support. Particularly, I am very grateful to my wife **K.Gayathri** for being understanding and patient with my predicament throughout the Ph.D.

ASHOK C

TABLE OF CONTENTS

CHAPTER NO. **TITLE** **PAGE NO.**

CHAPTER NO. **TITLE** **PAGE NO.**

CHAPTER NO. **TITLE** **PAGE NO.**

LIST OF TABLES

TABLE NO. **TITLE** **PAGE NO.**

LIST OF FIGURES

FIGURE NO. **TITLE** **PAGE NO.**

FIGURE NO. **TITLE** **PAGE NO.**

FIGURE NO. **TITLE** **PAGE NO.**

LIST OF SYMBOLS AND ABBREVIATIONS

AdS	-	Adjoined Subarray
AdS-MUSIC	-	Adjoined Subarray- Multiple Signal Classification
$\Delta\theta$	-	Angular separation
$\cong$	-	Approximately equal to
AR	-	Autoregressive
$\in$	-	Belongs to
B5G	-	Beyond Fifth Generation
$\mathrm{Card}\,(.)$	-	Cardinality of the set (.)
CAI	-	Classical Array Interpolation
CBF	-	Classical Beamformer
CCI	-	Co-Channel Interference
$(.)^H$	-	Conjugate Transpose of a Vector or Matrix (.)
CMA	-	Constant Modulus Algorithm
CACIS	-	Co-Prime Array with Compressed Inter-Element Spacing
CADiS	-	Co-Prime Array with Displaced Subarrays
CRLB	-	Cramer-Rao Lower Bound
dB	-	Decibel
DOF	-	Degrees-of-Freedom
diag {.}	-	Diagonal Matrix formed from the elements of {.}
DSP	-	Digital Signal Processor
θ	-	Direction Angle
DF	-	Direction-Finding
DOA	-	Direction-of-Arrival
DFT	-	Discrete Fourier Transform

δz	-	Discrete Root Interval
DECOM	-	DOA Estimation with Combined MUSIC for Coprime Array
$\notin$	-	Does Not Belongs to
λ	-	Eigenvalue
EVD	-	Eigenvalue Decomposition
ES-ESPRIT	-	Equirotational Stack - Estimation of Signal Parameters via Rotational Invariance
$\widehat{(.)}$	-	Estimate of a Vector or Matrix (.)
ESPRIT	-	Estimation of Signal Parameters via Rotational Invariance
(.)!	-	Factorial of (.)
FSD	-	Fast Subspace Decomposition
FCC	-	Federal Communications Commission
FOV	-	Field-of-View
5G	-	Fifth Generation
$\forall$	-	For every
FD	-	Fourier Domain
FDWLS	-	Fourier Domain Weighted Least-Squares
GCLA	-	General Co-Prime Linear Array
HAD	-	Hearing Aid Devices
$\mathbf{I}$	-	Identity Matrix
$\Im(.)$	-	Imaginary Part of (.)
$\langle .,. \rangle$	-	Inner Product
I	-	In-Phase
IoUT	-	Internet of Underwater Things
ISI	-	Inter-Symbol Interference
$(.)^{-1}$	-	Inverse of (.)
ILSP-CMA	-	Iterative Least Squares Projection - Constant Modulus Algorithm
KKT	-	Karush – Kuhn – Tucker

γ	-	Kernel Parameter
α	-	Lagrange Multiplier
ε	-	Limit of allowable error
LP	-	Linear Prediction
$\mathcal{L}[\mathbf{A}]$	-	Linear subspace spanned by the columns of $\mathbf{A}$
LCMV	-	Linearly Constrained Minimum Variance
$\mathbf{A}$	-	Matrix
max	-	Maximum
ME	-	Maximum Entropy
ML	-	Maximum Likelihood
$E(.)$	-	Expectation operator
MSE	-	Mean-Square Error
MRA	-	Minimal Redundant Array
min	-	Minimum
MVDR	-	Minimum Variance Distortionless Response
MHA	-	Minimum-Hole Array
$\langle\cdot\rangle$	-	Modulo Operator
MIMO	-	Multiple Input Multiple Output
MUSIC	-	Multiple Signal Classification
MI-ESPRIT	-	Multiple-Invariance - Estimation of Signal Parameters Via Rotational Invariance
NLA	-	Nested Linear Array
σ^2	-	Noise Power / Variance
ϕ	-	Non-Linear Transformation Function in SVR
NLA	-	Non-Uniform Linear Array
$\|\|.\|\|$	-	Norm of (.)
PHD	-	Pisarenko Harmonic Decomposition
P-SVR	-	Propagator-Support Vector Regression
QP	-	Quadratic Programming

Q	-	Quadrature
RBF	-	Radial Basis-Function
RBFNN	-	Radial Basis-Function Neural Network
RADAR	-	Radio Detection and Ranging
RAKE	-	Rank Reduction Estimator
RF	-	Radio Frequency
$\Re(.)$	-	Real Part (.)
RMSE	-	Root Mean Square Error
a	-	Scalar
$\mathbb{C}$	-	Set of all Complex Numbers
$\mathbb{R}$	-	Set of all Real Numbers
SNoI	-	Signal-Not-of-Interest
SoI	-	Signal-of-Interest
SNR	-	Signal-to-Noise Ratio
SONAR	-	Sound Navigation and Ranging
SLA	-	Sparse Linear Array
SDMA	-	Spatial Division Multiple Access
c	-	Speed of Light
$\subset$	-	Subset of
$\subseteq$	-	Subset of or Equal to
SVR	-	Support Vector Regression
$\oplus$	-	Hadamard Product
τ_n	-	Time Delay
$(.)^T$	-	Transpose of (.)
UCLA	-	Unfolded Co-Prime Linear Array
UCLA-MUSIC	-	Unfolded Co-Prime Linear Array - Multiple Signal Classification
ULA	-	Uniform Linear Array
$\cup$	-	Union

a	-	Vector
λ	-	Wavelength
WAI	-	Wiener Array Interpolation

CHAPTER 1

INTRODUCTION

In the last few decades, sensor array systems have gained considerable attention wherein the set of sensors is positioned in a specific configuration. It spatially captures the propagating signals from different sources in the field-of-view (FOV) and extracts the desired information from the observation in the presence of noise and interference (Manikas 2004). Sensor array systems are greatly supported by array signal processing techniques for its accomplishment. It processes the signals received by an array of sensors and brings out an estimation of the source signal parameters such as power, frequency and location based on the temporal and spatial characteristics. A combination of communication systems and array signal processing methods has been developed into a well-established technology. This technology is transitioning from traditional direction nulling phase arrays to sophisticated super-resolution spatiotemporal arrays. The MIMO array systems and arrayed wireless sensor networks use the channel's spatial and temporal features for handling multipath that improves the capacity and spectral efficiency (Liao *et al.*2018).

1.1 DOA ESTIMATION

In the research community of sensor array signal processing, estimation of the DOA of the source signals has long been of great interest in both civilian and military applications (Krim *et al.*1996). DOA estimation is an important problem seen in radar, sonar, geophysics, acoustics, bioengineering, seismology, multimedia, radio astronomy and wireless

communication. It finds applications in target localization and tracking in electronic warfare systems (Joshi *et al.* 2022), emergency rescue assistance, speech enhancement in hearing aid devices (HAD) (Tokgoz *et al.* 2021; Dehghan Firoozabadi *et al.* 2020), brain source localization (Albera *et al.* 2008), electronic surveillance, navigation, geophysical exploration, seismic exploration, freight tracking, intelligent transportation (Pohlmann *et al.* 2022), drone localization (Fu *et al.* 2019), parametric channel estimation (Wang *et al.*2020) and user localization in massive MIMO (Shu *et al.* 2018; Shu *et al.* 2020; Grenier *et al.*2016).

An adaptive antenna array is a potential technology for improvements in both military and civilian applications such as radar, electronic warfare systems, wireless communications and satellite navigation (Razavizadeh *et al.*2014; Balanis *et al.* 2007). Wireless technology is rapidly evolving, and 5G or beyond 5G (B5G) technology will soon take precedence (Shu *et al.* 2020) and for meeting its stringent demands, one potential solution is adaptive antenna array systems also known as smart antenna systems (Balanis *et al.* 2007; Gross 2005). In smart antenna systems, DOA estimation plays a key task in localizing the source signal directions. For instance, when the desired signal's DOA is known, adaptive beamforming methods can be used for steering the beams toward the desired source directions instead of the undesired directions (Bellofiore *et al.* 2002). In addition, DOA estimation plays a vital role in direction-finding (DF) for the next-generation mobile and stealth communication systems (Kiang *et al.* 2004).

In cellular radio systems, spatial division multiple access (SDMA) with its advanced spatial-processing capabilities allows it to distinguish the radio signals in the angular domain by forming a beam for each user based on its DOA. As a result, there is a significant increase in interference suppression and frequency reuse, leading to improved capacity and throughput of a

network with lower infrastructure costs (Balanis *et al.* 2007). DOA estimation of underwater targets plays a crucial role in SONAR systems for oceanographic and naval applications such as vessel navigation, torpedo localization and the internet of underwater things (IoUT) (Lan *et al.* 2021). High-resolution DOA estimation is an essential requirement of multiple-input and multiple-output (MIMO) RADAR systems for accurate localization and tracking of targets (Xu *et al.* 2022). Another usage for DOA estimation is in audio zooming for audio enhancement (Evers *et al.* 2018), in which, once the sound source has been located, it is possible to zoom in or amplify the specific sound to make it louder and clearer. In emergency rescue assistance, accurate localization of electromagnetic beacon sources is always necessary for search and rescue operations. The FCC (Federal Communications Commission 2022) has adopted a mandatory regulation for location accuracy in wireless emergency calls. Also, the localization of source nodes is crucial in sensor networks for optimal performance. Furthermore, the localization of animals and birds based on their sound is of great interest in bio-engineering studies.

DOA estimation is the process of determining the direction of the incoming source signals received by the sensor array, where the signals are located at a different point in space (Foutz *et al.* 2008). The DOAs of all the source signals are computed based on the temporal delays between the sensor array elements. In order to provide good insight, the problem of DOA estimation is explained with a human auditory system analogy (Balanis *et al.* 2007). A person's ability to ascertain the DOA of a sound can be viewed as the signals received by the ears, which function as acoustic sensors. The ears are separated and so each ear gets the signal with a distinct time delay. The brain, the human "signal processor" performs a large number of computations to correlate information and determine the direction of the received sound based on the temporal differences or delays received by the two ears. In a

similar way, the array of sensors is used in the measurement of the propagating fields. The propagating fields could be acoustic waves in hydrophone (sonar), microphone (acoustics), geophone (seismology), ultrasound probe (biomedical) array applications and electromagnetic waves in RF antenna array and optical receivers (wireless communication) (Manikas 2004). The digital signal processor (DSP) computes the DOA of the propagating fields based on the temporal differences or delays received by the sensor array.

1.2 OVERVIEW OF DOA ESTIMATION METHODS

The development of multi-source localization methods has been burgeoning in signal processing, communications, and underwater acoustics literature. There have been several reports concerning defense-oriented localization systems since World War I. Stansfield (Stansfield 1947) reports the statistical theory of emitter localization. Many further notable comprehensive reports followed, including a review work by Torrieri (Torrieri 1984), extensive reviews of array processing by Krim (Krim *et al.* 1996), Wax (Wax 1995) and a book devoted entirely to array processing by Van Trees (Van Trees 2022).

In general, DOA estimation methods can be broadly categorized into conventional methods, maximum likelihood (ML) methods, subspace-based methods, and integrated methods (Liberti *et al.* 1999). The conventional methods (also referred to as classical methods) for DOA estimation are essentially based on the concept of beamforming. Two methods are classified as conventional methods which are the delay-and-sum method (Bartlett 1961; Bartlett 1948) (also referred to as the classical beamformer (CBF) method or Fourier method or Bartlett method) and Capon's minimum variance method (also known as minimum variance distortionless response (MVDR)) (Capon 1969). The basic idea behind both the aforementioned methods is to steer a

beam in all possible directions and measure the output power from each direction. The directions for which the largest output power is observed are considered as the DOA of the source signals. These methods are simple in terms of implementation perspective and their non-parametric solutions are obtained without exploiting the statistics of the received signal. In the delay-and-sum method, the spatial power spectrum exhibits peaks when the beamforming weights are equal to the directional vectors of source signals. The angles corresponding to the peaks of the spatial spectrum are the DOA of the source signals. The major limitation of the delay-and-sum method is its poor angular resolution capability for resolving the DOA of multiple closely spaced source signals (Chen *et al* 2010). On the other hand, Capon's minimum variance method is designed for minimizing the output power for signal-not-of-interest (SNOI) and maximizing the output power for signal-of-interest (SOI) with the constraint of maintaining unity gain for the desired direction-of-interest. Capon's minimum variance method involves additional matrix inversion computation and exhibits better angular resolution compared to the delay-and-sum method. The downside of this approach is the inverse matrix computation that is expensive for large sensor arrays and becomes ill-conditioned (singular) in the presence of correlated source signals (Chen *et al.* 2010).

Research has been carried out on the maximum likelihood (ML) methods (Ziskind *et al.* 1988; Ziskind *et al.* 1990) for the DOA estimation problem which provides an optimal solution, especially at a low signal-to-noise ratio (SNR) and correlated source signal conditions. However, it is rarely used in practice because of its intense computational complexity to find the global maximum of the likelihood function.

Unlike the conventional methods and ML methods, the subspace-based methods exploit the statistics of the received signal and exhibit high-

resolution DOA estimation performance (Tuncer *et al.* 2009). Within the class of subspace-based methods, the multiple signal classification (MUSIC) and estimation of signal parameters via rotational invariance (ESPRIT) have been most widely examined. The MUSIC method proposed by Schmidt is a popular high-resolution eigenstructure method (Schmidt 1986). It yields an asymptotically unbiased DOA parameter estimate for multiple source signals and achieves superior estimation performance by exploiting the orthogonality between the signal and noise subspaces of the received signal array covariance matrix. In comparison to ML approaches, MUSIC performs a spectral search across a reduced parameter space, resulting in significantly lower computational complexity. However, it suffers in the presence of highly correlated source signals and the spectral search process involved may be computationally expensive for real-time applications. Moreover, it requires prior knowledge of the second-order spatial statistics of the signal and noise. Several efforts have been taken for enhancement of the resolution performance and reduction in computational complexity of the traditional MUSIC method. Xu has proposed the Fast Subspace Decomposition (FSD) technique for a reduction in the computational complexity seen in the MUSIC method (Xu *et al.*1994).

A search-free method called the Root-MUSIC method based on polynomial rooting has been proposed by Barbell (Barbell 1983). It offers improved resolution at low SNR levels and is computationally efficient compared to the traditional MUSIC method. However, it is applicable only for ULA configurations. The Cyclic MUSIC method suggested (Gardner 1988), is a selective direction-finding technique that takes advantage of the spectral coherence characteristics of the received signal to resolve signals that are spaced closer together than the array's resolution threshold. Additionally, Cyclic MUSIC does not adhere to the requirement of the total number of signals impinging on the array being lower than the total number of array

elements. The performance of MUSIC suffers greatly in a multipath environment where the signals received are strongly correlated. The array covariance matrix is subjected to a process known as spatial smoothing to overcome this drawback (Pillai *et al.*1989; Shan *et al.* 1985).

In addition, mean-square error-based approaches such as the linear prediction (LP) method (also referred to as the autoregressive (AR) method) (Johnson 1982) and Pisarenko harmonic decomposition (PHD) method (Pisarenko 1973) have been proposed. The maximum entropy (ME) method derived by Burg, maximizes the entropy function subject to certain constraints (Burg 1972). Kumaresan and Tufts (Kumaresan *et al.* 1983) have proposed a min-norm method based on the minimum norm vector residing in the noise subspace and its explanations are presented by Ermolaev and Gershman (Ermolaev *et al.* 1994). All the aforementioned methods such as LP, PHD, ME and min-norm exhibit an inferior estimation performance compared to the MUSIC method.

In reality, the resolution and estimation accuracy are limited by noise as well as inaccuracies in the presumed data model. Array calibration refers to the process of adjusting the presumed array response model for inaccuracies caused as a result of various imperfections such as phase errors, gain errors, uncertain sensor placements, an imbalance between the I (In-phase) and Q (Quadrature) channels, and an inaccurately defined mutual coupling model (Tuncer *et al.* 2009). Sakaguchi (Sakaguchi *et al.* 2002) has illustrated a hardware-based calibration technique. Auto-calibration is the other option where array response parameters are computed concurrently with the DOAs using the measured data (Li *et al.* 2003). Levi and Messer (Levi *et al.* 1990) and Rockah and Schultheiss (Rockah *et al.* 1987) have illustrated the fundamental constraints of the combined estimate of sensor locations and DOAs. Belloni (Belloni *et al.*2007) provided a more recent contribution in

which the array interpolation approach is effectively combined with the Root-MUSIC algorithm. The experimental results of array calibrations are presented in (Dandekar *et al.* 2000; Gupta *et al.* 2003; Pettersson *et al.* 2003; Pierre *et al.* 2004).

The aforementioned limitations of the MUSIC method have urged Roy and Kailath (Roy *et al.* 1989) to propose a method called ESPRIT through the exploitation of the rotational-invariance property of the sensor array. The major advantages of the ESPRIT method are its involvement of less computational complexity and the absence of the requirement of exhaustive spectral search and array calibration compared to the MUSIC method. Several variants such as unitary ESPRIT (Zoltowski *et al.* 1996), QR-ESPRIT (Strobach 1998), DFT-beamspace ESPRIT (Xu *et al.* 1994), Multiple-Invariance ESPRIT (MI-ESPRIT) (Swindlehurst *et al.* 1992) and Equirotational stack ESPRIT (ES-ESPRIT) (Strobach 2000) have been proposed for the enhancement of estimation performance and reduction in the computational complexity seen in the ESPRIT method.

The integrated method, which combines the property restoral and the subspace-based method, is the last category of DOA estimation methods. The property restoral method features the Iterative Least Squares Projection Based Constant Modulus Algorithm (ILSP-CMA) overcoming many of the challenges associated with Multistage CMA algorithms (Parra *et al.* 1995). Xu and Lin (Xu *et al.* 1995) have presented a novel technique by combining the ILSP-CMA with the subspace DOA approach for the enhancement of the DOF. Muhamed and Rappaport (Muhamed *et al.* 1996) demonstrated the improvement in estimation performance by combining the subspace-based approaches such as MUSIC and ESPRIT with the ILSP-CMA.

The practical aspects of design and applications of direction-finding (DF) systems are discussed in (Tuncer *et al.* 2009). A wide range of

contemporary DOA estimation methods is discussed in (Chandran 2005). Several attempts at higher-order statistics extension of subspace-based methods have been proposed (Chevalier *et al.* 2005). It offers enhanced DOF, insensitiveness to Gaussian background noise, and robustness to modeling errors. However, its main weakness is high computational complexity, poor angular resolution and higher sensitivity to finite sample effects (Tuncer *et al.* 2009).

Recently, nonuniform linear array (NULA) designs have gained popularity due to their offer of larger array aperture with fewer sensors (Tuncer *et al.* 2009). However, its estimation performance can be increased only when the information on the missing sensors is compensated. It can be obtained with the help of array mapping techniques (Tuncer *et al.* 2007). Various array-mapping techniques are seen in the literature such as Davies' transformation (Davies 1965) is one example that can be used in a variety of cases, but it is sensitive to parameter selection and array geometry. One of the most efficient techniques for array mapping is array interpolation (Bronez 1988).

Within array interpolation techniques, Classical Array Interpolation (CAI) (Friedlander *et al.* 1992) was introduced that interpolates using a mapping matrix with calibration angles. However, it is limited by small interpolation sectors and ill-condition of the inverse matrix involved in the mapping matrix. (Tuncer *et al.* 2007) have proposed a Wiener Array Interpolation (WAI) technique based on Mean-Square Error (MSE) for overcoming the limitations of CAI. It exhibits better performance than CAI at low SNR levels and is relevant for NULAs when fast algorithms like Root-MUSIC are applied. However, the computational complexity of these approaches is high due to the involvement of array mapping alongside the subspace methods such as Root-MUSIC and ESPRIT. To address this, several

relevant adaptations of Root-MUSIC and ESPRIT to more wide classes of array geometries have been proposed such as generalized ESPRIT (Gao *et al.* 2005), Fourier Domain (FD) Root-MUSIC (Rübsamen *et al.* 2008) FD-Weighted Least-Squares (FDWLS) Root-MUSIC algorithm (Rübsamen *et al.* 2009), and Rank Reduction Estimator (RARE) (Pesavento *et al.* 2002). In contrast, the orientation of designing a NULA in such a way that the conventional DOA estimation methods can be applied without compensating the missing sensor information by using array mapping techniques has gained significant interest. For this purpose, several SLA designs have been proposed.

Recently, co-prime linear array (CLA) designs such as general co-prime linear array (GCLA) (Vaidyanathan *et al.* 2011) and unfolded co-prime linear array (UCLA) (Zheng *et al.* 2018) have gained considerable research interest among the several SLA designs such as minimal redundant array (MRA) (Moffet 1968; Ishiguro 1980), minimum-hole array (MHA) (Vertatschitsch *et al.* 1986) and nested linear array (NLA) (Pal *et al.* 2010). Despite the potential advantages, both GCLA and UCLA suffer from the critical problem of ambiguity resulting in an ambiguous estimate of true DOAs. Specifically, GCLA suffers from the problem of pair-matching ambiguity in subarray-domain processing but both GCLA and UCLA suffer from the problem of grating-angle ambiguity.

1.3 OBJECTIVES OF DISSERTATION

In this thesis, the problem of estimating the DOA of the incoming source signals with a general co-prime linear array (GCLA) and unfolded co-prime linear array (UCLA) is of prime research interest.

The key objectives of this dissertation are as follows :

(i) To resolve the ambiguity problem such as pair-matching and grating-angle ambiguity in estimating the DOA of the incoming source signals with general co-prime linear array (GCLA) and unfolded co-prime linear array (UCLA).

(ii) To achieve a reliable estimation of true DOAs with superior estimation performances in terms of accuracy, angular resolution and degrees-of-freedom (DOF) compared to the existing methods.

(iii) To offer good generalization and robustness in estimation performance with reduced complexity in terms of computational complexity and execution time compared to the existing methods.

1.4 CONTRIBUTIONS OF DISSERTATION

The main contributions of the dissertation are summarized as follows :

(i) First, the proposed unambiguous DOA estimation method incorporates the initial estimation of DOAs through UCLA-MUSIC. The true DOAs are distinguished from ambiguous estimates obtained from UCLA-MUSIC using the estimated power of the transmitted source signals. The source power function is derived based on the signal subspace eigenvalues and its associated eigenvectors to estimate the power of the transmitted source signals. The proposed approach distinguishes and detects the true DOAs successfully without any ambiguity. The simulation results guarantee the superiority of the proposed method over the existing methods in terms of reliability and accuracy.

(ii) In the second solution, an improved polynomial rooting-based method for high-resolution unambiguous DOA estimation is proposed. A polynomial function is derived based on the orthogonality between the noise subspace eigenvectors and array directional vectors. A signal power function is derived based on spatial filtering for the selection of the signal roots that are associated with true DOAs over ambiguous roots obtained from the polynomial function. Furthermore, a maximum signal power function based on the second-order differential counterparts of the signal power function is proposed for the enhancement of the angular resolution capability of the signal power function in resolving DOAs of multiple closely spaced source signals. The error analysis is performed for confirmation of the achievement of better estimation accuracy of the proposed method that closely follows the fundamental limits of the Cramer-Rao lower bound **(**CRLB). The simulations have been performed to demonstrate the effectiveness and superiority of the proposed method in terms of reliability, accuracy, angular resolution and computational complexity.

(iii) In the third solution, a computationally efficient DOA estimation method based on support vector regression (SVR) has been proposed to address the ambiguity problem associated with GCLA and UCLA. The ambiguity problem is resolved by treating DOA estimation as approximating the unknown regression function that maps the signal subspace eigenvectors with the DOA of the incoming source signals. The proposed formulation uses only one regression model for the detection of multiple DOAs whereas the other SVR

formulation requires a multiple regression model. This provides computational efficiency for the proposed method. The proposed formulation estimates the DOAs involving full DOF without increasing the training complexity. It also offers good generalization for a varying number of sources and robustness in estimating the DOAs successfully without any ambiguity. The analysis and simulation findings show the proposed method outperforms the existing methods in terms of estimation reliability, estimation accuracy, computational complexity, execution time and DOF.

1.5 OUTLINE OF DISSERTATION

Chapter 1 introduces the thesis by presenting the following: array signal processing theory and its importance in various applications; definition of direction-of-arrival (DOA) estimation and its significant roles in various applications; evolutions of DOA estimation methods; motivation; objectives; main contributions and outline of the dissertation.

Chapter 2 lays the foundation for the thesis through the presentation of the ambiguity issues in DOA estimation with GCLA and UCLA with associated detailed literature reviews. The ULA is described first, along with its sensor array design, mathematical description of the received signal model, and the concept of spatial sampling. The GCLA and UCLA are then explained, along with its sensor array design and mathematical description of the received signal model and DOA estimation respectively. The Cramer-Rao lower bound (CRLB) for GCLA and UCLA is presented. Finally, a comprehensive investigation of ambiguity issues such as pair-matching ambiguity and grating-angle ambiguity in DOA estimation associated with GCLA and UCLA is discussed.

Chapter 3 presents the proposed method for the resolution of the critical issue of grating-angle ambiguity in the estimation of the DOA parameter with UCLA. Initially, the literature review related to the problem formulation and its existing solutions is detailed. Then, the mathematical description of the proposed unambiguous DOA estimation method based on the source power function is presented. The effectiveness of the proposed method is illustrated by several standard simulations.

Chapter 4 presents the mathematical description of an improved polynomial rooting-based method proposed to resolve the DOAs of multiple closely spaced source signals in the ambiguity problem situation. The simulation results presented show the effectiveness and superiority of the proposed method in terms of reliability, accuracy, angular resolution and computational complexity.

Chapter 5 presents a computationally efficient DOA estimation method based on support vector regression (SVR) for addressing the ambiguity problem associated with GCLA and UCLA. Initially, the literature related to the problem formulation and its existing solutions is detailed. Then, the mathematical formulation of the proposed SVR method for addressing the ambiguity problem with GCLA and UCLA is described. The complexity and DOF analysis of the proposed method in comparison with the existing methods is presented. The simulation results have been presented to show the effectiveness and superiority of the proposed method in terms of reliability, accuracy, computational complexity and execution time.

Chapter 6 summarizes the thesis highlighting the main contributions and discusses the future scope of the work presented in this dissertation.

CHAPTER 2

AMBIGUITY IN DIRECTION-OF-ARRIVAL ESTIMATION

2.1 INTRODUCTION

This chapter lays the foundation for the thesis through the presentation of the ambiguity problem in DOA estimation with the general co-prime linear array (GCLA) and the unfolded co-prime linear array (UCLA). The uniform linear array (ULA) is described first, along with its sensor array design, mathematical description of the received signal model, and the concept of spatial sampling. The GCLA and UCLA are then explained, along with its sensor array design, mathematical description of the received signal model and DOA estimation respectively. Finally, the investigation of ambiguity problems such as pair-matching and grating-angle in DOA estimation associated with GCLA and UCLA are discussed.

In general, DOA estimation has been widely investigated through the utilization of a ULA, in which the spacing between array elements is limited to less than half the signal wavelength (Van Trees 2022). However, the ULA design places restrictions on the effective array aperture and leads to mutual coupling between the array elements, affecting the performances of DOA estimation in terms of accuracy, resolution, and DOF (Tuncer *et al.* 2009). Typically, the idea of a large effective aperture provides high estimation accuracy and resolution in DOA estimation. This can be accomplished by increasing the number of array elements and the spacing between them. However, increasing the number of array elements could be

costly in terms of system hardware needs and computational complexity (He *et al.*2012).

The non-uniform linear array (NULA) designs, also known as the sparse linear array (SLA) designs (Moffet 1968; Ishiguro 1980; Vertatschitsch *et al.* 1986; Pal *et al.* 2010; Vaidyanathan *et al.* 2011) have been developed considering the restrictions of the ULA design. SLA design consists of array elements with an inter-element spacing of more than half the signal wavelength. It enables the SLA design to attain a large effective array aperture with fewer array elements and also mitigates the influence of mutual coupling between array elements. However, SLA suffers from the problem of spatial ambiguity due to the inter-element spacing being greater than half the signal wavelength. To prevent the formation of spatial aliasing in DOA estimation, array elements must be positioned optimally in SLA (Aboumahmoud *et al.* 2021). In the literature, numerous SLA designs have been proposed, including minimal redundant array (MRA) (Moffet 1968; Ishiguro 1980), minimum-hole array (MHA) (Vertatschitsch *et al.* 1986), and nested linear array (NLA) (Pal *et al.* 2010). MRA and MHA require an exhaustive search process for sensor positioning. In addition, an iterative process is involved in getting the suitable covariance matrix. In contrast, the NLA has an analytic expression for sensor positioning but it suffers from mutual coupling effects due to the dense distribution array elements in one subarray having an inter-element spacing of less than half the signal wavelength (Aboumahmoud *et al.* 2021).

Recently, the co-prime linear array (CLA) design (Vaidyanathan *et al.* 2011) has gained considerable research interest among the several SLA designs due to the following benefits: (i) the closed-form solution for positioning the array elements that make the design and analysis process simple, which lacks in the MRA and MHA (ii) the mutual coupling between

array elements is insignificant and provides higher estimation robustness compared to the NLA design (Tan *et al.*2014). A general CLA referred to as GCLA consists of two ULAs (subarrays), each with a co-prime number of array elements having more than half the signal wavelength as inter-element spacing (Vaidyanathan *et al.* 2011). Generalized CLA designs, such as co-prime array with compressed inter-element spacing (CACIS) and co-prime array with displaced subarrays (CADiS), have been suggested by (Qin *et al.* 2015) based on the difference-coarray of GCLA for enhancement of the DOF.

DOA estimation with GCLA is performed via two categories of approaches such as difference-coarray domain processing and subarray domain processing (Xiao *et al.* 2019). In the difference-coarray domain processing, the number of distinct consecutive covariance lags is virtually more than the number of physical array elements, providing the enhanced DOF (Liu *et al.*2015; Xie *et al.*2019). However, it is constrained by the presence of "holes" in the difference-coarray of GCLA and also entails a high degree of computational cost due to the requirement of a large number of snapshots. In subarray domain processing, the signal received from two subarrays is processed independently and the DOAs are estimated based on the co-prime property. In literature, numerous DOA estimators have been presented, in which subspace-based estimators such as MUSIC, ESPRIT and its variants offer superior estimation performances compared to the maximum likelihood estimators and beamformer estimators such as LCMV and MVDR (Schmidt 1986; Roy *et al.* 1989).

Zhou *et al.*(2013) have proposed a subspace-based estimator called DECOM, which decomposes the GCLA into two separate subarrays and applies the MUSIC estimator individually. The MUSIC spectrum of both the subarrays exhibits peaks at true DOAs and also peaks at ambiguous angle locations due to the inter-element spacing of the subarrays being greater than

half the signal wavelength. However, the co-prime property allows the peaks of the MUSIC spectrum of two subarrays to coincide for pair of angle locations that constitutes the true DOAs. Considerable efforts have been taken for the bypassing of spectral searching process in DECOM for GCLA by developing a partial spectral searching method (Sun *et al.*2015) and polynomial-rooting-based methods (Zhang *et al.* 2017; Liu *et al.* 2018; Yan *et al.* 2018). The major drawbacks of the above-aforementioned methods (Sun *et al.*2015; Zhang *et al.* 2017; Liu *et al.* 2018; Yan *et al.* 2018) are as follows (i) maximum DOF is equal to a subarray with a minimum number of array elements i.e., less than the total number of array elements (ii) estimation performances are limited in terms of resolution and accuracy (iii) additional complexity due to the pair-matching process (iv) suffers from pair-matching ambiguity in the case of signals are transmitted from multiple emitters (v) the information of the entire array is not utilized (Zheng *et al.* 2018).

To circumvent the restrictions mentioned above, the approach called adjoined subarray (AdS) based method presented by (Zheng *et al.* 2018) collectively utilizes the two subarrays rather than handling them separately. The method (Zheng *et al.* 2018), stacks the received signal from two subarrays of GCLA and applies the MUSIC estimator. Utilization of the entire array helps the method (Zheng *et al.* 2018) in the enhancement of the DOF and also in the elimination of the pair-matching process. However, the effective array aperture remains unchanged. As a result, there is no improvement seen in the estimation performance metrics such as resolution and accuracy.

Zheng *et al.* (2018) have proposed a new CLA design known as unfolded co-prime linear array (UCLA) also recognized as a co-prime array with adjoined subarrays (CAAdS) for meeting the aforementioned limitations.

The UCLA involves the cascading of two subarrays together, which results in the enlargement of the effective array aperture compared to the GCLA. This advantage helps the MUSIC estimator in its application to UCLA and it offers better estimation performances than GCLA. In (He *et al.*2020), a polynomial rooting approach called UCLA-Root MUSIC is proposed for the improvement of the resolution and avoidance of the spectral searching process where (Zheng *et al.* 2018) involves.

Despite the potential benefits of UCLA, it suffers from the critical issue of grating-angle ambiguity also referred to as directional matrix ambiguity or non-trivial ambiguity (Liu *et al.* 2013). It occurs due to the non-uniform linear array design of UCLA, in which there exists a set of DOAs with linearly dependent directional vectors. As a result, directional vectors that are not associated with true DOAs tend to reside in the signal subspace, yielding an estimate of true and ambiguous DOAs. The strategy proposed in (Yang *et al.*2019; Huang *et al.*2021) have used a beamformer-based approach to suppress the ambiguous estimate. However, it fails to resolve the problem of grating-angle ambiguity when the DOA of signals from multiple emitters is closely distributed. It also involves high computational complexity due to the spectral searching process and provides lower estimation performances in terms of reliability, accuracy and angular resolution.

2.2 UNIFORM LINEAR ARRAY

Figure 2.1 shows a ULA design consisting of N sensor elements that are uniformly spaced apart by distance 'd' and linearly positioned at $P_n = (nd, 0,0)\ ; n = 0,1,2,\ldots, N-1$ along the x-axis.

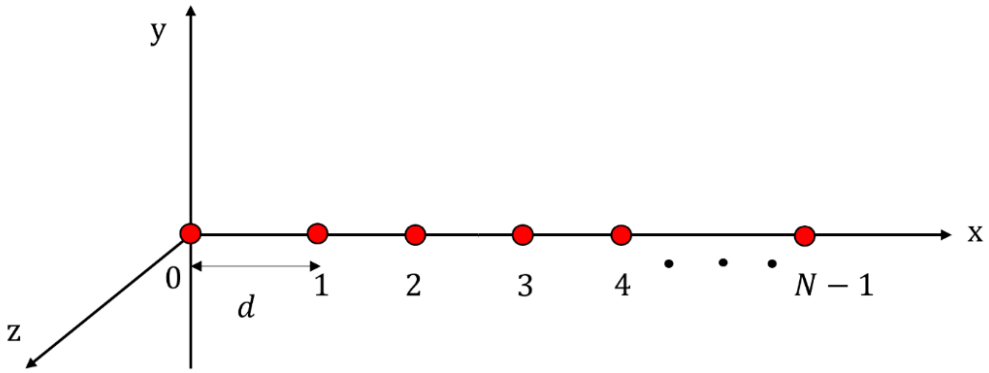

Figure 2.1 Design of ULA

2.2.1 Received Signal Model of ULA

Assume that an incoming far-field (plane wave) signal $s(t)$ impinges on the ULA from direction θ as shown in Figure 2.2. Let, $s(t)$ is a narrowband modulated signal and it is given by

$$s(t) = m(t)e^{j2\pi f_c t} \tag{2.1}$$

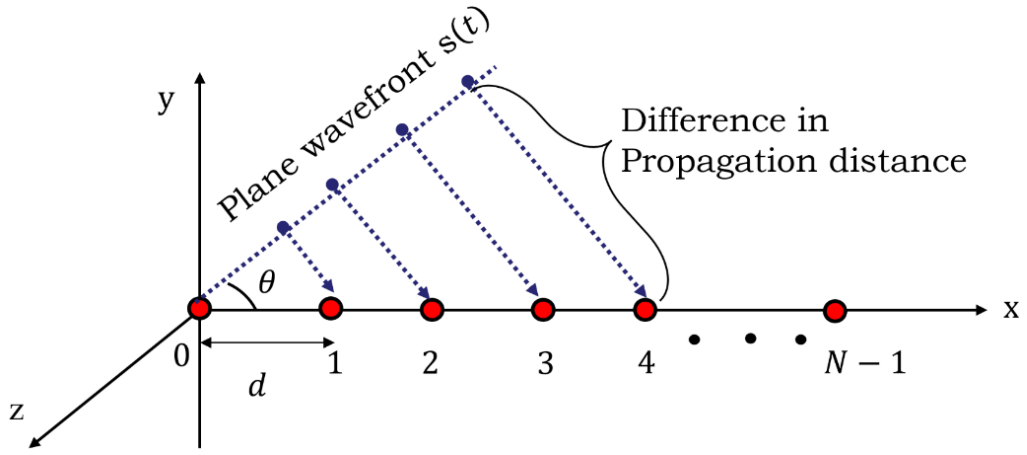

Figure 2.2 System model of ULA

where $m(t)$ denotes the modulated message or the complex envelope of $s(t)$ and f_c is the carrier frequency. Then, the signal received by ULA can be expressed as

$$\mathbf{x}_{ULA}(t) = \begin{bmatrix} x_0(t) \\ x_1(t) \\ \vdots \\ x_{N-1}(t) \end{bmatrix} = \begin{bmatrix} \mathrm{s}(t-\tau_0) \\ \mathrm{s}(t-\tau_1) \\ \vdots \\ \mathrm{s}(t-\tau_{N-1}) \end{bmatrix} \tag{2.2}$$

where $\mathrm{s}(t-\tau_n)$ is the signal received by the sensor element positioned at P_n, τ_n is the time delay of the received signal at the sensor element positioned at P_n. Generally, the time delay is expressed as

$$Time\ delay\ = \frac{Difference\ in\ propagation\ distance}{velocity} \tag{2.3}$$

Therefore, $\tau_n = \frac{nd\ sin\ (\theta)}{c}$. Now, the signal received at the sensor array can be written as

$$\mathbf{x}_{ULA}(t) = \begin{bmatrix} \mathrm{s}(t-\tau_0) \\ \mathrm{s}(t-\tau_1) \\ \vdots \\ \mathrm{s}(t-\tau_{N-1}) \end{bmatrix} = \begin{bmatrix} m(t-\tau_0)\, e^{j2\pi f_c(t-\tau_0)} \\ m(t-\tau_1)\, e^{j2\pi f_c(t-\tau_1)} \\ \vdots \\ m(t-\tau_{N-1})\, e^{j2\pi f_c(t-\tau_{N-1})} \end{bmatrix}$$

$$= \begin{bmatrix} m(t-\tau_0)\, e^{-j2\pi f_c\tau_0} \\ m(t-\tau_1)\, e^{-j2\pi f_c\tau_1} \\ \vdots \\ m(t-\tau_{N-1})\, e^{-j2\pi f_c\tau_{N-1}} \end{bmatrix} e^{j2\pi f_c t} \tag{2.4}$$

Let, $e^{-j2\pi f_c\tau_n} = e^{-j2\pi f_c\frac{nd\ sin\ (\theta)}{C}} = e^{-j2\pi\frac{nd\ sin\ (\theta)}{\lambda}} = e^{-jnk\ sin(\theta)}$, where $k = \frac{2\pi d}{\lambda}$. The bandwidth of $m(t)$ is narrow and substantially less than the carrier frequency. Thus, $m(t) \cong m(t-\tau_0) \cong m(t-\tau_1) \cong \ldots \cong m(t-\tau_{N-1})$. Then, the received signal vector can be written as

$$\mathbf{x}_{ULA}(t) = m(t)e^{j2\pi f_c t} \begin{bmatrix} 1 \\ e^{-jksin(\theta)} \\ \vdots \\ e^{-j(N-1)ksin(\theta)} \end{bmatrix} = \mathrm{s}(t)\ \mathbf{a}_{ULA}(\theta) \tag{2.5}$$

where $a_{ULA}(\theta)$ is the array directional vector, it can be also referred to as array response vector or array steering vector or array manifold vector and it contains the information about direction-of-arrival (θ). In practice, the number of source signals is more than one, and noise exists in the propagation environment. Consider, $M\,(M < N)$ source signals from directions $\Theta = \{\theta_m\}_{m=1}^{M}$ impinging on N element ULA with the field-of-view (FOV) such that $\theta_m \in (-90^o, +90^o)$. Then, the observed array output received signal vector can be expressed as

$$\mathbf{x}_{ULA}(t) = \begin{bmatrix} 1 & 1 & & 1 \\ e^{-jksin(\theta_1)} & e^{-jksin(\theta_2)} & \cdots & e^{-jksin(\theta_M)} \\ \vdots & \vdots & & \vdots \\ e^{-j(N-1)ksin(\theta_1)} & e^{-j(N-1)ksin(\theta_2)} & & e^{-j(N-1)ksin(\theta_M)} \end{bmatrix} \begin{bmatrix} s_1(t) \\ s_2(t) \\ \vdots \\ s_M(t) \end{bmatrix} + \begin{bmatrix} n_0(t) \\ n_1(t) \\ \vdots \\ n_{N-1}(t) \end{bmatrix} \quad (2.6)$$

The matrix form of the observed array output received signal vector is expressed as

$$\mathbf{x}_{ULA}(t) = \mathbf{A}_{ULA}\,\mathbf{s}(t) + \mathbf{n}(t) \quad (2.7)$$

where $\mathbf{A}_{ULA} = [\mathbf{a}(\theta_1)\ \mathbf{a}(\theta_2)\ldots\ \mathbf{a}(\theta_M)] \in \mathbb{C}^{N\,x\,M}$ is the array directional matrix, it can also be referred to as array steering or array manifold matrix or array response matrix. $\mathbf{a}_{ULA}(\theta_m) \in \mathbb{C}^{N\,x\,1}$ is the array directional vector associated with m^{th} source signal, $\mathbf{s}(t) = [s_1(t)\ s_2(t)\ldots\ s_M(t)]^T \in \mathbb{C}^{M\,x\,1}$ represents the incoming source signal vector and $\mathbf{n}(t) = [n_0(t)\ n_1(t)\ldots\ n_{N-1}(t)]^T \in \mathbb{C}^{N\,x\,1}$ represents the zero-mean

additive white noise vector with covariance $\mathrm{E}\{\mathbf{n}(t)\mathbf{n}^H(t)\} = \sigma_{\mathbf{n}}^2\mathbf{I}_N$, where $\sigma_{\mathbf{n}}^2$ is the noise power and $\mathbf{I}_N$ denotes the N x N identity matrix.

2.2.1.1 Concept of spatial sampling

This section briefs the choice of inter-element spacing 'd'through the concept of spatial sampling. The Nyquist frequency theorem implies that a minimum sampling frequency is necessary for avoiding aliasing in a time-sampled signal (Ifeachor *et al.* 2022) and is given by

$$f_s = \frac{1}{T_s} \geq 2f_{max} \tag{2.8}$$

where f_s denotes the sampling frequency, T_s denotes the sampling period and f_{max} denotes the maximum frequency of the signal in the frequency spectrum. Similarly, the spatial sampling with the ULA (McCowan 2001) can be expressed as

$$f_{x_s} = \frac{1}{d} \geq 2f_{max} \tag{2.9}$$

where f_{x_s} denotes the spatial sampling frequency, d denotes the spatial sampling period and f_{max} denotes the maximum frequency of the signal in the spatial spectrum. The spatial frequency $f_{max} = \frac{1}{\lambda}$, Thus, $\frac{1}{d} \geq 2\ \frac{1}{\lambda}$. Then, the Nyquist condition for avoiding aliasing in spatial sampling is given by

$$d \leq \frac{\lambda}{2} \tag{2.10}$$

Using the Nyquist condition to avoid aliasing in spatial sampling, the inter-element spacing of ULA is set as $d = \frac{\lambda}{2}$. Equation (2.6) is given as follows:

$$\mathbf{x}_{ULA}(t) = \begin{bmatrix} 1 & 1 & & 1 \\ e^{-jksin(\theta_1)} & e^{-jksin(\theta_2)} & \cdots & e^{-jksin(\theta_M)} \\ \vdots & \vdots & & \vdots \\ e^{-j(N-1)ksin(\theta_1)} & e^{-j(N-1)ksin(\theta_2)} & & e^{-j(N-1)ksin(\theta_M)} \end{bmatrix} \begin{bmatrix} s_1(t) \\ s_2(t) \\ \vdots \\ s_M(t) \end{bmatrix} + \begin{bmatrix} n_0(t) \\ n_1(t) \\ \vdots \\ n_{N-1}(t) \end{bmatrix} \quad (2.11)$$

where $k = \frac{2\pi d}{\lambda}$. Substituting $d = \frac{\lambda}{2}$, $k = \frac{2\pi\left(\frac{\lambda}{2}\right)}{\lambda} = \pi$, Then, the observed array output received signal vector can be written as

$$\mathbf{x}_{ULA}(t) = \begin{bmatrix} 1 & 1 & & 1 \\ e^{-j\pi sin(\theta_1)} & e^{-j\pi sin(\theta_2)} & \cdots & e^{-j\pi sin(\theta_M)} \\ \vdots & \vdots & & \vdots \\ e^{-j(N-1)\pi sin(\theta_1)} & e^{-j(N-1)\pi sin(\theta_2)} & & e^{-j(N-1)\pi sin(\theta_M)} \end{bmatrix} \begin{bmatrix} s_1(t) \\ s_2(t) \\ \vdots \\ s_M(t) \end{bmatrix} + \begin{bmatrix} n_0(t) \\ n_1(t) \\ \vdots \\ n_{N-1}(t) \end{bmatrix} \quad (2.12)$$

An N element ULA can resolve $N-1$ source signals through the use of subspace-based DOA estimators such as ESPRIT and MUSIC. The output of the sensors in an array is influenced by their neighboring sensors, and this impact manifests as mutual coupling. This scenario becomes more prevalent and adversely impacts the sensor output when the sensors are arranged closely in the array. This impact in the arrays is quantified through the use of the weight function, which defines the number of sensor pairs in the array with a given degree of inter-element spacing.

Definition: The weight function $\mathrm{w}(m)$ of an array refers to the number of sensor pairs corresponding to the index m which indicates the spacing between the underlined sensor pair (Liu *et al.* 2016) and it is given by

$$\mathrm{W}(m) = \{(n_1, n_2) \in \mathbb{S} \mid n_1 - n_2 = md\} \tag{2.13}$$

$$\mathrm{w}(m) = \mathrm{Card}\,(\mathrm{W}(m)\,) \tag{2.14}$$

where $\mathbb{S}$ is the set that contains the sensor positions of an array. $\mathrm{Card}\,(\mathrm{W}(m)\,)$ is the cardinality of the set $\mathrm{W}(m)$, which indicates the number of elements in the set $\mathrm{W}(m)$. Say, the first three weights, $\mathrm{w}(1)$, $\mathrm{w}(2)$, and $\mathrm{w}(3)$ denotes the number of sensor pairs in an array with d, $2d$, and $3d$ inter-element spacing respectively. For example, consider an 12 element ULA ($N = 12$) with its sensor positions $\mathbb{S} = \{0,1,2,3,4,5,6,7,8,9,10,11\}$, whose weight function is $\mathrm{w}(1) = 11$, indicates that 11 sensor pairs in an array have d inter-element spacing. It clearly shows that the ULA design has a significant effect on the mutual coupling between array elements and influences the DOA estimation performances.

2.3 CO-PRIME LINEAR ARRAY

Figure 2.3 shows the GCLA design with N sensor elements consisting of a superposition of two subarrays with one common element (Vaidyanathan *et al.* 2011). Subarray 1 has N_1 elements of ULA with the inter-element spacing of $d_1 = N_2\frac{\lambda}{2}$. Likewise, subarray 2 has N_2 elements of ULA with the inter-element spacing of $d_2 = N_1\frac{\lambda}{2}$, where λ is the wavelength of the source signal. Thus, the total number of sensor elements in GCLA is $N = N_1 + N_2 - 1$.

The effective array aperture obtained by GCLA is given by $((N_2 - 1)N_1 + 1)d$. For example, consider a $12-$element GCLA ($N = 12$ i.e., $N_1 = 7$ and $N_2 = 6$) with its inter-element spacing $d_1 = 6\frac{\lambda}{2}$ and $d_2 = 7\frac{\lambda}{2}$ respectively. The sensor position of subarray 1 is $\mathrm{S}_1 = \{0,6,12,18,24,30,36\}$ and subarray 2 is $\mathrm{S}_1 = \{0,7,14,21,28,35\}$. Thus, the sensor position of GCLA

is given by $S_1 \cup S_2 = \{0,6,7,12,14,18,21,24,28,30,35,36\}$. The first three weights of GCLA are $w(1) = 2, w(2) = 2, w(3) = 2$ indicating 2 sensor pairs in an array having d, $2d$ and $3d$ inter-element spacing respectively. The $12-$element GCLA can obtain $36d$ as an effective array aperture. It clearly shows that the GCLA design has significant improvement to counter mutual coupling and yields better sparsity (array aperture) compared to the ULA design.

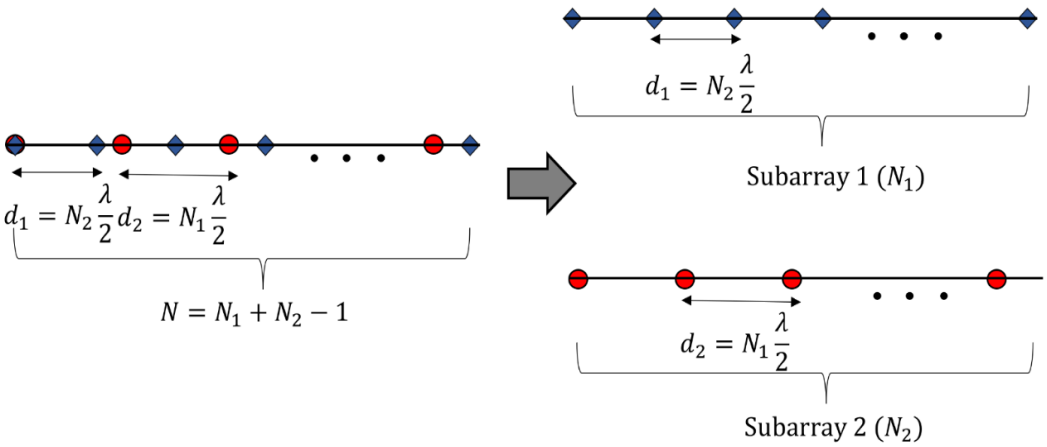

Figure 2.3 Design of GCLA

2.3.1 Received signal model of GCLA

Consider, M $(M < N)$ far-field source signals from directions $\Theta = \{\theta_m\}_{m=1}^{M}$ impinging on N element GCLA with the field-of-view (FOV) such that $\theta_m \in (-90^o, +90^o)$ as shown in Figure 2.4. Then, the observed array output received signal vector by i^{th}subarray of GCLA can be expressed as

$$\mathbf{x}_i(t) = \mathbf{A}_i\, \mathbf{s}(t) + \mathbf{n}_i(t) \quad ; \quad i = 1,2 \tag{2.15}$$

where $\mathbf{x}_1(t) \in \mathbb{C}^{N_1 \times 1}$ and $\mathbf{x}_2(t) \in \mathbb{C}^{N_2 \times 1}$ represents the received output vector of subarray 1 and subarray 2 of GCLA. Here, $\mathbf{A}_i$ represents the array directional matrix of i^{th}subarray and for each subarray, it is given by

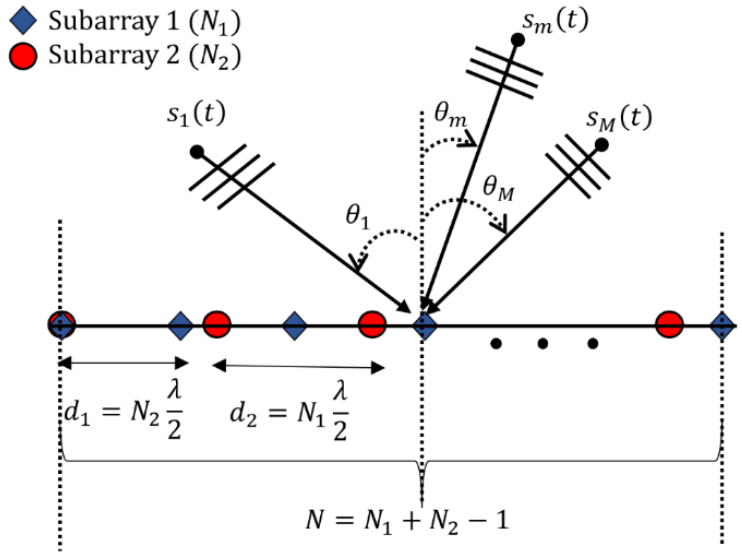

Figure 2.4 System model of GCLA

$$\mathbf{A}_1 = [\mathbf{a}_1(\theta_1)\ \mathbf{a}_1(\theta_2)\ldots\ \mathbf{a}_1(\theta_M)\ ] \in \mathbb{C}^{N_1 \mathrm{x}\, M} \tag{2.16}$$

$$\mathbf{A}_2 = [\mathbf{a}_2(\theta_1)\ \mathbf{a}_2(\theta_2)\ldots\ \mathbf{a}_2(\theta_M)\ ] \in \mathbb{C}^{N_2 \mathrm{x}\, M} \tag{2.17}$$

where $\mathbf{a}_1(\theta_m)$ and $\mathbf{a}_2(\theta_m)$ represents the array directional vector of subarray 1 and subarray 2 and it is given by

$$\mathbf{a}_1(\theta_m) = \left[1, e^{-j\pi N_2 \sin(\theta_m)}, \ldots, e^{-j\pi N_2 (N_1-1)\sin(\theta_m)}\right]^T \in \mathbb{C}^{N_1 \mathrm{x}\, 1} \tag{2.18}$$

$$\mathbf{a}_2(\theta_m) = \left[1, e^{-j\pi N_1 \sin(\theta_m)}, \ldots, e^{-j\pi N_1 (N_2-1)\sin(\theta_m)}\right]^T \in \mathbb{C}^{N_2 \mathrm{x}\, 1} \tag{2.19}$$

Then, the observed array output received signal vector of GCLA can be expressed as follows

$$\mathbf{x}_1(t) = \begin{bmatrix} 1 & 1 & & 1 \\ e^{-jN_2\pi \sin(\theta_1)} & e^{-jN_2\pi \sin(\theta_2)} & \cdots & e^{-jN_2\pi \sin(\theta_M)} \\ \vdots & \vdots & & \vdots \\ e^{-jN_2(N_1-1)\pi \sin(\theta_1)} & e^{-jN_2(N_1-1)\pi \sin(\theta_2)} & & e^{-jN_2(N_1-1)\pi \sin(\theta_M)} \end{bmatrix} \begin{bmatrix} s_1(t) \\ s_2(t) \\ \vdots \\ s_M(t) \end{bmatrix} + \begin{bmatrix} n_{1,0}(t) \\ n_{1,1}(t) \\ \vdots \\ n_{1,N_1-1}(t) \end{bmatrix} = \mathbf{A}_1\mathbf{s}(t) + \mathbf{n}_1(t) \tag{2.20}$$

$$\mathbf{x}_2(t) = \begin{bmatrix} 1 & 1 & \cdots & 1 \\ e^{-jN_1\pi sin(\theta_1)} & e^{-jN_1\pi sin(\theta_2)} & & e^{-jN_1\pi sin(\theta_M)} \\ \vdots & \vdots & & \vdots \\ e^{-jN_1(N_2-1)\pi sin(\theta_1)} & e^{-jN_1(N_2-1)\pi sin(\theta_2)} & & e^{-jN_1(N_2-1)\pi sin(\theta_M)} \end{bmatrix} \begin{bmatrix} s_1(t) \\ s_2(t) \\ \vdots \\ s_M(t) \end{bmatrix} + \begin{bmatrix} n_{2,0}(t) \\ n_{2,1}(t) \\ \vdots \\ n_{2,N_2-1}(t) \end{bmatrix} = \mathbf{A}_2\mathbf{s}(t) + \mathbf{n}_2(t) \quad (2.21)$$

Here, $\mathbf{s}(t) = [s_1(t)\ s_2(t) \ldots\ s_M(t)]^T \in \mathbb{C}^{M\,x\,1}$ represents the incoming source signal vector, $\mathbf{n}_1(t) \in \mathbb{C}^{N_1 x\,1}$ and $\mathbf{n}_2(t) \in \mathbb{C}^{N_2 x\,1}$ represents the zero-mean additive white noise of subarray 1 and subarray 2 with covariance $E\{\mathbf{n}_i(t)\mathbf{n}_i^H(t)\} = \sigma_{\mathbf{n}_i}^2\mathbf{I}_i$, $i = 1,2$, where $\sigma_{\mathbf{n}_i}^2$ is the noise power and $\mathbf{I}_i$ is the identity matrix (Vaidyanathan *et al.* 2011).

2.3.2 DOA Estimation with GCLA

The subarray-based method divides the GCLA into two ULAs (subarrays), and DOA estimation is performed independently on each ULA (Zhou *et al.*2013). The covariance of the received signal from two subarrays can be expressed as

$$\mathbf{R}_{\mathbf{x}_i} = E\{\mathbf{x}_i(t)\,\mathbf{x}_i{}^H(t)\}$$

$$= \mathbf{A}_i\,\mathbf{R}_s\,\mathbf{A}_i^H + \sigma_{\mathbf{n}_i}^2\mathbf{I}_i \ ; i = 1,2 \quad (2.22)$$

where $\mathbf{R}_s = \boldsymbol{E}\{\mathbf{s}\mathbf{s}^H\}$ denotes the source covariance matrix and $\mathbf{I}_i$ denotes the identity matrix. In practice, the actual covariance matrix $\mathbf{R}_{\mathbf{x}_i}$ is unknown, therefore its sample estimate $\widehat{\mathbf{R}}_{\mathbf{x}_i}$ is computed for K snapshots and it is given by

$$\widehat{\mathbf{R}}_{\mathbf{x}_i} = E\{\mathbf{x}_i(t)\,\mathbf{x}_i{}^H(t)\}$$

$$= \frac{1}{K}\sum_{t=1}^{K} \mathbf{x}_i(t)\,\mathbf{x}_i{}^H(t)\ ; i = 1,2 \tag{2.23}$$

The Equation (2.23) can be re-written as follows

$$\widehat{\mathbf{R}}_{\mathbf{x}_1} = E\{\mathbf{x}_1(t)\,\mathbf{x}_1{}^H(t)\} = \frac{1}{K}\sum_{t=1}^{K} \mathbf{x}_1(t)\,\mathbf{x}_1{}^H(t) \tag{2.24}$$

$$\widehat{\mathbf{R}}_{\mathbf{x}_2} = E\{\mathbf{x}_2(t)\,\mathbf{x}_2{}^H(t)\} = \frac{1}{K}\sum_{t=1}^{K} \mathbf{x}_2(t)\,\mathbf{x}_2{}^H(t) \tag{2.25}$$

The eigenvalue decomposition (EVD) of $\widehat{\mathbf{R}}_{\mathbf{x}_1} \in \mathbb{C}^{N_1 \mathrm{x}\, N_1}$ and $\widehat{\mathbf{R}}_{\mathbf{x}_2} \in \mathbb{C}^{N_2 \mathrm{x}\, N_2}$ yields

$$\widehat{\mathbf{R}}_{\mathbf{x}_1} = \hat{\mathbf{E}}_1 \widehat{\mathbf{D}}_1 \hat{\mathbf{E}}_1^H \tag{2.26}$$

$$\widehat{\mathbf{R}}_{\mathbf{x}_2} = \hat{\mathbf{E}}_2 \widehat{\mathbf{D}}_2 \hat{\mathbf{E}}_2^H \tag{2.27}$$

where $\hat{\mathbf{E}}_1 = \left[\mathbf{e}_1\ \mathbf{e}_2\ \mathbf{e}_3 \ldots \mathbf{e}_{N_1}\right] \in \mathbb{C}^{N_1 \mathrm{x}\, N_1}$, $\widehat{\mathbf{D}}_1 = \mathrm{diag}\left\{\lambda_1\ \lambda_2\ \lambda_3 \ldots \lambda_{N_1}\right\}, \hat{\mathbf{E}}_2 = \left[\mathbf{e}_1\ \mathbf{e}_2\ \mathbf{e}_3 \ldots \mathbf{e}_{N_2}\right] \in \mathbb{C}^{N_2 \mathrm{x}\, N_2}$, $\widehat{\mathbf{D}}_2 = \mathrm{diag}\left\{\lambda_1\ \lambda_2\ \lambda_3 \ldots \lambda_{N_2}\right\}$. The columns of $\hat{\mathbf{E}}_1$ and $\hat{\mathbf{E}}_2$ indicates the eigenvectors of $\widehat{\mathbf{R}}_{\mathbf{x}_1}$ and $\widehat{\mathbf{R}}_{\mathbf{x}_2}$ associated to eigenvalues of $\widehat{\mathbf{D}}_1$ and $\widehat{\mathbf{D}}_2$. In $\widehat{\mathbf{D}}_1$ and $\widehat{\mathbf{D}}_2$, only M eigenvalues are significant and related to the source signals and the remaining eigenvalues are approximately equal to noise power (Schmidt 1986). As a result, $\widehat{\mathbf{D}}_1, \widehat{\mathbf{D}}_2$ and its associated eigenvectors $\hat{\mathbf{E}}_1$, $\hat{\mathbf{E}}_2$ can be re-written as follows

$$\widehat{\mathbf{D}}_{s_1} = \mathrm{diag}\left\{\lambda_1\ \lambda_2\ \lambda_3 \ldots \lambda_M\right\} \tag{2.28}$$

$$\widehat{\mathbf{D}}_{s_2} = \mathrm{diag}\left\{\lambda_1\ \lambda_2\ \lambda_3 \ldots \lambda_M\right\} \tag{2.29}$$

$$\widehat{\mathbf{D}}_{n_1} = \text{diag}\{\lambda_{M+1}\ \lambda_{M+2}\ \lambda_{M+3}\ldots\lambda_{N_1}\} \tag{2.30}$$

$$\widehat{\mathbf{D}}_{n_2} = \text{diag}\{\lambda_{M+1}\ \lambda_{M+2}\ \lambda_{M+3}\ldots\lambda_{N_2}\} \tag{2.31}$$

$$\hat{\mathbf{E}}_{s_1} = [\mathbf{e}_1\ \mathbf{e}_2\ \mathbf{e}_3\ldots\mathbf{e}_M] \epsilon\ \mathbb{C}^{N_1 \text{ x } M} \tag{2.32}$$

$$\hat{\mathbf{E}}_{s_2} = [\mathbf{e}_1\ \mathbf{e}_2\ \mathbf{e}_3\ldots\mathbf{e}_M] \epsilon\ \mathbb{C}^{N_2 \text{ x } M} \tag{2.33}$$

$$\hat{\mathbf{E}}_{n_1} = [\mathbf{e}_{M+1}\ \mathbf{e}_{M+2}\ \mathbf{e}_{M+3}\ldots\mathbf{e}_{N_1}] \epsilon\ \mathbb{C}^{N_1 \text{ x } N_1-M} \tag{2.34}$$

$$\hat{\mathbf{E}}_{n_2} = [\mathbf{e}_{M+1}\ \mathbf{e}_{M+2}\ \mathbf{e}_{M+3}\ldots\mathbf{e}_{N_2}] \epsilon\ \mathbb{C}^{N_2 \text{ x } N_2-M} \tag{2.35}$$

Thus, $\widehat{\mathbf{R}}_{\mathbf{x}_1}$ and $\widehat{\mathbf{R}}_{\mathbf{x}_2}$ in Equation (2.26) and Equation (2.27) can be rewritten as

$$\widehat{\mathbf{R}}_{\mathbf{x}_1} = \hat{\mathbf{E}}_{s_1}\ \widehat{\mathbf{D}}_{s_1}\hat{\mathbf{E}}_{s_1}^H\ + \hat{\mathbf{E}}_{n_1}\ \widehat{\mathbf{D}}_{n_1}\ \hat{\mathbf{E}}_{n_1}^H \tag{2.36}$$

$$\widehat{\mathbf{R}}_{\mathbf{x}_2} = \hat{\mathbf{E}}_{s_2}\ \widehat{\mathbf{D}}_{s_2}\hat{\mathbf{E}}_{s_2}^H\ + \hat{\mathbf{E}}_{n_2}\ \widehat{\mathbf{D}}_{n_2}\ \hat{\mathbf{E}}_{n_2}^H \tag{2.37}$$

The columns of $\hat{\mathbf{E}}_{s_1}$ and $\hat{\mathbf{E}}_{s_2}$ (eigenvectors) that span the space is referred to as the signal subspace of $\widehat{\mathbf{R}}_{\mathbf{x}_1}$ and $\widehat{\mathbf{R}}_{\mathbf{x}_2}$ respectively. Similarly, the columns of $\hat{\mathbf{E}}_{n_1}$ and $\hat{\mathbf{E}}_{n_2}$ (eigenvectors) that span the space is referred to as the noise subspace of $\widehat{\mathbf{R}}_{\mathbf{x}_1}$ and $\widehat{\mathbf{R}}_{\mathbf{x}_2}$ respectively. Furthermore, the signal subspace and directional vector of the source signals span the same space and are orthogonal to the noise subspace (Pal *et al.*2011). As a result, the directional vector can be used in the search for all possible angles across the noise subspace to determine the DOA of transmitted source signals, and the MUSIC null spectrum of each subarray is provided by

$$\hat{f}_1(\theta) = \mathbf{a}_1^H(\theta)\ \hat{\mathbf{E}}_{n_1}\ \hat{\mathbf{E}}_{n_1}^H\ \mathbf{a}_1(\theta)\ = \left\|\hat{\mathbf{E}}_{n_1}^H\ \mathbf{a}_1(\theta)\right\|^2 \tag{2.38}$$

$$\hat{f}_2(\theta) = \mathbf{a}_2^H(\theta)\ \hat{\mathbf{E}}_{n_2}\ \hat{\mathbf{E}}_{n_2}^H\ \mathbf{a}_2(\theta)\ = \left\|\hat{\mathbf{E}}_{n_2}^H\ \mathbf{a}_2(\theta)\right\|^2 \tag{2.39}$$

The pseudo spectrum of Equation (2.38) and Equation (2.39) can also be expressed as

$$\hat{f}_1(\theta) = \frac{1}{\mathbf{a}_1^H(\theta)\,\hat{\mathbf{E}}_{n_1}\,\hat{\mathbf{E}}_{n_1}^H\,\mathbf{a}_1(\theta)} = \frac{1}{\|\hat{\mathbf{E}}_{n_1}^H\,\mathbf{a}_1(\theta)\|^2} \tag{2.40}$$

$$\hat{f}_2(\theta) = \frac{1}{\mathbf{a}_2^H(\theta)\,\hat{\mathbf{E}}_{n_2}\,\hat{\mathbf{E}}_{n_2}^H\,\mathbf{a}_2(\theta)} = \frac{1}{\|\hat{\mathbf{E}}_{n_2}^H\,\mathbf{a}_2(\theta)\|^2} \tag{2.41}$$

The MUSIC spectrum of subarray 1 $\hat{f}_1(\theta)$ exhibits peaks at true DOAs $(\hat{\theta}_m)$ and ambiguous angles $(\hat{\theta}_m^{amb})$ are taken into consideration as the candidate angles $(\hat{\theta}_{1,m}^{cand})$. As a result, the following relationship exists between $\hat{\theta}_m$ and $\hat{\theta}_{1,m}^{cand}$ and it is given by

$$sin(\hat{\theta}_m) - sin(\hat{\theta}_{1,m}^{cand}) = \frac{2J_{N_1}}{N_2} \tag{2.42}$$

where J_{N_1} is an integer. $\hat{\theta}_{1,m}^{cand}$ corresponds to true DOA at $J_{N_1} = 0$ and for $J_{N_1} = -(N_2 - 1), .., -1, 1, \ldots, (N_2 - 1)$, $\hat{\theta}_{1,m}^{cand}$ corresponds to ambiguous angles. Similarly, the MUSIC spectrum of subarray 2 has the following relationship

$$sin(\hat{\theta}_m) - sin(\hat{\theta}_{2,m}^{cand}) = \frac{2J_{N_2}}{N_1} \tag{2.43}$$

where J_{N_2} is an integer. $\hat{\theta}_{2,m}^{cand}$ corresponds to true DOA at $J_{N_2} = 0$ and for $J_{N_2} = -(N_1 - 1), .., -1, 1, \ldots, (N_1 - 1), \hat{\theta}_{2,m}^{cand}$ corresponds to ambiguous angles. By using Equation (2.42) and Equation (2.43), the relationship between the two spectra can be obtained and it is expressed as

$$sin(\hat{\theta}_{2,m}^{cand}) - sin(\hat{\theta}_{1,m}^{cand}) = 2\left(\frac{J_{N_1}}{N_2} - \frac{J_{N_2}}{N_1}\right) \tag{2.44}$$

As a result, the uniqueness of DOA estimation is given by $\hat{\theta}_{1,m}^{cand} = \hat{\theta}_{2,m}^{cand} = \hat{\theta}_m$ exist for $J_{N_1} = J_{N_2} = 0$. For $J_{N_1} \neq 0$ and $J_{N_2} \neq 0$, the two spectrum exhibit $\hat{\theta}_{1,m}^{cand} \neq \hat{\theta}_{2,m}^{cand}$ under N_1 and N_2 are co-prime integers referred to as co-prime property (Zhou *et al.*2013). Hence, the common angle pairs in the two spectra are considered to be the true DOAs $\hat{\theta}_m$. A partial spectral search method (Sun *et al.*2015) and polynomial rooting-based methods (Zhang *et al.* 2017; Liu *et al.* 2018; Yan *et al.* 2018) have been proposed for a reduction in the computational complexity seen in the (Zhou *et al.* 2013) method. The DOF achieves by N element GCLA in subarray domain processing is $min(N_1, N_2) - 1$ (Zheng *et al.* 2018).

2.4 UNFOLDED CO-PRIME LINEAR ARRAY

Figure 2.5 shows the UCLA design with N sensor elements consisting of cascading of two subarrays with one element as common (Zheng *et al.* 2018). Here, subarray 2 is cascaded with subarray 1. As a result, the total number of sensor elements in UCLA is $N = N_1 + N_2 - 1$. The inter-element spacing of each subarray is defined as $d_1 = N_2\frac{\lambda}{2}$ and $d_2 = N_1\frac{\lambda}{2}$ respectively, where λ is the wavelength of the source signal.

The effective array aperture obtained by UCLA is given by $((N_2 - 1)N_1 + (N_1 - 1)N_2 + 1)d$. For example, consider a $12-$element UCLA ($N = 12$ i. e., $N_1 = 7$ and $N_2 = 6$) with its inter-element spacing $d_1 = 6\frac{\lambda}{2}$ and $d_2 = 7\frac{\lambda}{2}$ respectively. The sensor position of subarray 2 is $\mathbb{S}_2 = \{0,7,14,21,28,35\}$ and subarray 1 is $\mathbb{S}_1 = \{35,41,47,53,59,65,71\}$. Thus, the sensor position of UCLA is given by $\mathbb{S}_1 \cup \mathbb{S}_2 = \{0,7,14,21,28,35,41,47,53,59,65,71\}$.

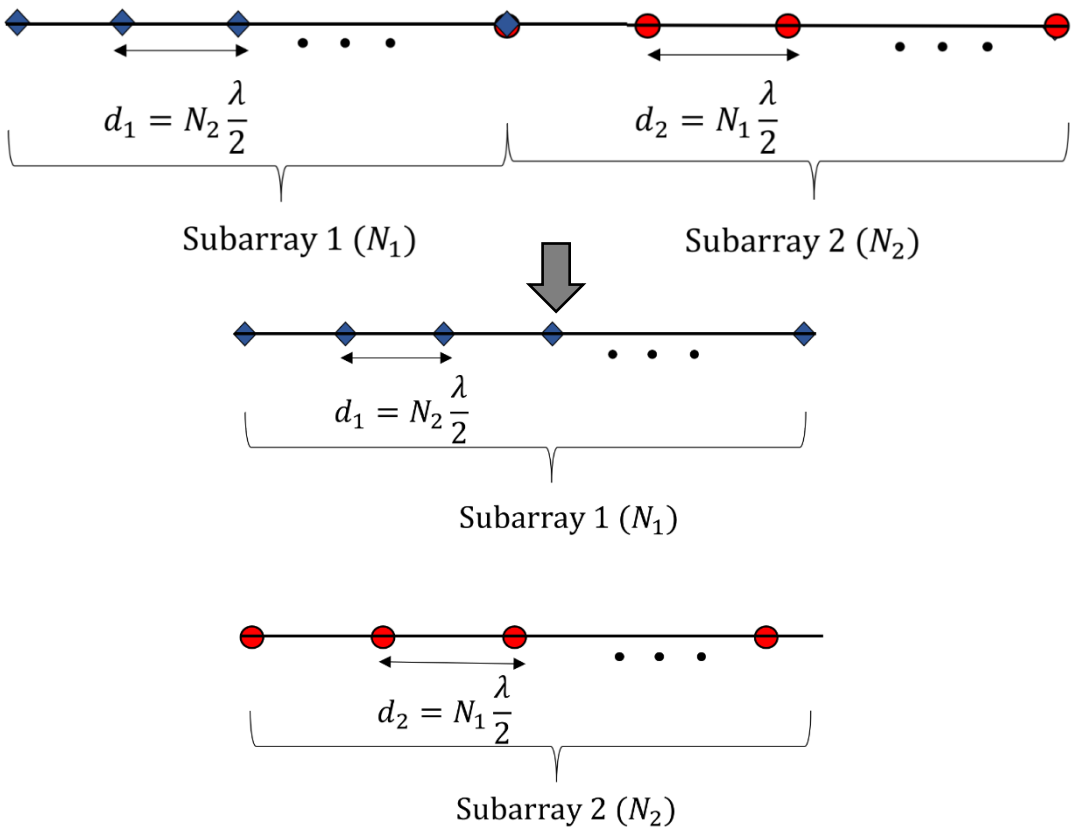

Figure 2.5 Design of UCLA

The first three weights of UCLA are $\mathrm{w}(1) = \mathrm{w}(2) = \mathrm{w}(3) = 0$ indicating no sensor pairs in an array having d, $2d$, and $3d$ inter-element spacing respectively. The $12-$element UCLA can obtain $72d$ as an effective array aperture. It clearly shows the UCLA design has significant mitigation of mutual coupling effects and yields good sparsity (enhanced array aperture) compared to the GCLA design.

2.4.1 Received Signal Model of UCLA

Consider, M $(M < N)$ far-field source signals from directions $\Theta = \{\theta_m\}_{m=1}^{M}$ impinging on N element UCLA with the field-of-view (FOV)

such that $\theta_m \epsilon (-90^o, +90^o)$ as shown in Figure 2.6. Then, the observed array output received signal vector $\mathbf{x}_{UCLA}(t) \epsilon \mathbb{C}^{N \times 1}$ of UCLA is given by

$$\mathbf{x}_{UCLA}(t) = \mathbf{A}_{UCLA}\,\mathbf{s}(t) + \mathbf{n}(t) \tag{2.45}$$

where $\mathbf{A}_{UCLA} = [\mathbf{a}(\theta_1)\ \mathbf{a}(\theta_2) \ldots \mathbf{a}(\theta_M)] \epsilon \mathbb{C}^{N \times M}$ represents the array directional matrix and $\mathbf{a}(\theta_m) = [\mathbf{a}_1^T(\theta_m)\ \mathbf{a}_2^T(\theta_m)]^T \epsilon \mathbb{C}^{N \times 1}$ represents the array directional vector of UCLA. The directional vector of $\mathbf{a}_1(\theta_m)$ and $\mathbf{a}_2(\theta_m)$ in UCLA can be expressed as

$$\mathbf{a}_1(\theta_m) = \left[1,\ e^{-j\pi N_2 \sin(\theta_m)}, \ldots,\ e^{-j\pi N_2 (N_1-1) \sin(\theta_m)}\right]^T \tag{2.46}$$

$$\mathbf{a}_2(\theta_m) = \left[e^{-j\pi (N_2(N_1-1)+N_1) \sin(\theta_m)}, \ldots,\ e^{-j\pi (N_2(N_1-1)+N_1(N_2-1)) \sin(\theta_m)}\right]^T \tag{2.47}$$

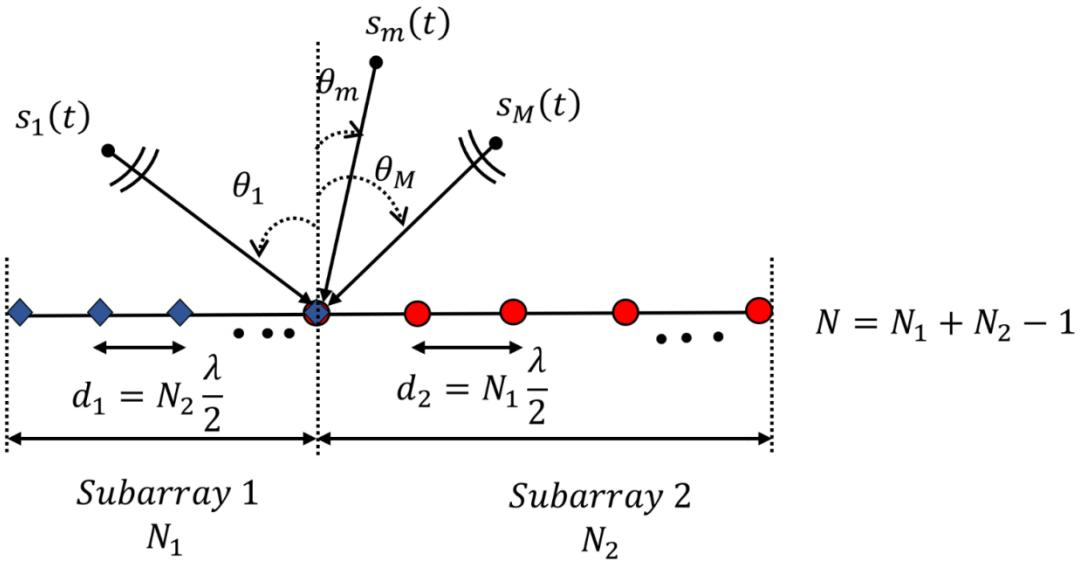

Figure 2.6 System model of UCLA

As a result, $\mathbf{a}(\theta_m) \epsilon \mathbb{C}^{N \times 1}$ of UCLA can be written as

$$\mathbf{a}(\theta_m) = [1,\ e^{-j\pi N_2 \sin(\theta_m)}, \ldots,\ e^{-j\pi N_2 (N_1-1) \sin(\theta_m)}, e^{-j\pi (N_2(N_1-1)+N_1) \sin(\theta_m)},$$

$$\ldots, e^{-j\pi (N_2(N_1-1)+N_1(N_2-1)) \sin(\theta_m)}]^T \tag{2.48}$$

$\mathbf{s}(t) = [s_1(t)\ s_2(t) \ldots\ s_M(t)]^T \in \mathbb{C}^{M\,x\,1}$ represents the vector of emitter signal amplitudes and $\mathbf{n}(t) = [n_0(t)\ n_1(t) \ldots n_{N-1}(t)\ ]^T \in \mathbb{C}^{N\,x\,1}$ represents the zero-mean additive white noise with covariance $E\{\mathbf{n}(t)\mathbf{n}^{\boldsymbol{H}}(t)\} = \sigma_{\mathbf{n}}^{\mathbf{2}}\mathbf{I}_N$, where $\sigma_{\mathbf{n}}^{\mathbf{2}}$ is the noise power and $\mathbf{I}_N$ denotes the $N\,x\,N$ identity matrix (Zheng *et al.* 2018). The observed array output received signal vector $\mathbf{x}_{UCLA}(t) \in \mathbb{C}^{Nx\,1}$ of UCLA can be expressed as follows

$$\mathbf{x}_{UCLA}(t) =$$

$$\begin{bmatrix} 1 & 1 & & 1 \\ e^{-j\pi N_2 \sin(\theta_1)} & e^{-j\pi N_2 \sin(\theta_m)} & & e^{-j\pi N_2 \sin(\theta_M)} \\ \vdots & \vdots & & \vdots \\ e^{-j\pi N_2(N_1-1)\sin(\theta_1)} & e^{-j\pi N_2(N_1-1)\sin(\theta_m)} & \cdots & e^{-j\pi N_2(N_1-1)\sin(\theta_M)} \\ e^{-j\pi(N_2(N_1-1)+N_1)\sin(\theta_1)} & e^{-j\pi(N_2(N_1-1)+N_1)\sin(\theta_m)} & & e^{-j\pi(N_2(N_1-1)+N_1)\sin(\theta_M)} \\ \vdots & \vdots & & \vdots \\ e^{-j\pi(N_2(N_1-1)+N_1(N_2-1))\sin(\theta_1)} & e^{-j\pi(N_2(N_1-1)+N_1(N_2-1))\sin(\theta_m)} & & e^{-j\pi(N_2(N_1-1)+N_1(N_2-1))\sin(\theta_M)} \end{bmatrix}$$

$$\begin{bmatrix} s_1(t) \\ s_2(t) \\ \vdots \\ s_M(t) \end{bmatrix} + \begin{bmatrix} n_0(t) \\ n_1(t) \\ \vdots \\ n_{N-1}(t) \end{bmatrix} \qquad (2.49)$$

2.4.2 DOA Estimation with UCLA

UCLA is considered as a single array design, and so the covariance $\mathbf{R}_{\mathbf{x}} \in \mathbb{C}^{Nx\,N}$ of the received signal $\mathbf{x}_{UCLA}(t) \in \mathbb{C}^{Nx\,1}$ is directly obtained instead from two subarrays separately and it is given by

$$\mathbf{R}_{\mathbf{x}} = E\{\mathbf{x}_{UCLA}(t)\,\mathbf{x}_{UCLA}^{H}(t)\}$$

$$= \mathbf{A}_{UCLA}\,\mathbf{R}_{\mathbf{s}}\,\mathbf{A}_{UCLA}^{H} + \sigma_{\mathbf{n}}^{\mathbf{2}}\mathbf{I}_N \qquad (2.50)$$

where $\mathbf{R}_{\mathbf{s}} = \boldsymbol{E}\{\mathbf{s}\mathbf{s}^{H}\}$ denotes the source covariance matrix, $\sigma_{\mathbf{n}}^{\mathbf{2}}$ is the noise power and $\mathbf{I}_N$ denotes the $N\,x\,N$ identity matrix. In practice, the actual

covariance matrix $\mathbf{R_x}$ is unknown, therefore its sample estimate $\widehat{\mathbf{R}}_\mathbf{x}$ is computed for K snapshots and it is given by

$$\widehat{\mathbf{R}}_\mathbf{x} = \frac{1}{K}\sum_{t=1}^{K} \mathbf{x}_{UCLA}(t)\, \mathbf{x}_{UCLA}^{H}(t) = \begin{bmatrix} \widehat{\mathbf{R}}_1 & \widehat{\mathbf{R}}_2 \\ \widehat{\mathbf{R}}_3 & \widehat{\mathbf{R}}_4 \end{bmatrix} \tag{2.51}$$

Here, the array covariance $\widehat{\mathbf{R}}_\mathbf{x}$ inherently contains the self and mutual information relating to two subarrays due to the utilization of the entire array. It can be seen via the block matrices such as $\widehat{\mathbf{R}}_1$, $\widehat{\mathbf{R}}_4$ as the array auto-covariance and $\widehat{\mathbf{R}}_2$, $\widehat{\mathbf{R}}_3$ as the array cross-covariance of two subarrays in $\widehat{\mathbf{R}}_\mathbf{x}$ of Equation (2.51) (Zheng *et al.* 2018). The eigenvalue decomposition (EVD) of $\widehat{\mathbf{R}}_\mathbf{x}$ yields

$$\widehat{\mathbf{R}}_\mathbf{x} = \hat{\mathbf{E}}_s\, \hat{\mathbf{D}}_s \hat{\mathbf{E}}_s^H + \hat{\mathbf{E}}_n\, \hat{\mathbf{D}}_n\, \hat{\mathbf{E}}_n^H \tag{2.52}$$

where $\hat{\mathbf{E}}_s \triangleq [\mathbf{e}_1, \mathbf{e}_2, \ldots, \mathbf{e}_M] \in \mathbb{C}^{N \times M}$ and $\hat{\mathbf{E}}_n \triangleq [\mathbf{e}_{M+1}, \mathbf{e}_{M+2}, \ldots, \mathbf{e}_N]\, \mathbb{C}^{N \times N-M}$ contains the signal- and noise-subspace eigenvectors of $\widehat{\mathbf{R}}_\mathbf{x}$ corresponding to the eigenvalues in the diagonal matrix $\hat{\mathbf{D}}_s \triangleq \text{diag}\{\lambda_1, \lambda_2, \ldots, \lambda_M\}$ and $\hat{\mathbf{D}}_n \triangleq \text{diag}\{\lambda_{M+1}, \lambda_{M+2}, \ldots, \lambda_N\}$. Furthermore, the signal subspace and directional vector of the source signals span the same space and are orthogonal to the noise subspace. As a result, the directional vector can be used in the search for all possible angles across the noise subspace to determine the DOA of transmitted source signals, and the UCLA-MUSIC pseudo spectrum is given by

$$\hat{f}_{UCLA-MUSIC}(\theta) = \frac{1}{\mathbf{a}^H(\theta)\, \hat{\mathbf{E}}_n\, \hat{\mathbf{E}}_n^H\, \mathbf{a}(\theta)} = \frac{1}{\| \hat{\mathbf{E}}_n^H\, \mathbf{a}(\theta) \|^2} \tag{2.53}$$

Thus, the angles (θ) correspond with the highest peaks of $\hat{f}_{UCLA-MUSIC}(\theta)$ are the DOA of the transmitted source signals. He *et al.* (2018) have proposed a polynomial rooting approach called UCLA-Root

MUSIC for the improvement of the resolution and avoidance of the spectral searching process involved in UCLA-MUSIC (Zheng *et al.* 2018). The DOF achieved by N element UCLA using UCLA-MUSIC (Zheng *et al.* 2018) and UCLA-Root MUSIC (He *et al.* 2020) is $N_1 + N_2 - 1$.

2.5 AMBIGUITY IN DOA ESTIMATION WITH GCLA AND UCLA

This section deals with the ambiguity issues such as pair-matching and grating-angle in DOA estimation associated with GCLA and UCLA.

2.5.1 Pair-Matching Ambiguity

In the subarray-based DOA estimation with GCLA, the common angle pairs in the MUSIC spectra of two subarrays are regarded as the true DOAs $\hat{\theta}_m$ based on the co-prime property. However, the uniqueness of DOA estimation given in section 2.3.2 is not always true in the case of multiple incoming source signals (Xiao *et al.*2019). Let us consider, that two signals impinge on GCLA from different directions θ_1 and θ_2 i.e., $\theta_1 \neq \theta_2$. The MUSIC spectrum of subarray 1 exhibits two ambiguous angles $\hat{\theta}_{1,1}^{amb}$ and $\hat{\theta}_{1,2}^{amb}$ associated to θ_1 and θ_2 respectively by having the following relationship

$$sin(\hat{\theta}_1) - sin(\hat{\theta}_{1,1}^{amb}) = \frac{2J_{N_{1,1}}}{N_2} \tag{2.54}$$

$$sin(\hat{\theta}_2) - sin(\hat{\theta}_{1,2}^{amb}) = \frac{2J_{N_{1,2}}}{N_2} \tag{2.55}$$

where $J_{N_{1,1}}$ and $J_{N_{1,2}}$ are integers in the range $-(N_2 - 1)$ to $(N_2 - 1)$ i.e., $-(N_2 - 1), .., -1, 1, \ldots, (N_2 - 1)$. Similarly, the MUSIC spectrum of subarray 2 exhibits two ambiguous angles $\hat{\theta}_{2,1}^{amb}$ and $\hat{\theta}_{2,2}^{amb}$ associated to θ_1 and θ_2 respectively by having the following relationship

$$sin(\hat{\theta}_1) - sin(\hat{\theta}_{2,1}^{amb}) = \frac{2J_{N_{2,1}}}{N_1} \tag{2.56}$$

$$sin(\hat{\theta}_2) - sin(\hat{\theta}_{2,2}^{amb}) = \frac{2J_{N_{2,2}}}{N_1} \tag{2.57}$$

where $J_{N_{2,1}}$ and $J_{N_{2,2}}$ are integers in the range $-(N_1 - 1)$ to $(N_1 - 1)$ i. e.,$-(N_1 - 1), .., -1, 1, \ldots, (N_1 - 1)$. Thus, the relationship between the two spectra that can be obtained based on Equation (2.42) and Equation (2.43) respectively is expressed as follows

$$\sin(\hat{\theta}_1) - \sin(\hat{\theta}_2) = 2\left(\frac{J_{N_{2,1}}}{N_1} - \frac{J_{N_{1,2}}}{N_2}\right) \tag{2.58}$$

$$\sin(\hat{\theta}_1) - \sin(\hat{\theta}_2) = 2\left(\frac{J_{N_{1,1}}}{N_2} - \frac{J_{N_{2,2}}}{N_1}\right) \tag{2.59}$$

By Subtracting the Equations (2.56),(2.55),(2.58) and Equations (2.57),(2.54),(2.59) respectively results as follow

$$\sin(\hat{\theta}_{1,2}^{amb}) = \sin(\hat{\theta}_{2,1}^{amb}) \tag{2.60}$$

$$\sin(\hat{\theta}_{1,1}^{amb}) = \sin(\hat{\theta}_{2,2}^{amb}) \tag{2.61}$$

Thus, the MUSIC spectrum of subarray 1 and subarray 2 exhibits common angle pairs (overlapped peaks) at the ambiguous angles in addition to the true DOA angles are referred to be pair-matching errors. As a result, it leads to the ambiguous estimate of true DOAs referred to as pair-matching ambiguity in DOA estimation with GCLA (Xiao *et al.*2019).

For example, consider two source signals ($M = 2$) from the direction $\theta_1 = 10.00^{\circ}$ and $\theta_2 = 39.11^{\circ}$ impinges on GCLA with $N = 11$ elements $(N_1 = 5, N_2 = 7)$ under signal-to-noise ratio (SNR) of 10 dB and a snapshot of $K = 200$. The method proposed in (Zhou *et al.*2013)

exhibits overlapped peaks for a set of angles that includes true DOAs such as $\hat{\theta}_1 = 10.00^{\circ}$ and $\hat{\theta}_2 = 39.11^{\circ}$ as well as ambiguous angles such as $\hat{\theta}_3^{amb} = -13.09^{\circ}$ and $\hat{\theta}_4^{amb} - 75.75^{\circ}$ as shown in Figure 2.7. Similarly, the partial spectral search-based method (Sun *et al.*2015) also suffered from this ambiguity problem. Furthermore, the polynomial rooting-based methods (Zhang *et al.* 2017; Liu *et al.* 2018; Yan *et al.* 2018) result in more than $M = 2$ common roots i.e., 4 roots (closer to unit magnitude) related to $\hat{\theta}_1 = 10.00^{\circ}, \hat{\theta}_2 = 39.11^{\circ}, \hat{\theta}_3^{amb} = -13.09^{\circ}$ and $\hat{\theta}_4^{amb} - 75.75^{\circ}$ leading to an ambiguous estimate of true DOAs which can be seen in Table A1.1 of Appendix 1. Persistence of pair-matching ambiguity is seen for at least any two direction angles of the set $\{10.00^{\circ}, 39.11^{\circ}, -13.09^{\circ}, -75.75^{\circ}\}$ (Xiao *et al.*2019).

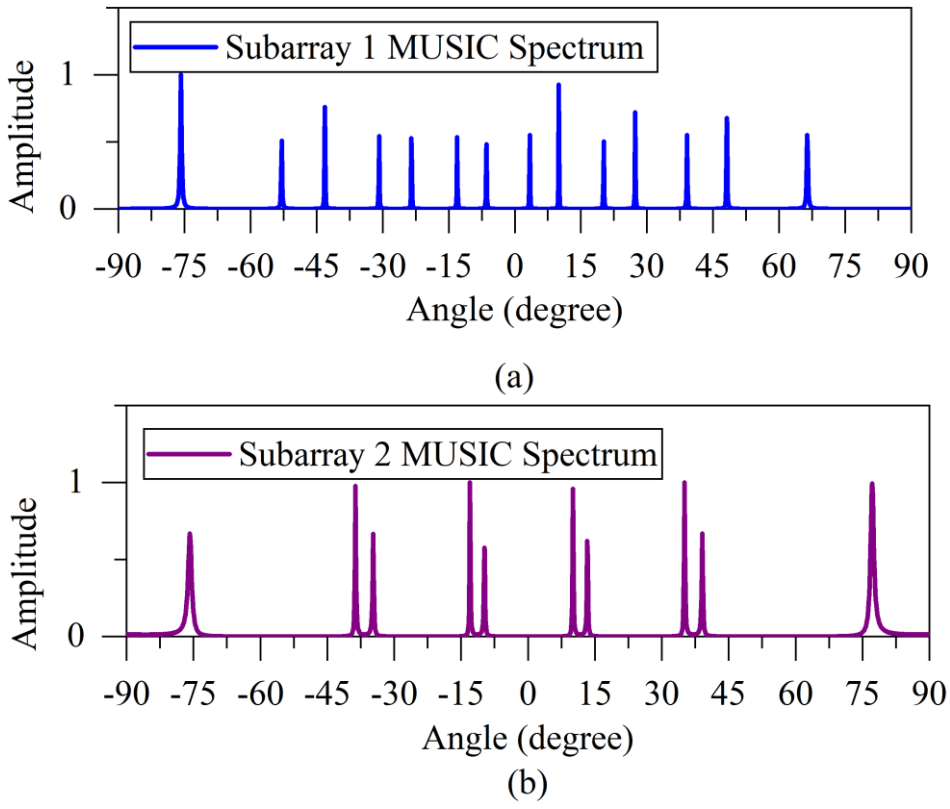

Figure 2.7 (Continued)

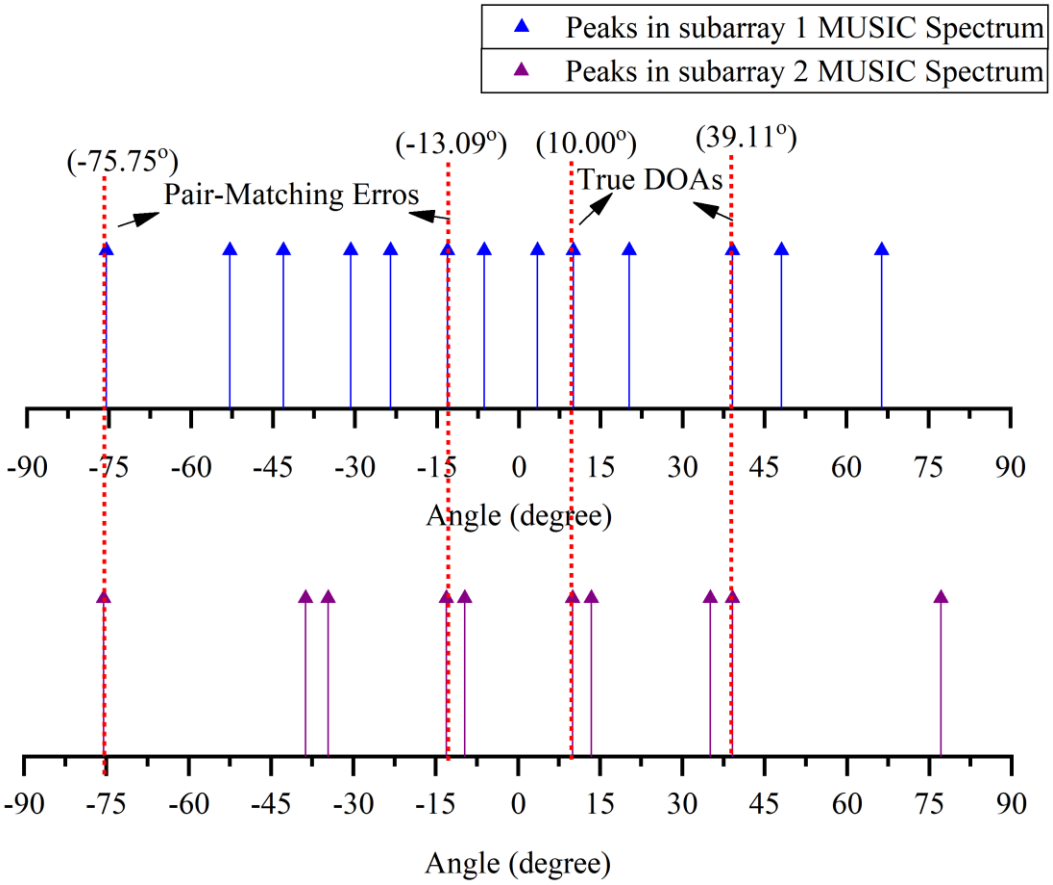

(c)

Figure 2.7 The problem of pair-matching ambiguity in GCLA: (a) Subarray 1 MUSIC Spectrum (b) Subarray 2 MUSIC Spectrum (c) Pair-matching error diagram

The problem of pair-matching ambiguity in DOA estimation with GCLA is resolved through the use of adjoined subarray (AdS) based method. The method (Zheng *et al.* 2018) stacks the signal received from two subarrays together and applies the MUSIC estimator. The received array output signal vector of subarray 1 $\mathbf{x}_1(t)$ and subarray 2 $\mathbf{x}_2(t)$ of GCLA are stacked. This can be expressed as

$$\begin{bmatrix} \mathbf{x}_1(t) \\ \mathbf{x}_2(t) \end{bmatrix} = \begin{bmatrix} 1 & 1 & & 1 \\ e^{-j\pi N_2 sin(\theta_1)} & e^{-j\pi N_2 sin(\theta_m)} & & e^{-j\pi N_2 sin(\theta_M)} \\ \vdots & \vdots & & \vdots \\ e^{-j\pi N_2 (N_1-1) sin(\theta_1)} & e^{-j\pi N_2 (N_1-1) \sin(\theta_m)} & \cdots & e^{-j\pi N_2 (N_1-1) sin(\theta_M)} \\ 1 & 1 & & 1 \\ e^{-jN_1 \pi sin(\theta_1)} & e^{-jN_1 \pi sin(\theta_2)} & & e^{-jN_1 \pi sin(\theta_M)} \\ \vdots & \vdots & & \vdots \\ e^{-jN_1 (N_2-1)\pi sin(\theta_1)} & e^{-jN_1 (N_2-1)\pi sin(\theta_2)} & & e^{-jN_1 (N_2-1)\pi sin(\theta_M)} \end{bmatrix} \begin{bmatrix} s_1(t) \\ s_2(t) \\ \vdots \\ s_M(t) \end{bmatrix} + \begin{bmatrix} n_{1,0}(t) \\ n_{1,1}(t) \\ \vdots \\ n_{1,N_1-1}(t) \\ n_{2,0}(t) \\ n_{2,1}(t) \\ \vdots \\ n_{2,N_2-1}(t) \end{bmatrix} \quad (2.62)$$

$$\mathbf{x}(t) = \begin{bmatrix} \mathbf{x}_1(t) \\ \mathbf{x}_2(t) \end{bmatrix} = \begin{bmatrix} \mathbf{A}_1 \\ \mathbf{A}_2 \end{bmatrix} \mathbf{s}(t) + \begin{bmatrix} \mathbf{n}_1(t) \\ \mathbf{n}_2(t) \end{bmatrix}$$

$$= \mathbf{A}\,\mathbf{s}(t) + \mathbf{n}(t) \quad (2.63)$$

where $\mathbf{A} = \begin{bmatrix} \mathbf{A}_1 \\ \mathbf{A}_2 \end{bmatrix} = [\mathbf{A}_1^T\ \mathbf{A}_2^T\ ]^T = [\mathbf{a}(\theta_1)\ \mathbf{a}(\theta_2) \ldots \mathbf{a}(\theta_M)] \in \mathbb{C}^{(N_1+N_2)\ x\ M}$ is the array directional matrix. Here, $\mathbf{a}(\theta_m)$ is the array directional vector and it can be written as $\mathbf{a}(\theta_m) = [\mathbf{a}_1{}^T(\theta_m)\ \ \mathbf{a}_2{}^T(\theta_m)\ ]^T \in \mathbb{C}^{(N_1+N_2)\ x\ 1}$, $\mathbf{s}(t)$ and $\mathbf{n}(t) = [\mathbf{n}_1{}^T(t)\ \ \mathbf{n}_2{}^T(t)\ ]^T \in \mathbb{C}^{(N_1+N_2)\ x\ 1}$ represents the source signal vector and noise vector respectively.

In adjoined subarray (AdS) based DOA estimation method (Zheng *et al.*2018), the estimated covariance $\widehat{\mathbf{R}}_{\mathbf{x}} \in \mathbb{C}^{(N_1+N_2)\ x\ (N_1+N_2)}$ of the array output signal vector $\mathbf{x}(t) \in \mathbb{C}^{\ (N_1+N_2)\ x\ 1}$ with K snapshots can be given as

$$\widehat{\mathbf{R}}_{\mathbf{x}} = \frac{1}{K}\sum_{t=1}^{K} \mathbf{x}(t)\,\mathbf{x}^H(t)\ = \begin{bmatrix} \widehat{\mathbf{R}}_1 & \widehat{\mathbf{R}}_2 \\ \widehat{\mathbf{R}}_3 & \widehat{\mathbf{R}}_4 \end{bmatrix} \quad (2.64)$$

Utilization of the two subarrays together through the stacking of its received array output signal vector helps the array covariance $\widehat{\mathbf{R}}_{\mathbf{x}}$ containing the self and mutual information of two subarrays. It can be seen via block matrices such as $\widehat{\mathbf{R}}_1$, $\widehat{\mathbf{R}}_4$ as the array auto-covariance and $\widehat{\mathbf{R}}_2$, $\widehat{\mathbf{R}}_3$ as the array cross-covariance of two subarrays respectively. The adjoined subarray (AdS) based method has been utilizing the self and mutual information whereas the subarray-based method utilizes only the self-information of two subarrays. The eigenvalue decomposition (EVD) of $\widehat{\mathbf{R}}_{\mathbf{x}}$ yields

$$\widehat{\mathbf{R}}_{\mathbf{x}} = \widehat{\mathbf{E}}_s \, \widehat{\mathbf{D}}_s \widehat{\mathbf{E}}_s^H \; + \widehat{\mathbf{E}}_n \, \widehat{\mathbf{D}}_n \, \widehat{\mathbf{E}}_n^H \tag{2.65}$$

where $\widehat{\mathbf{E}}_s \triangleq [\mathbf{e}_1, \mathbf{e}_2, \ldots, \mathbf{e}_M] \in \mathbb{C}^{(N_1+N_2)\mathrm{x}\, M}$ and $\widehat{\mathbf{E}}_n \triangleq \left[\mathbf{e}_{M+1}, \mathbf{e}_{M+2}, \ldots, \mathbf{e}_{(N_1+N_2)}\right] \mathbb{C}^{(N_1+N_2)\,\mathrm{x}\,((N_1+N_2)-M)}$ contains the signal- and noise-subspace eigenvectors of $\widehat{\mathbf{R}}_{\mathbf{x}}$ corresponding to the eigenvalues in the diagonal matrix $\widehat{\mathbf{D}}_s \triangleq \mathrm{diag}\{\lambda_1, \lambda_2, \ldots, \lambda_M\}$ and $\widehat{\mathbf{D}}_n \triangleq \mathrm{diag}\{\lambda_{M+1}, \lambda_{M+2}, \ldots, \lambda_{(N_1+N_2)}\}$. Furthermore, the signal subspace and directional vector of the source signals span the same space and are orthogonal to the noise subspace. As a result, the directional vector can be used in the search for all possible angles across the noise subspace to determine the DOA of the transmitted source signals, and the adjoined subarray (AdS) MUSIC pseudo spectrum is given by

$$\hat{f}_{AdS-MUSIC}(\theta) = \frac{1}{[\mathbf{a}_1(\theta)\ \mathbf{a}_2(\theta)]\, \widehat{\mathbf{E}}_n \widehat{\mathbf{E}}_n^H \left[\mathbf{a}_1{}^T(\theta)\ \mathbf{a}_2{}^T(\theta)\right]^T} \tag{2.66}$$

Thus, the angles (θ) corresponds with the highest peaks of $\hat{f}_{AdS-MUSIC}(\theta)$ are the DOA of the transmitted source signals. In (He *et al.* 2020), a polynomial rooting extension of adjoined subarray (AdS) MUSIC is proposed to improve resolution with reduced computational complexity. The estimation results with the associated observations on the existence of ambiguity, DOF and complexity of the above-aforementioned

methods such as subarray-based methods (Zhou *et al.*2013; Sun *et al.*2015; Zhang *et al.* 2017; Liu *et al.* 2018; Yan *et al.* 2018) and adjoined subarray-based methods (Zheng *et al.*2018; He *et al.*2020) in the case of pair-matching ambiguity for GCLA are summarized in Table A1.1 of Appendix 1.

2.5.2 Grating-Angle Ambiguity

DOA estimation performance has a significant influence from the array directional vector $\mathbf{a}(\theta_m)$, which contains information about the DOA parameter θ_m (Tuncer *et al.* 2009). Generally, the unique solution of the DOA estimation is assured if the mapping of the DOA parameter $\theta_m \in \mathbb{R}^1$ to array directional vector $\mathbf{a}(\theta_m) \in \mathbb{C}^N$ is one-to-one by having array directional matrix $\mathbf{A}$ as full rank i.e., $rank(\mathbf{A}) = M$ (Manikas 2004). Due to the large inter-element spacing of each subarray in GCLA and UCLA, the one-to-one mapping is not assured and arises a problem of ambiguity in estimating the true DOAs.

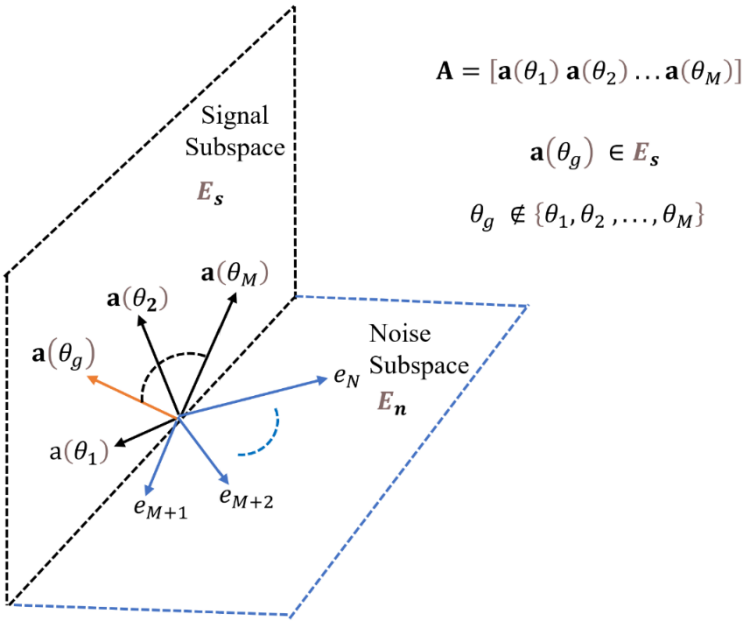

Figure 2.8 Geometric view of grating-angle ambiguity

Specifically, both GCLA and UCLA suffer from a type of array ambiguity known as grating-angle ambiguity, also known as directional matrix ambiguity or non-trivial ambiguity (Liu *et al.*2013). It occurs when the directional vector $\mathbf{a}_1(\theta_m)$ and $\mathbf{a}_2(\theta_m)$ of both the subarrays are identical for different direction angles and resulting in columns of $\mathbf{A}$ that are linearly dependent i.e., $rank(\mathbf{A}) < M$. For instance, consider $\theta_g \notin \Theta$; $\forall\Theta = \{\theta_m\}_{m=1}^{M}$, the array directional vector of θ_g belongs to the signal subspace spanned by the columns of $\mathbf{A}$ such that $\mathbf{a}(\theta_g) \in \mathcal{L}[\mathbf{A}]$ where θ_g is the grating (ambiguous) angle as shown in Figure 2.8. It happens due to the linear dependence of array directional vector $\mathbf{a}(\theta_g)$ on the array directional vectors of $\mathbf{A}$ and it is expressed as

$$\mathbf{a}(\theta_g) = \sum_{m=1}^{M} \propto_m \mathbf{a}(\theta_m) = \propto_1 \mathbf{a}(\theta_1) + \propto_2 \mathbf{a}(\theta_2) + \cdots . + \propto_M \mathbf{a}(\theta_M) \quad (2.67)$$

Alternatively, Equation (2.67) can be written as

$$\begin{bmatrix}\mathbf{a}_1(\theta_g)\\ \mathbf{a}_2(\theta_g)\end{bmatrix} = \propto_1 \begin{bmatrix}\mathbf{a}_1(\theta_1)\\ \mathbf{a}_2(\theta_1)\end{bmatrix} + \propto_2 \begin{bmatrix}\mathbf{a}_1(\theta_2)\\ \mathbf{a}_2(\theta_2)\end{bmatrix} + \ldots + \propto_M \begin{bmatrix}\mathbf{a}_1(\theta_M)\\ \mathbf{a}_2(\theta_M)\end{bmatrix} \quad (2.68)$$

where $\propto_m$ represents the constant coefficient.

The problem of grating-angle ambiguity is seen with the use of Gram matrix $\mathbf{G}(\theta) \epsilon\, \mathbb{C}^{J \times J}$ (Nannuru *et al.*2017) and it is given by

$$\mathbf{G}(\theta) = \mathbf{a}^H(\theta)\, \mathbf{a}(\theta) \quad (2.69)$$

The Gram matrix is computed for each $\theta \epsilon \left(-90^o, +90^o\right)$ and it is given by $= -90^o + (j-1)\,\Delta\theta \;;\; j = 1, 2, 3, \ldots, J$, where $\Delta\theta$ is the angular separation. For instance, if $\Delta\theta = 1^o$ then $J = 181$, and if $\Delta\theta = 0.1^o$ then $J = 1801$. Using Equation (2.69) with $\Delta\theta = 0.1^o$, $J = 1801$, the Gram

matrix $\mathbf{G}(\theta)$ is computed for ULA having $N_{ULA} = 11$ with the inter-sensor spacing of $d_{ULA} = \frac{\lambda}{2}$, Figure 2.9 shows each angle having one major lobe (no spatial aliasing). Whereas, for UCLA having $N = 11$ i. e., $N_1 = 5$ and $N_2 = 7$ with its inter-element spacing $d_1 = 7\frac{\lambda}{2}$ and $d_2 = 5\frac{\lambda}{2}$ respectively, resulting in one main lobe for each angle and side lobes with substantial strength (spatial aliasing), as depicted in Figure 2.10.

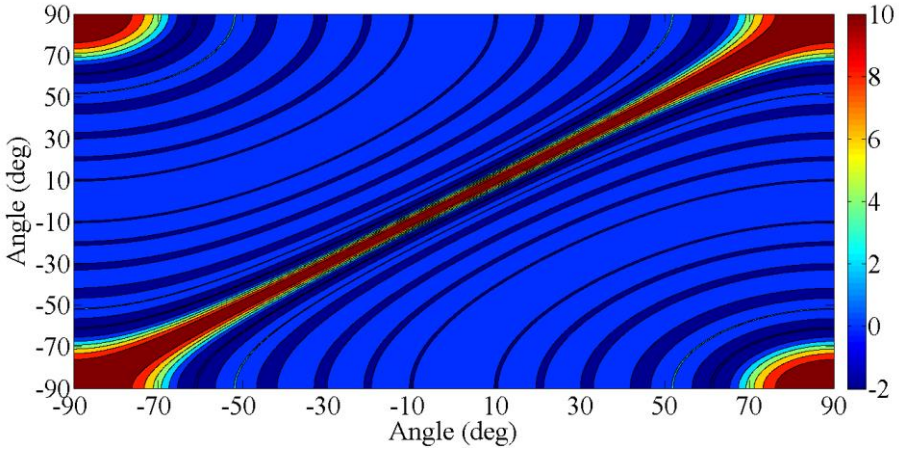

Figure 2.9 Gram matrix of ULA ($N_{ULA} = 11$ with $d_{ULA} = \frac{\lambda}{2}$)

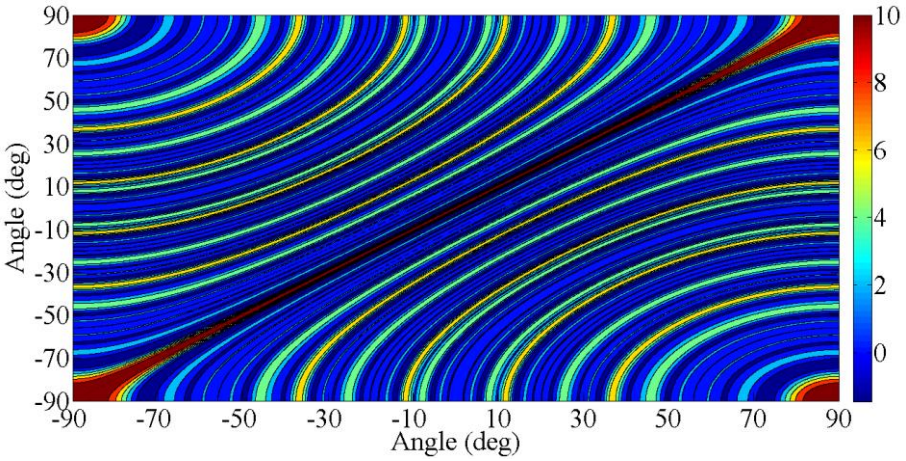

Figure 2.10 Gram matrix of UCLA ($N = 11\ i.e., N_1 = 5$ and $N_2 = 7$ with $d_1 = 7\frac{\lambda}{2}$ and $d_2 = 5\frac{\lambda}{2}$)

The subspace-based method for DOA estimation demands that the signal eigenvectors and directional vectors of the source signals should span

the same subspace. However, UCLA's non-uniform linear array design leads to the existence of a set of direction angles with linearly dependent directional vectors. As a result, directional vectors that are not associated with true DOAs also reside in the signal subspace, resulting in an ambiguous estimate. This is referred to as the grating-angle ambiguity problem (Tan *et. al* 2002).

For instance, consider a UCLA having $N = 11$ i.e., $N_1 = 5$ and $N_2 = 7$ with its inter-element spacing $d_1 = 7\frac{\lambda}{2}$ and $d_2 = 5\frac{\lambda}{2}$ respectively. For this design, the set of direction angles $\{10.00^o, 27.35^o, 35.01^o, 59.25^o\}, \{20.00^o, 38.88^o, 47.90^o, -76.47^o\}$ and $\{12.37^o, 30.00^o, 37.92^o, 64.16^o\}$ that satisfies Equation (2.68) is given by $\mathbf{a}_1(\theta_1) = \mathbf{a}_1(\theta_3)$; $\mathbf{a}_2(\theta_1) = \mathbf{a}_2(\theta_2)$; $\mathbf{a}_1(\theta_4) = \mathbf{a}_1(\theta_2)$ and $\mathbf{a}_2(\theta_4) = \mathbf{a}_2(\theta_3)$ (Xiao *et al.* 2019). As a result, the directional vector of each four angles can be linear dependent on the other three directional vectors and it is given by

$$\begin{bmatrix}\mathbf{a}_1(\theta_4^{amb})\\ \mathbf{a}_2(\theta_4^{amb})\end{bmatrix} = -\begin{bmatrix}\mathbf{a}_1(\theta_1)\\ \mathbf{a}_2(\theta_1)\end{bmatrix} + \begin{bmatrix}\mathbf{a}_1(\theta_2)\\ \mathbf{a}_2(\theta_2)\end{bmatrix} + \begin{bmatrix}\mathbf{a}_1(\theta_3)\\ \mathbf{a}_2(\theta_3)\end{bmatrix} \tag{2.70}$$

Here θ_4^{amb} is the grating (ambiguous) angle (θ_g).

Different examples are considered for the purpose of illustration of the grating-angle ambiguity. Firstly, assume $M = 3$ transmitted source signals impinges on GCLA with $N = 11$ elements $(N_1 = 5, N_2 = 7)$ from the direction $\theta_1 = 12.37^o, \theta_2 = 30.00^o$ and $\theta_3 = 37.92^o$ under signal-to-noise ratio (SNR) of 10 dB and a snapshot of $K = 200$. The method proposed in (Zhou *et al.*2013) exhibits overlapped peaks for a set of angles that includes true DOAs such as $\hat{\theta}_1 = 12.37^o$, $\hat{\theta}_2 = 30.00^o$ and $\hat{\theta}_3 = 37.92^o$ as well as ambiguous angles such as $\hat{\theta}_4^{amb} = 64.16^o$ as shown in Figure 2.11. Similarly, the partial spectral search-based method (Sun *et al.*2015) also suffered from this ambiguity problem. The polynomial rooting-based methods

suggested by (Zhang *et al.* 2017; Liu *et al.* 2018; Yan *et al.* 2018) result in more than $M = 3$ common roots i.e., 4 roots (closer to unit magnitude) related to $\hat{\theta}_1 = 12.37^{o}$, $\hat{\theta}_2 = 30.00^{o}$, $\hat{\theta}_3 = 37.92^{o}$ and $\hat{\theta}_4^{amb} = 64.16^{o}$ leading to an ambiguous estimate of true DOAs and it can be seen in Table A1.2 of Appendix 1.

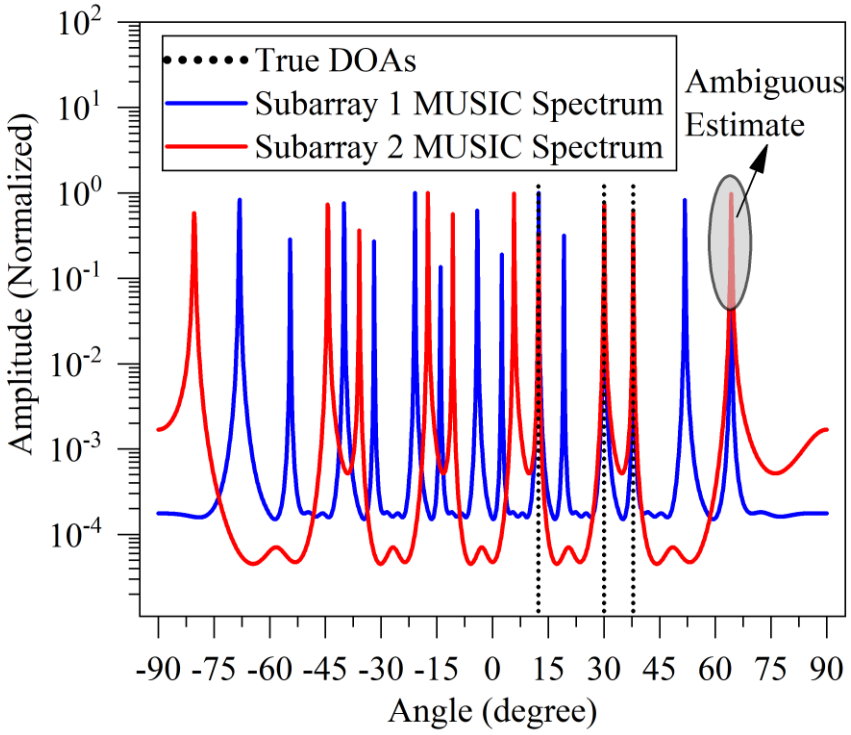

Figure 2.11 The problem of grating-angle ambiguity in GCLA for the case of $M = 3$

Now, assume $M = 3$ transmitted source signals impinges on UCLA with $N = 11$ elements $(N_1 = 5, N_2 = 7)$ from the direction $\theta_1 = 10.00^{o}$, $\theta_2 = 27.35^{o}$ and $\theta_3 = 35.01^{o}$ under signal-to-noise ratio (SNR) of 10 dB and a snapshot of $K = 200$. The UCLA- MUSIC estimator (Zheng *et al.*2018) is expected to exhibit the three highest peaks at the true angle location of the spectrum. However, the issue of grating-angle ambiguity leads to the UCLA-MUSIC estimator in the exhibition of significant peaks at true and ambiguous angle locations i.e., $\theta_{true} = \{10.00^{o}, 27.35^{o}, 35.01^{o}\}$ and $\theta_g = \{59.25^{o}\}$ as shown in

Figure 2.12. Likewise, the method (He *et al.*2020) also exhibits more than three roots that lie inside the unit circle with the largest magnitude i.e., three signal roots related to $\theta_{true} = \{10.00^o, 27.35^o, 35.01^o\}$ and one ambiguous root related to $\theta_g = \{59.25^o\}$ and it can be seen in Table A1.3 of Appendix 1.

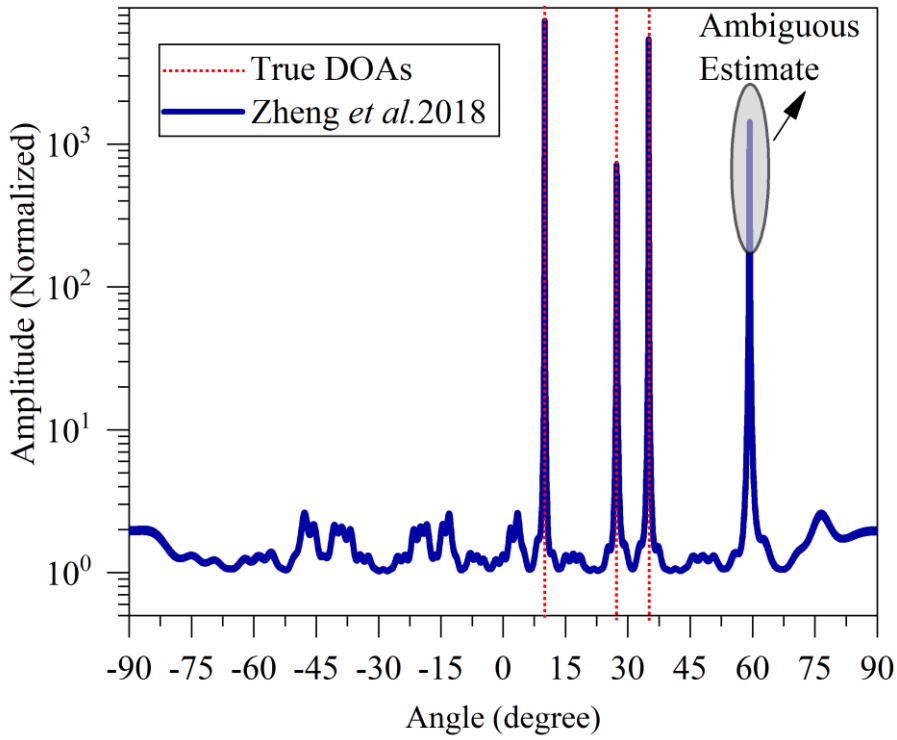

Figure 2.12 The problem of grating-angle ambiguity in UCLA for the case of $M = 3$

Similarly, consider $M = 6$ transmitted source signals from the direction $\theta_1 = 10.00^o, \theta_2 = 27.35^o, \theta_3 = 35.01^o, \theta_4 = 30.00^o, \theta_5 = 12.37^o, \theta_6 = 64.16^o$ with an SNR of 10 dB and a snapshot of $K = 200$. The UCLA-MUSIC estimator (Zheng *et al.*2018) is expected to exhibit the six highest peaks at the true angle location of the spectrum. However, the issue of grating-angle ambiguity leads to the UCLA-MUSIC estimator in the exhibition of significant peaks at true and ambiguous angle locations i.e., $\theta_{true} = \{10.00^o, 27.35^o, 35.01^o, 30.00^o, 12.37^o, 64.16^o\}$and

$\theta_g = \{59.25^o, 37.92^o\}$ as shown in Figure 2.13. Likewise, the method (He *et al.*2020) also exhibits more than six roots that lie inside the unit circle with the largest magnitude i.e., six signal roots related to $\theta_{true} = \{10.00^o, 27.35^o, 35.01^o, 30.00^o, 12.37^o, 64.16^o\}$ and two ambiguous roots related to $\theta_g = \{59.25^o, 37.92^o\}$. In both cases, the method suggested by (Zheng *et al.*2018) shows peaks at ambiguous angle locations as noticeably high compared to the peaks of the true angle locations, resulting in indistinguishability of the ambiguous peaks and leading to the ambiguous estimation of true DOAs. Similarly, the method suggested by (He *et al.*2020) shows the roots related to ambiguous angles as significantly high compared to the roots related to true angles, resulting in the indistinguishability of the ambiguous roots and leading to the ambiguous estimation of true DOAs.

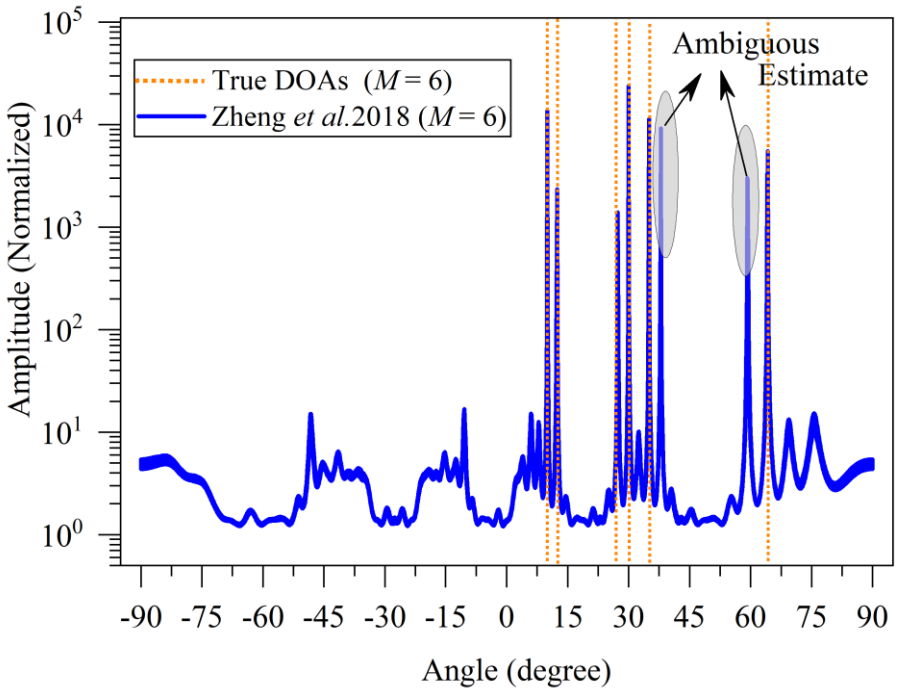

Figure 2.13 The problem of grating-angle ambiguity in UCLA for the case of $M = 6$

The "beamformer-like" approaches proposed by (Yang *et al.*2019; Huang *et al.*2021) help resolution of the grating-angle ambiguity where the Classical Beamforming (CBF) approach is utilized in the identification of the true DOAs and ambiguous angles resulting from the MUSIC method based on the CBF power values. However, it fails to resolve the ambiguity when the DOA of the transmitted signals from multiple sources are closely distributed. It also involves high computational complexity due to the spectral searching process and offers lower estimation performances in terms of reliability, accuracy and angular resolution.

To illustrate this, consider $M = 5$ (closely spaced case) transmitted source signals from directions $\theta_1 = 10.00^o, \theta_2 = 27.35^o, \theta_3 = 35.01^o, \theta_4 = 57^o, \theta_5 = 62^o$ impinges on UCLA with $N = 11$. Figure 2.14 (a) shows that the UCLA-MUSIC spectrum exhibits peaks at the true and ambiguous angle locations i. e., $\theta_{true} = \{10.00^o, 27.35^o, 35.01^o\}$ and $\theta_g = \{59.25^o\}$ under SNR of 10 dB and a snapshot of $K = 200$. Figure 2.14 (b) and Table 2.1 clearly show the CBF power at a grating (ambiguous) angle $\theta_g = 59.25^o$ as substantial in comparison with the CBF power of true DOAs.

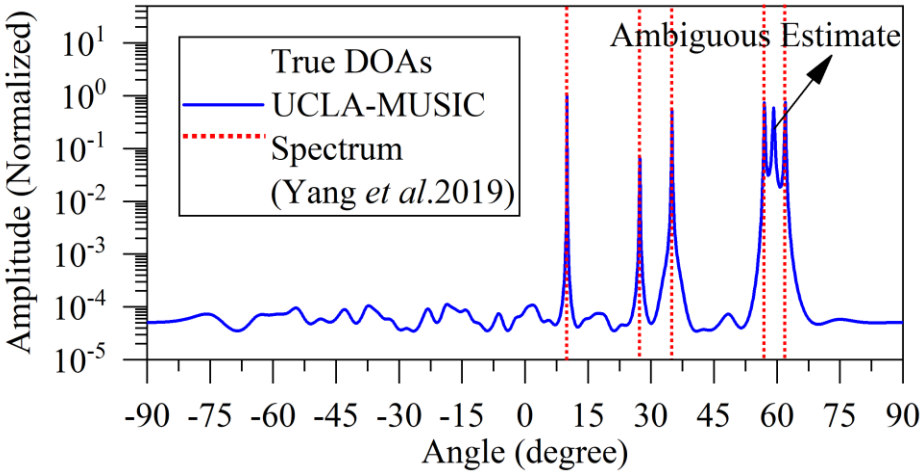

(a)

Figure 2.14 (Continued)

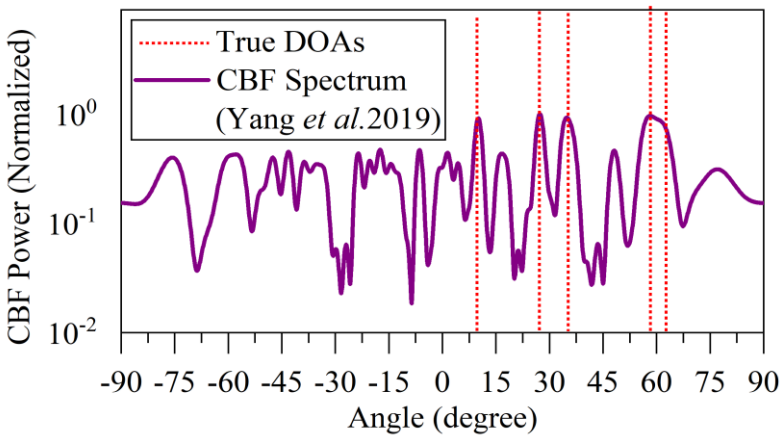

(b)

Figure 2.14 (a) The UCLA-MUSIC spectrum for the case of $M = 5$ (b) The CBF power spectrum for the case of $M = 5$

Table 2.1 DOA estimation result of the Yang *et al.*2019 method for the case of $M = 5$

Set of Angles	True θ_1 10.00°	True θ_2 27.35°	True θ_3 35.01°	True θ_4 57°	True θ_5 62°	Generated Ambiguous θ_g 59.25°
$\hat{\theta}_{UCLA-MUSIC}$	10.00°	27.35°	35.01°	57°	62°	59.25°
$\hat{P}_{CBF}$	0.6805	0.8611	0.4930	0.5277	0.4444	0.5486
True or Ambiguous	True	True	True	True	Ambiguous	True

The estimation results with associated observations on the existence of ambiguity, DOF and complexity of the above-aforementioned methods: subarray-based methods (Zhou *et al.*2013; Sun *et al.*2015; Zhang *et al.* 2017; Liu *et al.* 2018; Yan *et al.* 2018) and adjoined subarray-based methods (Zheng *et al.* 2018; He *et al.*2020) in the general case of grating-angle ambiguity for GCLA are summarized in Table A1.2 of Appendix 1. Similarly, the estimation results with associated observations on the existence of ambiguity, DOF and complexity of the above-aforementioned methods: subarray-based

methods (Zhou *et al.*2013; Sun *et al.*2015; Zhang *et al.* 2017; Liu *et al.* 2018; Yan *et al.* 2018), adjoined subarray-based methods (Zheng *et al.* 2018; He *et al.*2020) and beamforming-like methods (Yang *et al.*2019; Huang *et al.*2021) in the general and closely distributed cases of grating-angle ambiguity for UCLA are summarized in Table A1.3, Table A1.4 and Table A.15 respectively of Appendix 1. Table 2.1, Table A1.4 and Table A1.5 show the failure of the beamforming-like method involving CBF (Yang *et al.*2019; Huang *et al.*2021) to distinguish the true DOAs and results in the ambiguous estimation of true DOAs.

2.6 CRAMER-RAO LOWER BOUND (CRLB)

This section briefs the Cramer-Rao lower bound (CRLB) for GCLA and UCLA. The CRLB is one of the important tools used in parameter estimation problems providing the lower bound on the accuracy of unbiased estimators (Cramer 1951). In DOA estimation problems, CRLB is considered as one of the key performance metrics in the assessment of the accuracy of unbiased DOA estimators (Stoica *et al.*1990). According to (Zheng *et al.* 2018), the CRLB for GCLA is given as follows

$$\mathrm{CRLB}_{GCLA} = \frac{\sigma^2}{2K}\left\{\Re\left[\mathbf{U} \oplus \left(\widehat{\mathbf{R}}_{\mathrm{s}}\, \mathbf{A}_{GCLA}^{H} \widehat{\mathbf{R}}_{\mathbf{x}}^{\,-\mathbf{1}} \mathbf{A}_{GCLA}\, \widehat{\mathbf{R}}_{\mathrm{s}}\right)\right]^{T}\right\}^{-\mathbf{1}} \tag{2.71}$$

where

$$\mathbf{A}_{GCLA} = \begin{bmatrix}\mathbf{A}_1 \\ \mathbf{A}_2\end{bmatrix} = [\mathbf{A}_1^T\, \mathbf{A}_2^T\,]^T = [\mathbf{a}(\theta_1)\, \mathbf{a}(\theta_2) \ldots \mathbf{a}(\theta_M)]$$

$$\mathbf{U} = \dot{\mathbf{A}}_{GCLA}^{H}[\mathbf{I} - \mathbf{A}_{GCLA}(\mathbf{A}_{GCLA}^{H}\mathbf{A}_{GCLA})^{-1}\mathbf{A}_{GCLA}^{H}]\dot{\mathbf{A}}_{GCLA}$$

$$\widehat{\mathbf{R}}_{\mathrm{x}} = \mathbf{A}_{GCLA}\, \widehat{\mathbf{R}}_{\mathrm{s}}\, \mathbf{A}_{GCLA}^{H} + \sigma^2 \mathbf{I}_N$$

$$\widehat{\mathbf{R}}_{\mathbf{s}} = \frac{1}{K}\sum_{t=1}^{K} \mathrm{s}(t)\, \mathrm{s}^{H}(t)$$

Here, $\dot{\mathbf{A}}_{GCLA}$ is the first-order derivative of $\mathbf{A}_{GCLA}$ i. e., $\dot{\mathbf{A}}_{GCLA} = \frac{\partial \mathbf{A}_{GCLA}}{\partial \boldsymbol{\theta}}$ and $\dot{\mathbf{a}}(\theta_m) = \frac{\partial \mathbf{a}\,(\theta_m)}{\partial \theta_m}$ where $\mathbf{a}(\theta_m) = [\mathbf{a}_1{}^{T}(\theta_m)\ \mathbf{a}_2{}^{T}(\theta_m)\,]^{T}$, $\Re[.]$ represents the real part and $\oplus$ denotes the Hadamard product. Similarly, the extension of CRLB for UCLA is straightforward and is given as follows

$$\mathrm{CRLB}_{UCLA} = \frac{\sigma^2}{2K}\left\{\Re\left[\mathbf{U} \oplus \left(\widehat{\mathbf{R}}_{\mathrm{s}}\, \mathbf{A}_{UCLA}^{H} \widehat{\mathbf{R}}_{\mathrm{x}}{}^{-\mathbf{1}} \mathbf{A}_{UCLA}\, \widehat{\mathbf{R}}_{\mathrm{s}}\right)\right]^{T}\right\}^{-\mathbf{1}} \qquad (2.72)$$

$$\mathbf{U} = \dot{\mathbf{A}}_{UCLA}^{H}[\mathbf{I} - \mathbf{A}_{UCLA}(\mathbf{A}_{UCLA}^{H}\mathbf{A}_{UCLA})^{-1}\mathbf{A}_{UCLA}^{H}]\dot{\mathbf{A}}_{UCLA}$$

$$\dot{\mathbf{A}}_{UCLA} = [\dot{\mathbf{a}}(\theta_1)\ \dot{\mathbf{a}}(\theta_2)\ldots\dot{\mathbf{a}}(\theta_M)] = \left[\frac{\partial \mathbf{a}(\theta_1)}{\partial \theta_1}\ \frac{\partial \mathbf{a}(\theta_2)}{\partial \theta_2}\ldots\ \frac{\partial \mathbf{a}(\theta_M)}{\partial \theta_M}\right]$$

$$\widehat{\mathbf{R}}_{\mathrm{x}} = \mathbf{A}_{UCLA}\, \widehat{\mathbf{R}}_{\mathrm{s}}\, \mathbf{A}_{UCLA}^{H} + \sigma^2 \mathbf{I}_N$$

$$\widehat{\mathbf{R}}_{\mathrm{s}} = \frac{1}{K}\sum_{t=1}^{K} \mathrm{s}(t)\, \mathrm{s}^{H}(t)$$

2.7 SUMMARY

This chapter has provided the groundwork for the rest of the thesis by addressing ambiguity concerns in DOA estimation using GCLA and UCLA. Initially, a description of the ULA design has been provided with its mutual coupling impacts via weight function. Then, the mathematical description of the received signal model, and the concept of spatial sampling for the choice of inter-element spacing in ULA have been discussed. A description of the design of GCLA and UCLA has been provided with its mutual coupling impacts and sparsity via weight function. It is shown that, compared to GCLA, the UCLA design has enhanced effective array aperture

and mitigates the mutual coupling effects. Then, the mathematical description of the received signal model and DOA estimation with GCLA and UCLA is discussed. The DOA estimation with UCLA offers better estimation performance than GCLA due to the enlarged effective array aperture of UCLA over GCLA. Finally, the comprehensive investigation of ambiguity problems such as pair-matching and grating-angle in DOA estimation associated with GCLA and UCLA has been discussed. Since ambiguity problems are crucial in DOA estimation, the following chapters focus on resolving ambiguity problems with superior estimation performances in terms of reliability, accuracy, and angular resolution with low computational complexity and execution time.

CHAPTER 3

AMBIGUITY ELIMINATION METHOD BASED ON THE ESTIMATION OF SOURCE POWER

3.1 INTRODUCTION

The ambiguity issues in DOA estimation with co-prime linear arrays have been discussed in chapter 2. As a result, there is a potential need to address the critical issue of grating-angle ambiguity in estimating the direction-of-arrival (DOA) parameter with unfolded co-prime linear array (UCLA). In the proposed method, the true DOAs are distinguished from ambiguous estimates obtained from UCLA-MUSIC using the estimated power of the source signals. The source power function based on the signal subspace eigenvalues and its associated eigenvectors has been derived to estimate the power of the source signals. Simulation studies are carried out to validate the proposed method's performance in terms of estimation accuracy and reliability.

3.2 SIGNAL MODEL

Consider, M $(M < N)$ far-field source signals from directions $\Theta = \{\theta_m\}_{m=1}^{M}$ impinging on N element UCLA with the field-of-view (FOV) such that $\theta_m \in (-90^o, +90^o)$ as shown in Figure 2.6 of chapter 2. Then, the observed array output received signal vector $\mathbf{x}_{UCLA}(t) \in \mathbb{C}^{N\text{x}\,1}$ of UCLA is given by

$$\mathbf{x}_{UCLA}\,(t) = \mathbf{A}_{UCLA}\,\mathbf{s}\,(t) + \mathbf{n}\,(t) \tag{3.1}$$

where $\mathbf{A}_{UCLA} = \left[\mathbf{a}\,(\theta_1)\ \mathbf{a}\,(\theta_2)\ldots\ \mathbf{a}\,(\theta_M)\right] \epsilon\, \mathbb{C}^{N\,x\,M}$ represents the array directional matrix and $\mathbf{a}\,(\theta_m) = [\mathbf{a}_1^T(\theta_m)\ \mathbf{a}_2^T(\theta_m)]^T \epsilon\, \mathbb{C}^{N\,x\,1}$ represents the array directional vector of UCLA. The directional vector of $\mathbf{a}_1(\theta_m)$ and $\mathbf{a}_2(\theta_m)$ in UCLA can be expressed as

$$\mathbf{a}_1(\theta_m) = \left[1,\ e^{-j\pi N_2\, sin(\theta_m)},\ldots,\ e^{-j\pi N_2(N_1-1)\, sin(\theta_m)}\right]^T \tag{3.2}$$

$$\mathbf{a}_2(\theta_m) = \left[e^{-j\pi(N_2(N_1-1)+N_1)\, sin(\theta_m)},\ldots,\ e^{-j\pi(N_2(N_1-1)+N_1(N_2-1))\, sin(\theta_m)}\right]^T \tag{3.3}$$

As a result, $\mathbf{a}\,(\theta_m)\ \epsilon\ \mathbb{C}^{N\,x\,1}$ of UCLA can be written as

$$\mathbf{a}\,(\theta_m) = [1,\ e^{-j\pi N_2\, sin(\theta_m)},\ldots,\ e^{-j\pi N_2(N_1-1)\, sin(\theta_m)}, e^{-j\pi(N_2(N_1-1)+N_1)\, sin(\theta_m)}, \ldots, e^{-j\pi(N_2(N_1-1)+N_1(N_2-1))sin(\theta_m)}]^T \tag{3.4}$$

$\mathbf{s}\,(t) = [s_1(t)\ s_2(t)\ldots\ s_M(t)]^T\ \epsilon\ \mathbb{C}^{M\,x\,1}$ represents the vector of emitter signal amplitudes and $\mathbf{n}(t) = [n_0(t)\ n_1(t)\ldots n_{N-1}(t)\ ]^T \epsilon\ \mathbb{C}^{N\,x\,1}$ represents the zero-mean additive white noise with covariance $\mathrm{E}\{\mathbf{n}(t)\mathbf{n}^{\boldsymbol{H}}(t)\} = \sigma_{\mathbf{n}}^{\mathbf{2}}\mathbf{I}_N$, where $\sigma_{\mathbf{n}}^{\mathbf{2}}$ is the noise power and $\mathbf{I}_N$ denotes the $N\,x\,N$ identity matrix (Zheng *et al.* 2018). The observed array output received signal vector $\mathbf{x}_{UCLA}\,(t)\ \epsilon\ \mathbb{C}^{Nx\,1}$ of UCLA can be expressed as follows

$$\mathbf{x}_{UCLA}\,(t) =$$

$$\begin{bmatrix} 1 & 1 & & 1 \\ e^{-j\pi N_2\, sin(\theta_1)} & e^{-j\pi N_2\, sin(\theta_m)} & & e^{-j\pi N_2\, sin(\theta_M)} \\ \vdots & \vdots & & \vdots \\ e^{-j\pi N_2(N_1-1)\, sin(\theta_1)} & e^{-j\pi N_2(N_1-1)\, sin(\theta_m)} & \ldots & e^{-j\pi N_2(N_1-1)\, sin(\theta_M)} \\ e^{-j\pi(N_2(N_1-1)+N_1)\, sin(\theta_1)} & e^{-j\pi(N_2(N_1-1)+N_1)\, sin(\theta_m)} & & e^{-j\pi(N_2(N_1-1)+N_1)\, sin(\theta_M)} \\ \vdots & \vdots & & \vdots \\ e^{-j\pi(N_2(N_1-1)+N_1(N_2-1))sin(\theta_1)} & e^{-j\pi(N_2(N_1-1)+N_1(N_2-1))sin(\theta_m)} & & e^{-j\pi(N_2(N_1-1)+N_1(N_2-1))sin(\theta_M)} \end{bmatrix}$$

$$\begin{bmatrix} s_1(t) \\ s_2(t) \\ \vdots \\ s_M(t) \end{bmatrix} + \begin{bmatrix} n_0(t) \\ n_1(t) \\ \vdots \\ n_{N-1}(t) \end{bmatrix} \tag{3.5}$$

The signal model given in Equation (3.5) is seen as similar to the signal model given in Equation (2.49).

3.3 PROPOSED METHOD

This section describes the method proposed for the elimination of the ambiguous angles estimated from the UCLA-MUSIC. UCLA is considered as a single-array design, and so the covariance $\mathbf{R_x} \in \mathbb{C}^{N \times N}$ of the received signal $\mathbf{x}_{UCLA}(t) \in \mathbb{C}^{N \times 1}$ is directly obtained instead from two subarrays separately and it is given by

$$\mathbf{R_x} = E\{\mathbf{x}_{UCLA}(t)\, \mathbf{x}_{UCLA}^{H}(t)\}$$

$$= \mathbf{A}_{UCLA}\, \mathbf{R}_s\, \mathbf{A}_{UCLA}^{H} + \sigma_{\mathbf{n}}^{2} \mathbf{I}_N \tag{3.6}$$

where $\mathbf{R}_s = \boldsymbol{E}\{\mathbf{s}\mathbf{s}^H\}$ denotes the source covariance matrix, $\sigma_{\mathbf{n}}^{2}$ is the noise power and $\mathbf{I}_N$ denotes the $N \times N$ identity matrix. In practice, the actual covariance matrix $\mathbf{R_x}$ is unknown, therefore its sample estimate $\widehat{\mathbf{R}}_{\mathbf{x}}$ is computed for K snapshots and it is given by

$$\widehat{\mathbf{R}}_{\mathbf{x}} = \frac{1}{K} \sum_{t=1}^{K} \mathbf{x}_{UCLA}(t)\, \mathbf{x}_{UCLA}^{H}(t) = \begin{bmatrix} \widehat{\mathbf{R}}_1 & \widehat{\mathbf{R}}_2 \\ \widehat{\mathbf{R}}_3 & \widehat{\mathbf{R}}_4 \end{bmatrix} \tag{3.7}$$

Here, the array covariance $\widehat{\mathbf{R}}_{\mathbf{x}}$ inherently contains the self and mutual information of two subarrays due to the utilization of the entire array. It can be seen via the block matrices such as $\widehat{\mathbf{R}}_1$, $\widehat{\mathbf{R}}_4$ are the array auto-covariance and $\widehat{\mathbf{R}}_2$, $\widehat{\mathbf{R}}_3$ are the array cross-covariance of two subarrays in $\widehat{\mathbf{R}}_{\mathbf{x}}$ of Equation (3.7) (Zheng *et al.* 2018). The eigenvalue decomposition (EVD) of $\widehat{\mathbf{R}}_{\mathbf{x}}$ yields

$$\widehat{\mathbf{R}}_{\mathbf{x}} = \widehat{\mathbf{E}}_s\, \widehat{\mathbf{D}}_s \widehat{\mathbf{E}}_s^{H} + \widehat{\mathbf{E}}_n\, \widehat{\mathbf{D}}_n\, \widehat{\mathbf{E}}_n^{H} \tag{3.8}$$

where $\hat{\mathbf{E}}_s \triangleq [\mathbf{e}_1, \mathbf{e}_2, \ldots, \mathbf{e}_M] \in \mathbb{C}^{N \times M}$ and $\hat{\mathbf{E}}_n \triangleq [\mathbf{e}_{M+1}, \mathbf{e}_{M+2}, \ldots, \mathbf{e}_N]\, \mathbb{C}^{N \times N-M}$ contains the signal- and noise-subspace eigenvectors of $\hat{\mathbf{R}}_{\mathbf{x}}$ corresponding to the eigenvalues in the diagonal matrix $\hat{\mathbf{D}}_s \triangleq \text{diag}\{\lambda_1, \lambda_2, \ldots, \lambda_M\}$ and $\hat{\mathbf{D}}_n \triangleq \text{diag}\{\lambda_{M+1}, \lambda_{M+2}, \ldots, \lambda_N\}$. Furthermore, the signal subspace and directional vector of the source signals span the same space and are orthogonal to the noise subspace. As a result, the directional vector can be used in the search for all possible angles from -90° to $+90^{\circ}$ across the noise-subspace to determine the DOA of transmitted source signals, and the UCLA-MUSIC pseudo spectrum is given by

$$\hat{f}_{UCLA-MUSIC}(\theta) = \frac{1}{\mathbf{a}^H(\theta)\, \hat{\mathbf{E}}_n\, \hat{\mathbf{E}}_n^H\, \mathbf{a}(\theta)} = \frac{1}{\|\hat{\mathbf{E}}_n^H\, \mathbf{a}(\theta)\|^2} \tag{3.9}$$

Thus, the angles (θ) corresponding with the highest peaks of $\hat{f}_{UCLA-MUSIC}(\theta)$ are the DOA of the transmitted source signals.

In the case of grating-angle ambiguity, the $\hat{f}_{UCLA-MUSIC}(\theta)$ fails to exhibit the highest peaks at true DOAs as illustrated in section 2.5.2 of chapter 2. A source covariance function is derived for distinguishing and eliminating the ambiguous angles from the initial estimate of UCLA-MUSIC. To start with, using Equation (3.6), the source covariance matrix $\mathbf{R}_{\mathbf{s}}$ can be expressed as $\mathbf{R}_{\mathbf{s}} = \boldsymbol{E}\{\mathbf{s}\mathbf{s}^H\}$ and it is generally unknown in practice. Thus, a relation is established through consideration of only the contribution of source signals using Equations (3.6) and Equation (3.8) and it is given by

$$\mathbf{A}_{UCLA}\, \hat{\mathbf{R}}_{\mathbf{s}}\, \mathbf{A}_{UCLA}^H \triangleq \hat{\mathbf{E}}_{\mathrm{s}} \hat{\mathbf{D}}_{\mathrm{s}} \hat{\mathbf{E}}_{\mathrm{s}}{}^H \tag{3.10}$$

Upon multiplying $\hat{\mathbf{E}}_s$ and $\hat{\mathbf{E}}_s{}^H$ to $\mathbf{A}_{UCLA}\, \hat{\mathbf{R}}_{\mathrm{s}}\, \mathbf{A}_{UCLA}^H$ in Equation (3.10) results in

$$\hat{\mathbf{E}}_{\mathrm{s}}{}^H \mathbf{A}_{UCLA}\, \hat{\mathbf{R}}_{\mathbf{s}}\, \mathbf{A}_{UCLA}^H \hat{\mathbf{E}}_{\mathrm{s}} = \text{diag}\,\{\lambda_1\ \lambda_2 \ldots \lambda_M\} = \hat{\mathbf{D}}_{\mathrm{s}} \tag{3.11}$$

Equation (3.11) allows for the following derivation of $\widehat{\mathbf{R}}_{\mathrm{s}}$ and it is given by

$$\widehat{\mathbf{R}}_{\mathrm{s}} = \left(\widehat{\mathbf{E}}_{\mathrm{s}}{}^{H}\mathbf{A}_{UCLA}\right)^{-1}\widehat{\mathbf{D}}_{\mathrm{s}}\left(\mathbf{A}_{UCLA}^{H}\widehat{\mathbf{E}}_{\mathrm{s}}\right)^{-1} \tag{3.12}$$

The diag$\{\widehat{\mathbf{R}}_{\mathrm{s}}\}$ contains the estimate of the power of the transmitted source signals. In the case of grating-angle ambiguity, the $\hat{f}_{UCLA-MUSIC}(\theta)$ exhibits more than M highest peaks given by L $(L \geq M)$. Assume the total number of peaks exhibited by $\hat{f}_{UCLA-MUSIC}(\theta)$ is given by T $(T \geq L)$. Now, for the computation of the total number of highest peaks L $(L \geq M)$ from the total number of peaks T $(T \geq L)$ exhibited by $\hat{f}_{UCLA-MUSIC}(\theta)$, the amplitudes of the T peaks are sorted in descending order and it is given by $y_1 > y_2 > \ldots > y_T$. The angles associated with y_1, y_2,..., y_T can be indicated as θ_1, θ_2,..., θ_D. The total number of L $(L \geq M)$ highest peaks can be computed by

$$L = \arg\ \underset{u}{max}\ D(u) \tag{3.13}$$

where $D(u) = \frac{y_u - y_{u+1}}{y_{u+1}}$, $u = 1,2,3,\ldots,T-1$. Here, the $D(u)$ result is low when both the y_u and y_{u+1} are nearly equal, while $D(u)$ result is high when y_u is low and y_{u+1} is high and vice versa. Then, the angles associated with the highest peaks L $(L \subseteq T)$ exhibited by $\hat{f}_{UCLA-MUSIC}(\theta)$ can be represented as

$$\Theta = \{\theta_l\}_{l=1}^{L} \tag{3.14}$$

The existence of ambiguity can be confirmed through the use of the following conditions (i) *if* $L > M$ then *ambiguity exists* (ii) *if* $L = M$ then *ambiguity does not exists.* In the case of ambiguity, the set of possible combinations of angles can be obtained and it is given by

$$\Theta^{i} = \left\{\theta_{i,p}\right\}_{p=1}^{M},\ i = 1,2,\ldots,h \tag{3.15}$$

where $h = \mathrm{C}_M^L = \frac{L!}{M!\,(L-M)!}$, $\theta_{i,p}$ can be obtained from the initial estimate (Θ) and it is given by

$$\theta_{i,p} = \Theta[\langle p - i \rangle_L] \tag{3.16}$$

where $\langle \cdot \rangle_L$ is the modulo operation i.e., $\langle p - i \rangle_L = (p - i) \bmod L$. The equivalent array directional matrix $\widehat{\mathbf{A}}_{UCLA}^{i}$ for Θ^i can be computed and expressed as

$$\widehat{\mathbf{A}}_{UCLA}^{i} = [\hat{\mathbf{a}}(\theta_{i,1})\ \hat{\mathbf{a}}(\theta_{i,2}) \ldots \hat{\mathbf{a}}(\theta_{i,M})], i = 1,2,\ldots,h \tag{3.17}$$

The signal source power function (matrix) $\widehat{\mathbf{R}}_{\mathrm{s}}$ for each $\widehat{\mathbf{A}}_{UCLA}^{i}$ can be computed and it is given by

$$\widehat{\mathbf{R}}_{\mathbf{s}}^{i} = \left(\hat{\mathbf{E}}_{\mathrm{s}}{}^{H} \widehat{\mathbf{A}}_{UCLA}^{i}\right)^{-1} \widehat{\mathbf{D}}_{\mathrm{s}} \left(\widehat{\mathbf{A}}_{UCLA}^{iH} \hat{\mathbf{E}}_{\mathrm{s}}\right)^{-1} \tag{3.18}$$

Because the diagonal of $\widehat{\mathbf{R}}_{\mathrm{s}}^{i}$ comprises the estimate of the power of the transmitted source signals, the trace $(\widehat{\mathbf{R}}_{\mathrm{s}}^{i})$ is computed and it is given by

$$w_i = \text{trace}\ (\widehat{\mathbf{R}}_{\mathbf{s}}^{i}) \tag{3.19}$$

The index of minimum value of w_i can be used for getting the source covariance matrix $\widehat{\mathbf{R}}_{\boldsymbol{s}}$ related to the transmitted source signals and it can be expressed as

$$r = \arg \min_{i}\ (w_i) \tag{3.20}$$

Finally, the M true DOAs can be obtained through the utilization of the index (r) and it is given by

$$\widehat{\Theta} = \{\theta_{r,p}\}_{p=1}^{M} \tag{3.21}$$

Thus, the M true DOAs of the transmitted source signals can be obtained without ambiguity from $\widehat{\Theta}$ defined in Equation (3.21). Table 3.1 summarizes the steps of the proposed method.

Table 3.1 Steps of the proposed method

Step 1	Estimate the sample covariance matrix $\widehat{\mathbf{R}}_{\mathbf{x}}$ using Equation (3.7)
Step 2	Perform EVD on $\widehat{\mathbf{R}}_{\mathbf{x}}$ and obtain the $\widehat{\mathbf{E}}_s$, $\widehat{\mathbf{E}}_n$ and $\widehat{\mathbf{D}}_s$.
Step 3	Using pseudo spectrum $\hat{f}_{UCLA-MUSIC}(\theta)$ in Equation (3.9) obtain the initial estimate $\Theta = \{\theta_l\}_{l=1}^{L}$
Step 4	Construct the equivalent array directional matrix $\widehat{\mathbf{A}}_{UCLA}^{i}$ for Θ^i using Equation (3.17)
Step 5	Obtain the source covariance matrix $\widehat{\mathbf{R}}_{\mathrm{s}}^{i}$ for each $\widehat{\mathbf{A}}_{UCLA}^{i}$ using Equation (3.18)
Step 6	Find the $\widehat{\mathbf{R}}_{\mathrm{s}}$ corresponds to the true DOAs using Equation (3.19) and Equation (3.20)
Step 7	Obtain the M true DOAs using Equation (3.21)

3.4 SIMULATION RESULTS AND DISCUSSION

This section details the simulations used for validation of the proposed method's estimation performances in terms of reliability and accuracy.

3.4.1 Estimation Reliability

To show the estimation reliability of the proposed method, two cases are considered such that case 1: $M = 3$ and case 2: $M = 6$. In case 1 of $M = 3$ transmitted source signals from directions $\theta_1 = 10.00^{\mathrm{o}}, \theta_2 = 27.35^{\mathrm{o}}, \theta_3 = 35.01^{\mathrm{o}}$ impinges on UCLA with $N = 11$ under the SNR of 10 dB and a snapshot of $K = 200$. Figure 3.1 and Figure 3.2 show the failure of

the method (Zheng *et al.* 2018) and method (He *et al.*2020) in the consistent estimate of the true DOAs for 10 unbiased simulation trials. The method proposed by (Zheng *et al.* 2018) helps estimation correctly only once due to the exhibition of highest peaks at true DOAs, whereas it fails in the remaining simulation trials due to the exhibition of the highest peaks at $\theta_{amb} = 59.25^{o}$ instead of $\theta_2 = 27.35^{o}$. The method (He *et al.*2020) estimates correctly twice, whereas it fails in the remaining simulation trials due to the existence of ambiguous roots related to $\theta_{amb} = 59.25^{o}$ that lie close to the unit circle. In contrast, Figure 3.3 shows the proposed method overcoming the problem of grating-angle ambiguity and successfully estimating the true DOAs for all 10 unbiased simulation trials.

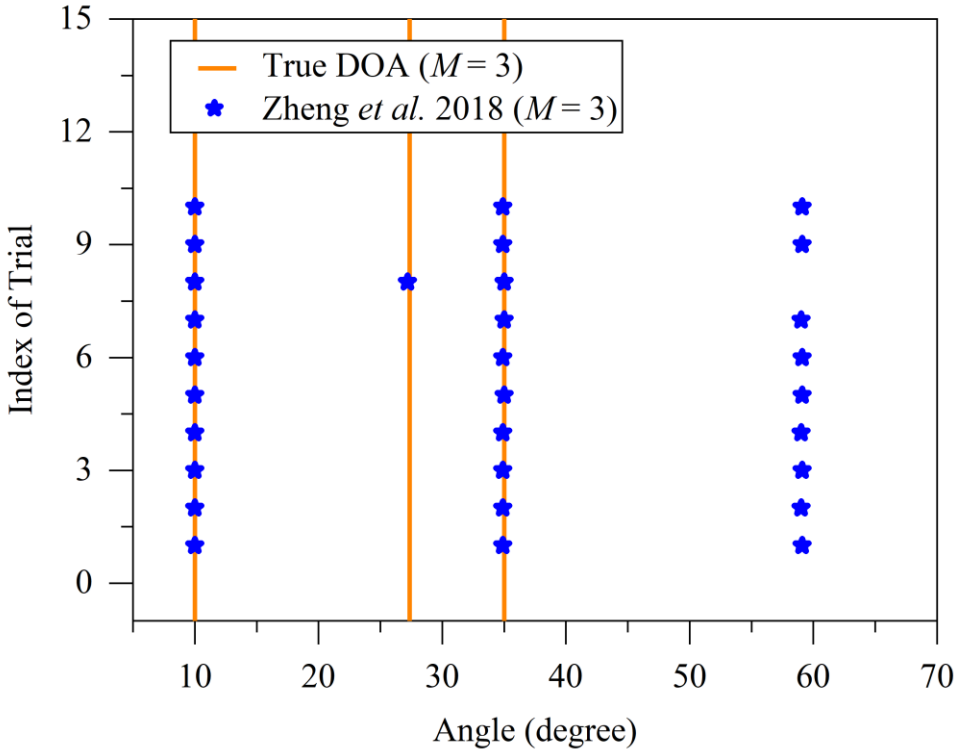

Figure 3.1 Estimation reliability of Zheng *et al.* 2018 method for the case of $M = 3$

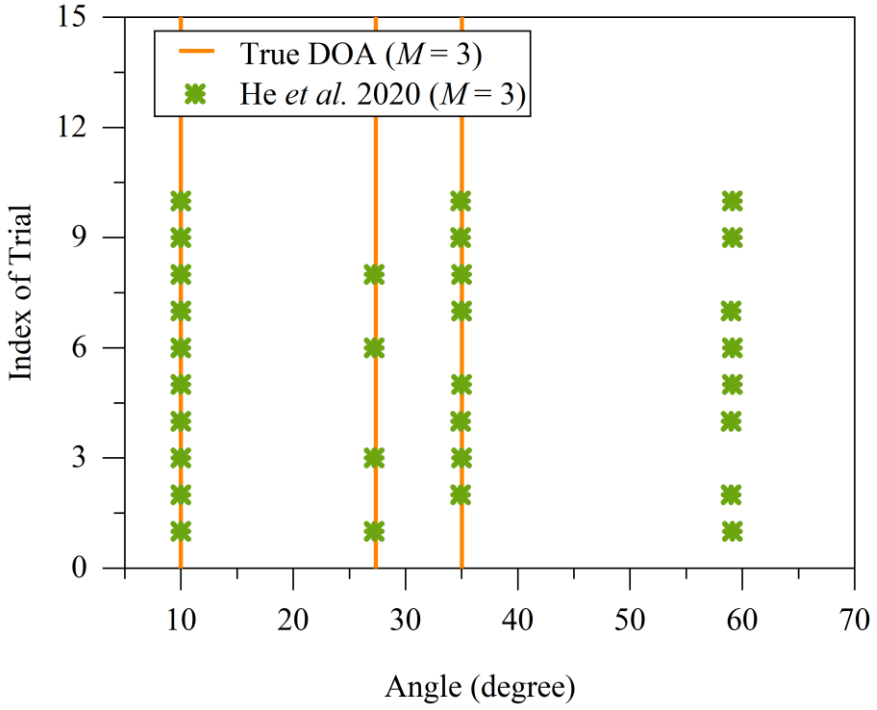

Figure 3.2 Estimation reliability of He *et al.*2020 method for the case of $M = 3$

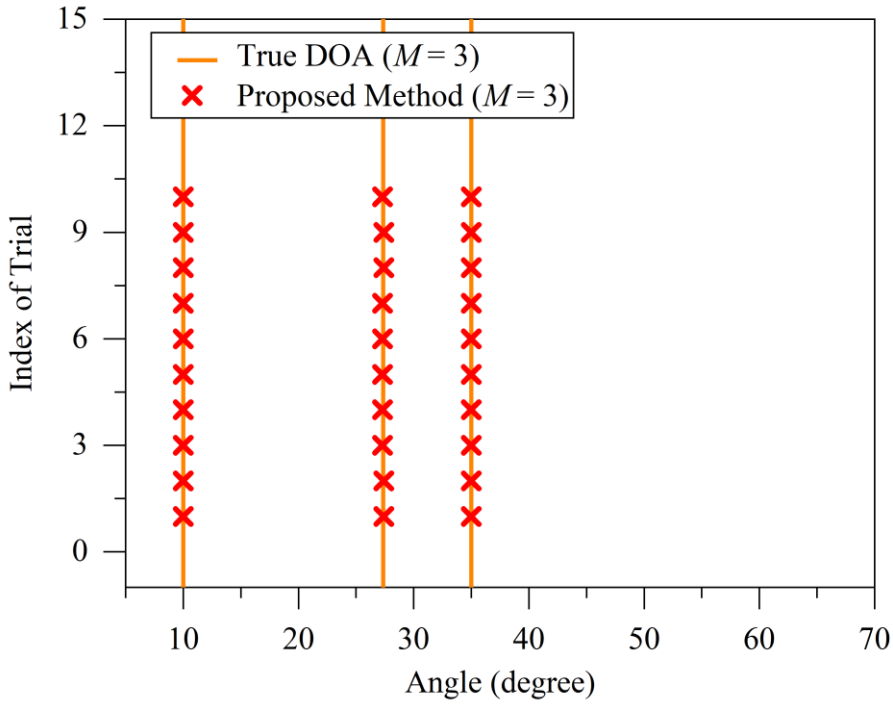

Figure 3.3 Estimation reliability of the proposed method for the case of $M = 3$

Consider case 2 of $M = 6$ transmitted source signals from directions $\theta_1 = 10.00^o, \theta_2 = 27.35^o, \theta_3 = 35.01^o, \theta_4 = 30.00^o, \theta_5 = 12.37^o, \theta_6 = 64.16^o$ impinges on UCLA with $N = 11$ under the SNR of 10 dB and a snapshot of $K = 200$ for demonstration of the superiority of the proposed method. Figure 3.4 shows the method proposed by (Zheng *et al.* 2018) fails in the estimation of true DOAs due to the existence of the highest peaks at $\theta_{amb} = \{59.25^o, 37.92^o\}$. Figure 3.5 shows the failure of the method (He *et al.*2020) due to the existence of ambiguous roots related to $\theta_{amb} = \{59.25^o, 37.92^o\}$ that lie closest to the unit circle. However, the proposed method yields a reliable estimation of true DOAs consistently without any ambiguity as shown in Figure 3.6. It is worth noting that the proposed method achieves superior estimation reliability compared to the existing methods even if the number of transmitted signal sources increases.

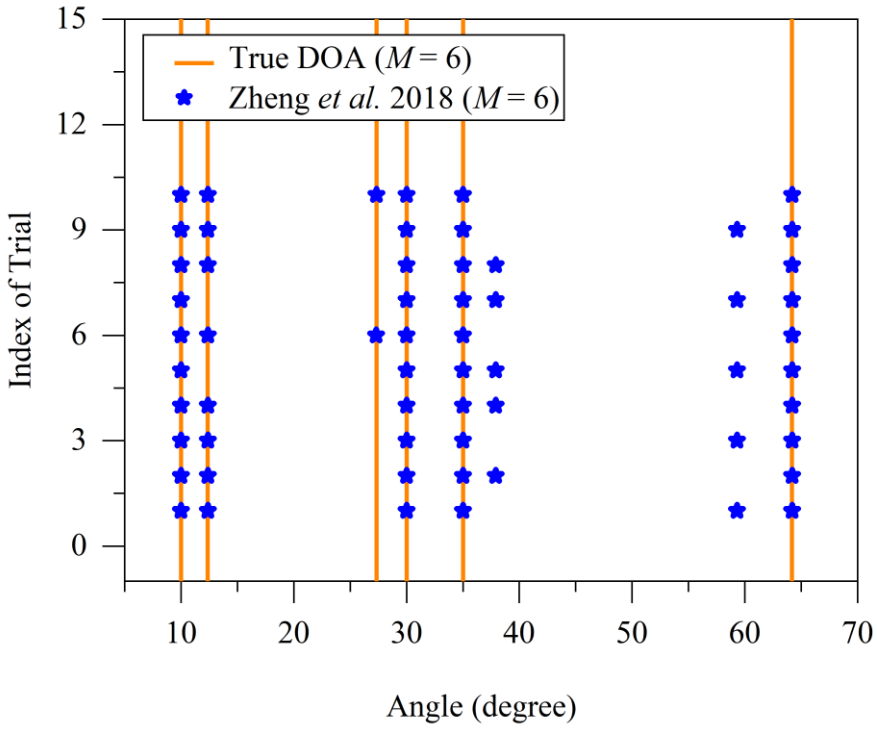

Figure 3.4 Estimation reliability of the Zheng *et al.* 2018 method for the case of $M = 6$

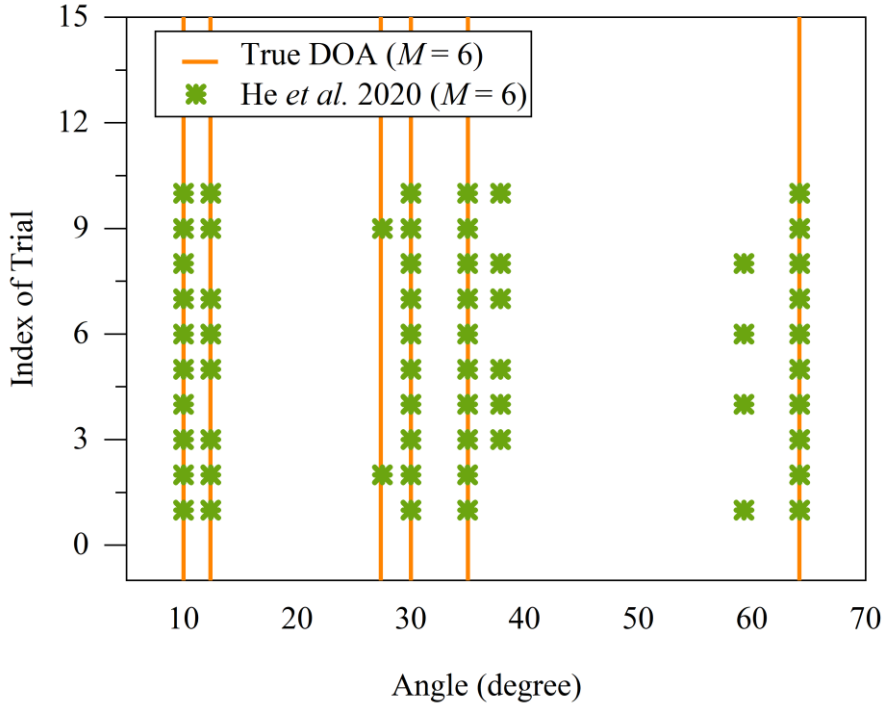

Figure 3.5 Estimation reliability of the He *et al.*2020 method for the case of $M = 6$

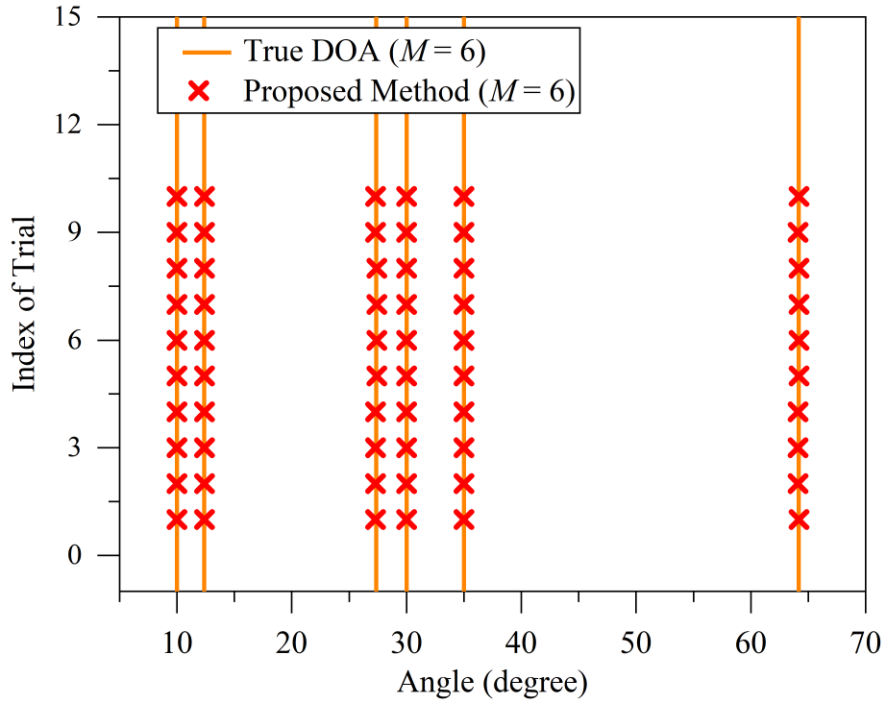

Figure 3.6 Estimation reliability of the proposed method for the case of $M = 6$

3.4.2 Estimation Accuracy

To show the estimation accuracy of the proposed method with method (Zheng *et al.* 2018) and method (He *et al.*2020), a performance metric called Root mean square error (RMSE) is used and it is expressed by

$$\text{RMSE} = \sqrt{\frac{1}{MQ}\sum_{m=1}^{M}\sum_{q=1}^{Q}\left(\hat{\theta}_{m,q} - \theta_m\right)^2} \tag{3.22}$$

where $\hat{\theta}_{m,q}$ is the estimate of m^{th}DOA at q^{th} Monte-Carlo simulation trial of its total Q and θ_m is the m^{th} true DOA. Firstly, RMSE is evaluated for different SNR (dB) varying from -20 to 20 with the step of 5 for $Q = 500$ Monte-Carlo simulation trails. Considering case 1 of $M = 3$ transmitted source signals from directions $\theta_1 = 10.00^{\text{o}}, \theta_2 = 27.35^{\text{o}}, \theta_3 = 35.01^{\text{o}}$ impinges on UCLA with $N = 11$ under the fixed snapshot of $K = 200$. Figure 3.7 shows the proposed method outperforming the existing method (Zheng *et al.* 2018) and method (He *et al.*2020) by offering better estimation accuracy. Furthermore, the proposed method closely follows the limits of the Cramer-Rao lower bound (CRLB) even at low SNR levels.

Evaluation of RMSE has been done for case 2 of $M = 6$ transmitted source signals from directions $\theta_1 = 10.00^{\text{o}}, \theta_2 = 27.35^{\text{o}}, \theta_3 = 35.01^{\text{o}}, \theta_4 = 30.00^{\text{o}}, \theta_5 = 12.37^{\text{o}}, \theta_6 = 64.16^{\text{o}}$ impinges on UCLA with $N = 11$, under a fixed snapshot of $K = 200$ for demonstration of the superiority of the proposed method. Figure 3.8 shows that the proposed method exhibits better estimation accuracy compared to the method (Zheng *et al.* 2018) and method (He *et al.*2020) as the SNR increases and also closely follows the limits of CRLB.

Finally, evaluation of RMSE has been done for different snapshots with variations from 30 to 1100 with fixed SNR of 10 dB for the above-mentioned case 1 of $M = 3$ and case 2 of $M = 6$ source signals. Figure 3.9 and Figure 3.10 show the proposed method's RMSE as lower compared to the method (Zheng *et al.* 2018) and method (He *et al.*2020). Furthermore, the RMSE performance of the proposed method closely follows the limits of the CLRB even at the lower number of snapshots.

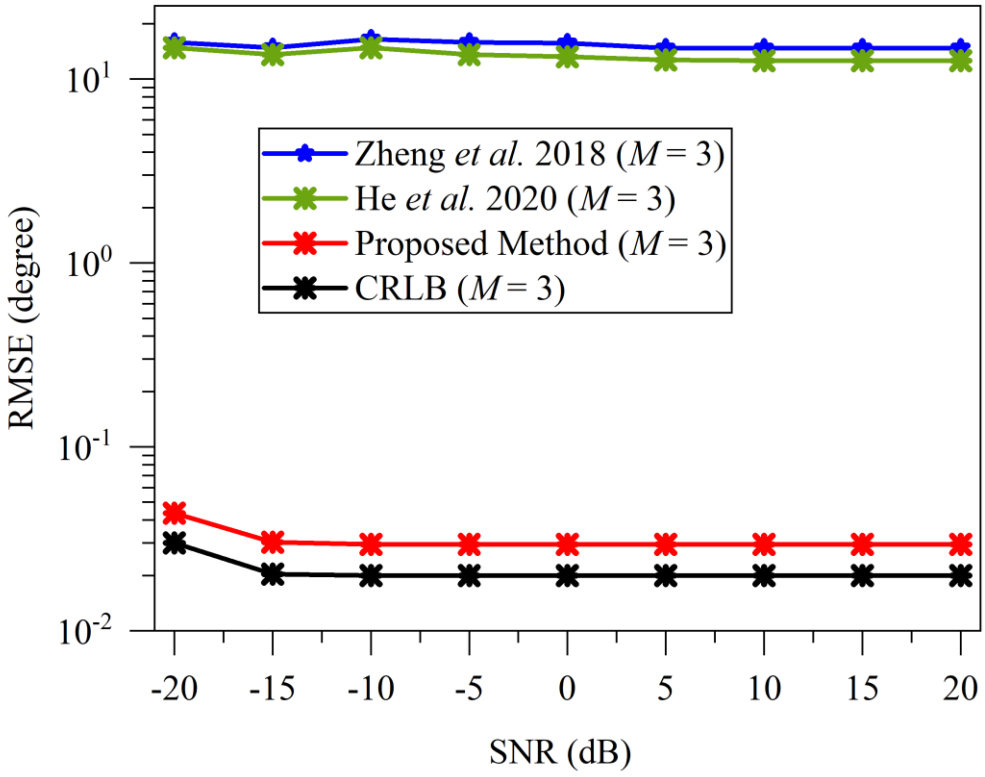

Figure 3.7 RMSE versus SNR for the case of $M = 3$

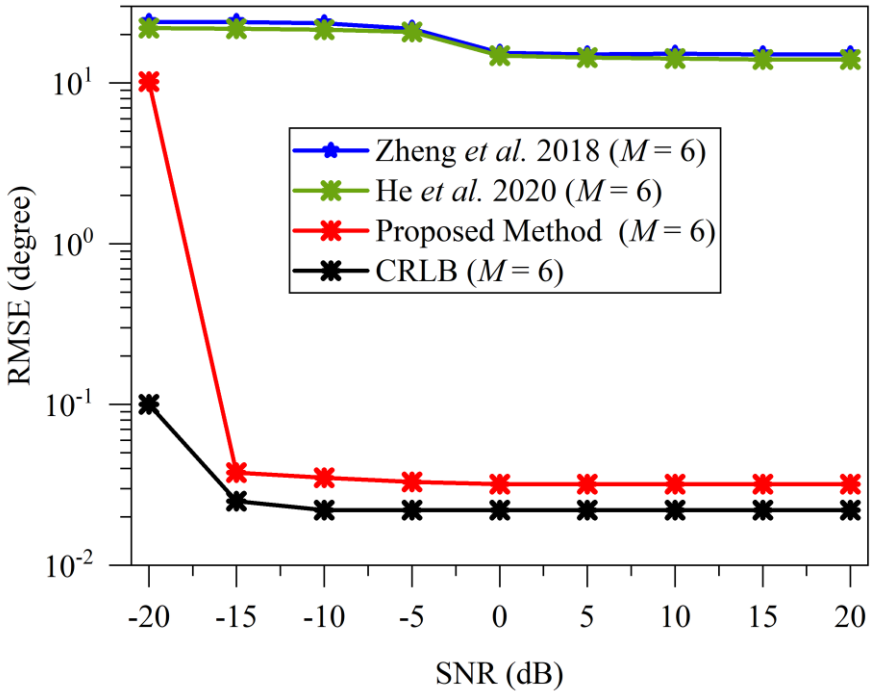

Figure 3.8 RMSE versus SNR for the case of $M = 6$

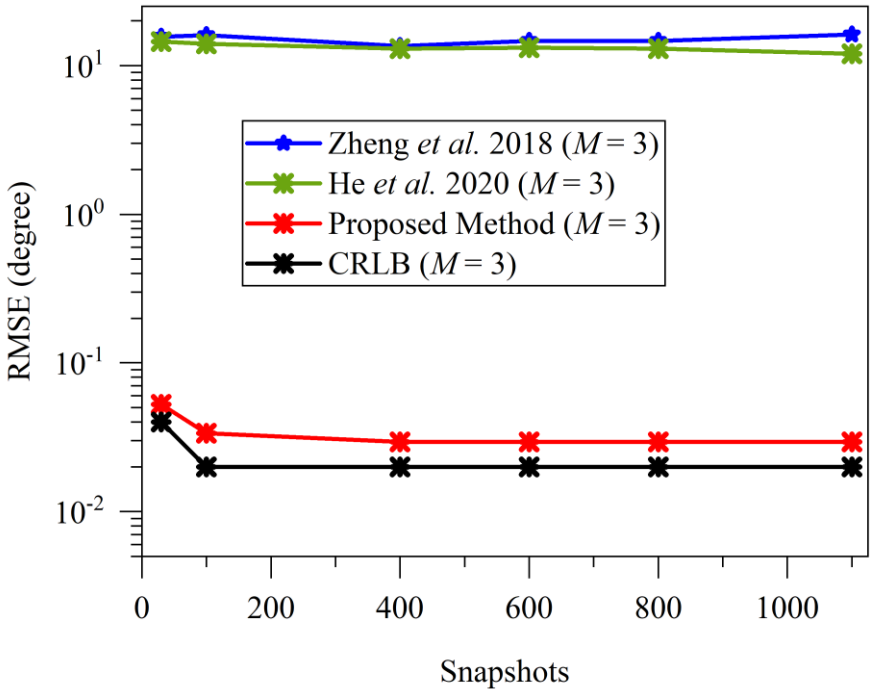

Figure 3.9 RMSE versus snapshots for the case of $M = 3$

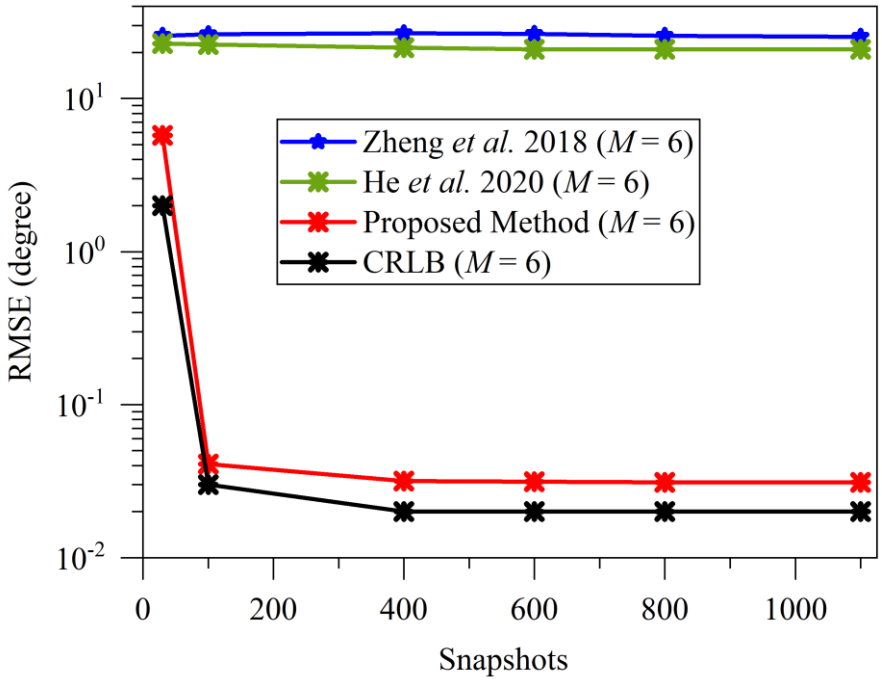

Figure 3.10 RMSE versus snapshots for the case of $M = 6$

3.5 SUMMARY

In this chapter, a method has been proposed for the resolution of the critical issue of grating-angle ambiguity in the estimation of the DOA parameter with UCLA. The proposed unambiguous DOA estimation method incorporates an initial estimation of DOAs through UCLA-MUSIC. The true DOAs are distinguished from ambiguous estimates obtained from UCLA-MUSIC with the use of the estimated power of the transmitted source signals. The source power function based on the signal subspace eigenvalues and its associated eigenvectors has been used in the estimation of the power of the source signals transmitted. The proposed approach distinguishes and detects the true DOAs successfully without any ambiguity. The simulation results guarantee the outperformance of the proposed method over the existing methods through the exhibition of superior estimation in terms of reliability and accuracy.

CHAPTER 4

AN IMPROVED POLYNOMIAL ROOTING-BASED METHOD FOR HIGH-RESOLUTION UNAMBIGUOUS DOA ESTIMATION

4.1 INTRODUCTION

Despite the method based on the source covariance function proposed in chapter 3 successfully resolving the ambiguity problem, the estimation performances are limited in terms of angular resolution. It also involves high computational complexity due to the spectral searching process involved in UCLA-MUSIC (Zheng *et al.* 2018). An improved polynomial rooting-based method has been proposed for overcoming the limitations of the aforementioned method and for the resolution of the ambiguity problem.

The proposed method derives a polynomial function for DOA estimation with UCLA based on the orthogonality between the noise subspace eigenvectors and array directional vectors spanned by the signal subspace. A signal power function based on spatial filtering is established for the selection of the signal roots that are related to true DOAs over ambiguous roots for circumventing the grating-angle ambiguity. A maximum signal power function based on the second-order differential counterparts of the signal power function is proposed for the enhancement of the angular resolution capability of the signal power function in resolving DOAs of closely spaced signal emitters. The error analysis is carried out for establishing the achievement of better estimation accuracy by the proposed method that

closely follows the fundamental limits of the CRLB. The proposed method overcomes the grating-angle ambiguity and estimates the true DOAs successfully with improved estimation performances in terms of reliability, accuracy and angular resolution involving low computational complexity. Finally, the simulations have been performed to show the effectiveness and superiority of the proposed method.

4.2 SIGNAL MODEL

Consider, $M\ (M < N)$ far-field source signals from directions $\Theta = \{\theta_m\}_{m=1}^{M}$ impinging on N element UCLA with the field-of-view (FOV) such that $\theta_m \in (-90^o,\ +90^o)$ as shown in Figure 2.6 of chapter 2. Then, the observed array output received signal vector $\mathbf{x}_{UCLA}\ (n) \in \mathbb{C}^{N\,x\,1}$ of UCLA is given by

$$\mathbf{x}_{UCLA}\ (n) = \mathbf{A}_{UCLA}\ \mathbf{s}\ (n) + \mathbf{v}\ (n) \tag{4.1}$$

where $\mathbf{A}_{UCLA} = [\mathbf{a}\ (\theta_1)\ \ \mathbf{a}\ (\theta_2) \ldots\ \mathbf{a}\ (\theta_M)] \in \mathbb{C}^{N\,x\,M}$ represents the array directional matrix and $\mathbf{a}\ (\theta_m) = [\mathbf{a}_1^T(\theta_m)\ \ \mathbf{a}_2^T(\theta_m)]^T \in \mathbb{C}^{N\,x\,1}$ represents the array directional vector of UCLA. The directional vector of $\mathbf{a}_1(\theta_m)$ and $\mathbf{a}_2(\theta_m)$ in UCLA can be expressed as

$$\mathbf{a}_1(\theta_m) = \left[1,\ e^{-j\pi N_2\, sin(\theta_m)}, \ldots,\ e^{-j\pi N_2(N_1-1)\, sin(\theta_m)}\right]^T \tag{4.2}$$

$$\mathbf{a}_2(\theta_m) = \left[e^{-j\pi(N_2(N_1-1)+N_1)\, sin(\theta_m)}, \ldots,\ e^{-j\pi(N_2(N_1-1)+N_1(N_2-1))\, sin(\theta_m)}\right]^T \tag{4.3}$$

As a result, $\mathbf{a}\ (\theta_m) \in \mathbb{C}^{N\,x\,1}$ of UCLA can be written as

$$\mathbf{a}\ (\theta_m) = [1,\ e^{-j\pi N_2\, sin(\theta_m)}, \ldots,\ e^{-j\pi N_2(N_1-1)\, sin(\theta_m)}, e^{-j\pi(N_2(N_1-1)+N_1)\, sin(\theta_m)},$$

$$\ldots, e^{-j\pi(N_2(N_1-1)+N_1(N_2-1))\, sin(\theta_m)}]^T \tag{4.4}$$

$\mathbf{s}(n) = [s_1(n)\ s_2(n) \ldots\ s_M(n)]^T \in \mathbb{C}^{M \times 1}$ represents the vector of emitter signal amplitudes and $\mathbf{v}(n) = [v_0(n)\ v_1(n) \ldots v_{N-1}(n)\ ]^T \in \mathbb{C}^{N \times 1}$ represents the zero-mean additive white noise with covariance $\mathrm{E}\{\mathbf{v}(n)\mathbf{v}^{\boldsymbol{H}}(n)\} = \sigma_{\mathbf{v}}^2 \mathbf{I}_N$, where $\sigma_{\mathbf{v}}^2$ is the noise power and $\mathbf{I}_N$ denotes the N x N identity matrix (Zheng *et al.* 2018). The observed array output received signal vector $\mathbf{x}_{UCLA}(n) \in \mathbb{C}^{N \times 1}$ of UCLA can be expressed as follows

$$\mathbf{x}_{UCLA}(n) =$$

$$\begin{bmatrix} 1 & 1 & & 1 \\ e^{-j\pi N_2 \sin(\theta_1)} & e^{-j\pi N_2 \sin(\theta_m)} & & e^{-j\pi N_2 \sin(\theta_M)} \\ \vdots & \vdots & & \vdots \\ e^{-j\pi N_2 (N_1-1) \sin(\theta_1)} & e^{-j\pi N_2 (N_1-1) \sin(\theta_m)} & \cdots & e^{-j\pi N_2 (N_1-1) \sin(\theta_M)} \\ e^{-j\pi (N_2(N_1-1)+N_1) \sin(\theta_1)} & e^{-j\pi (N_2(N_1-1)+N_1) \sin(\theta_m)} & & e^{-j\pi (N_2(N_1-1)+N_1) \sin(\theta_M)} \\ \vdots & \vdots & & \vdots \\ e^{-j\pi (N_2(N_1-1)+N_1(N_2-1)) \sin(\theta_1)} & e^{-j\pi (N_2(N_1-1)+N_1(N_2-1)) \sin(\theta_m)} & & e^{-j\pi (N_2(N_1-1)+N_1(N_2-1)) \sin(\theta_M)} \end{bmatrix}$$

$$\begin{bmatrix} s_1(n) \\ s_2(n) \\ \vdots \\ s_M(n) \end{bmatrix} + \begin{bmatrix} v_0(n) \\ v_1(n) \\ \vdots \\ v_{N-1}(n) \end{bmatrix} \tag{4.5}$$

The signal model given in Equation (4.5) is seen as similar to the signal model given in Equation (2.49).

4.3 PROPOSED METHOD

The estimated covariance matrix $\widehat{\mathbf{R}}_{\mathbf{x}} \in \mathbb{C}^{N \times N}$ of the array output received signal vector $\mathbf{x}_{UCLA}(n)$ with K snapshots can be expressed as

$$\begin{aligned} \widehat{\mathbf{R}}_{\mathbf{x}} &= \frac{1}{K} \sum_{i=1}^{K} \mathbf{x}_{UCLA}(n_i) \mathbf{x}_{UCLA}^H(n_i) \\ &= \frac{1}{K}\, \mathbf{x}_{UCLA}\, \mathbf{x}_{UCLA}^H \\ &= \begin{bmatrix} \widehat{\mathbf{R}}_1 & \widehat{\mathbf{R}}_2 \\ \widehat{\mathbf{R}}_3 & \widehat{\mathbf{R}}_4 \end{bmatrix} \end{aligned} \tag{4.6}$$

where $\mathbf{x}_{UCLA} = [\mathbf{x}_{UCLA}(n_1),\ \mathbf{x}_{UCLA}(n_2),\ldots,\mathbf{x}_{UCLA}(n_K)\ ] \in \mathbb{C}^{N\ x\ K}$, block matrices such as $\widehat{\mathbf{R}}_1$, $\widehat{\mathbf{R}}_4$ are the array auto-covariance and $\widehat{\mathbf{R}}_2$, $\widehat{\mathbf{R}}_3$ are the array cross-covariance that contain the self and mutual information of two subarrays respectively. The eigenvalue decomposition (EVD) of $\widehat{\mathbf{R}}_{\mathbf{x}}$ results $\widehat{\mathbf{R}}_{\mathbf{x}} = \hat{\mathbf{E}}\hat{\mathbf{D}}\hat{\mathbf{E}}^H = \hat{\mathbf{E}}_s\hat{\mathbf{D}}_s\hat{\mathbf{E}}_s^H + \hat{\mathbf{E}}_n\hat{\mathbf{D}}_n\hat{\mathbf{E}}_n^H$, where $\hat{\mathbf{E}} = \left[\hat{\mathbf{E}}_s, \hat{\mathbf{E}}_n\right]$, $\hat{\mathbf{E}}_s \triangleq [\mathbf{e}_1, \mathbf{e}_2,\ldots,\mathbf{e}_M] \in \mathbb{C}^{N\ x\ M}$ and $\hat{\mathbf{E}}_n \triangleq [\mathbf{e}_{M+1}, \mathbf{e}_{M+2},\ldots,\mathbf{e}_N]\ \mathbb{C}^{N\ x\ N-M}$ contains the signal- and noise-subspace eigenvectors of $\widehat{\mathbf{R}}_{\mathbf{x}}$ corresponding to the eigenvalues in the diagonal matrix $\hat{\mathbf{D}}_s \triangleq \text{diag}\{\lambda_1,\lambda_2,\ldots,\lambda_M\}$ and $\hat{\mathbf{D}}_n \triangleq \text{diag}\{\lambda_{M+1},\lambda_{M+2},\ldots,\lambda_N\}$. Here, $\hat{\mathbf{E}} = \left[\hat{\mathbf{E}}_s, \hat{\mathbf{E}}_n\right]$ is a unitary matrix, hence the signal subspace $\hat{\mathbf{E}}_s$ and noise subspace $\hat{\mathbf{E}}_n$ are orthogonal to each other i. e., $\hat{\mathbf{E}}_s^H\hat{\mathbf{E}}_n \triangleq 0$. The co-prime property and joint utilization of self and mutual information of two subarrays in UCLA allows the space spanned by $\hat{\mathbf{E}}_s$ and columns of $\mathbf{A}_{UCLA}$ to be equal and orthogonal to $\hat{\mathbf{E}}_n$. As a result, the array directional vectors of $\mathbf{A}_{UCLA}$and eigenvectors of noise subspace are orthogonal and hold a property $\| \hat{\mathbf{E}}_n^H\mathbf{A}_{UCLA} \| \triangleq 0$. Using this property, a polynomial function $f(z)$ is defined by

$$f(z) = \mathbf{a}^T(1/z)\hat{\mathbf{E}}_n\hat{\mathbf{E}}_n^H\,\mathbf{a}(z) \tag{4.7}$$

where $\mathbf{a}(z)$ is the array directional vector of UCLA and it can be expressed as $\mathbf{a}(z) = [\mathbf{a}_1{}^T(z)\ \ \mathbf{a}_2{}^T(z)\ ]^T$. Then, $\mathbf{a}_1(z)$ and $\mathbf{a}_2(z)$ can be written as

$$\mathbf{a}_1(z)|_{z=e^{-j\pi sin(\theta)}} = \left[1\ \ z^{N_2}\ \ z^{2N_2}\ldots\ \ z^{(N_1-1)N_2}\right]^T \tag{4.8}$$

$$\mathbf{a}_2(z)|_{z=e^{-j\pi sin(\theta)}} = \left[\ z^{(N_1-1)N_2+N_1}\ \ z^{(N_1-1)N_2+2N_1}\ldots\ \ z^{(N_1-1)N_2+(N_2-1)N_1}\right]^T \tag{4.9}$$

Thus, $\mathbf{a}(z)$ can be written as

$$\mathbf{a}(z)|_{z=e^{-j\pi sin(\theta)}} = [1\ \ z^{N_2}\ \ z^{2N_2}\ldots z^{(N_1-1)N_2}\ z^{(N_1-1)N_2+N_1}\ z^{(N_1-1)N_2+2N_1}\ldots z^{\overbrace{(N_1-1)N_2+(N_2-1)N_1}^{\tilde{r}}}]^T \tag{4.10}$$

The solution to polynomial function $f(z)$ results in $2r$ number of roots where $r = 2N_1N_2 - N_1 - N_2$. Here, the $2r$ roots appear as conjugate reciprocal pairs $\{z_p\}_{p=1}^{r}$ and $\{1/z_p^*\}_{p=1}^{r}$ and the roots that lie inside the unit circle have information about the DOA of the emitter signals. Therefore, the roots that lie inside the unit circle with the highest magnitude such that $\{z_m\}_{m=1}^{M} \subset \{z_p\}_{p=1}^{r}$ are used in the estimation of the M DOAs. In the situation of grating-angle ambiguity, there exist more than M roots that lie closest to the unit circle and are not distinguishable concerning true DOAs. Therefore, a signal power function $s(z)$ is defined based on the spatial filtering technique to find the M signal roots corresponding to the true DOAs. The signal power function $s(z)$ is defined as the mean power of $\mathbf{x}'_{UCLA}(n)$, where $\mathbf{x}'_{UCLA}(n)$ is the weighted linear combination of array output signal vector $\mathbf{x}_{UCLA}$ and it is given by

$$\mathbf{x}'_{UCLA}(n) = \mathbf{w}^H \mathbf{x}_{UCLA} \tag{4.11}$$

Here, the weight vector $\mathbf{w}$ is equal to the array response vector $\mathbf{a}(z)$ (Tuncer *et al.* 2009) and the signal power function $s(z)$ can be expressed as

$$\begin{aligned} s(z) &= E\{|\mathbf{x}'_{UCLA}(n)|^2\} \\ &= E\{|\mathbf{a}^H(z)\, \mathbf{x}_{UCLA}(n)|^2\} \\ &= \mathbf{a}^H(z)(E\{\mathbf{x}_{UCLA}(n)\, \mathbf{x}_{UCLA}^H(n)\})\, \mathbf{a}(z) \\ &= \mathbf{a}^H(z) \left(\underbrace{\frac{1}{K} \sum_{i=1}^{K} \mathbf{x}_{UCLA}(n_i) \mathbf{x}_{UCLA}^H(n_i)}_{\widehat{\mathbf{R}}_{\mathbf{x}}} \right) \mathbf{a}(z) \\ &= \mathbf{a}^T(z^{-1}) \widehat{\mathbf{R}}_{\mathbf{x}}\, \mathbf{a}(z) \end{aligned} \tag{4.12}$$

The signal power function $s(z)$ yields a higher power for signal roots but is unable to resolve the closely distributed signal roots with a higher power. Therefore, the second-order differential of $s(z)$ is defined to improve the resolution and it is expressed as

$$s''(z) \triangleq \frac{ds(z)}{dz} = \frac{-s(z-\delta z)+s(z)+s(z+\delta z)}{\delta z} \tag{4.13}$$

where $\delta z = e^{-j\pi \sin \delta\theta}$ is a discrete root interval. Here, $s''(z)$ being local maxima for convex upward of $s(z)$, it resolves the closely spaced signal roots with higher power and simultaneously yields higher power for other roots. Therefore, a maximum signal power function $p(z)$ is defined as a product of $s(z)$ and its second-order differential counterparts $s''(z)$ to find the signal roots related to true DOAs and it is given by

$$p(z) = s(z).\ s''(z) \tag{4.14}$$

Thus, $p(z)$ yields higher power for $\{z_m\}_{m=1}^{M}$ signal roots relating to M true DOAs among $\{z_p\}_{p=1}^{r}$ roots. Finally, using $z_m = e^{-j\pi \sin(\theta_m)}$, the DOA of the emitter signals is obtained from $\{z_m\}_{m=1}^{M}$ signal roots are given by

$$\hat{\theta}_m = -\sin^{-1}\left(\frac{\varphi(z_m)}{\pi}\right);\ \ m = 1,2,\ldots,M \tag{4.15}$$

where $\varphi(z_m) = \tan^{-1}(\Im(z_m)/\Re(z_m))$ is the phase angle of z_m, $\Im(z_m)$ and $\Re(z_m)$ are the imaginary- and real- parts of z_m. Table 4.1 summarizes the processing steps of the proposed method.

Table 4.1 Processing steps of the proposed method

Step 1	Estimate the array covariance matrix $\widehat{\mathbf{R}}_{\mathbf{x}}$ using Equation (4.6)
Step 2	Perform EVD on $\widehat{\mathbf{R}}_{\mathbf{x}}$ and obtain the noise subspace $\widehat{\mathbf{E}}_n$
Step 3	Obtain the roots of the polynomial function $f(z)$ defined in Equation (4.7)
Step 4	Obtain M signal roots i. e., $\{z_m\}_{m=1}^{M}$ using maximum signal power function $p(z)$ defined in Equation (4.14)
Step 5	From $\{z_m\}_{m=1}^{M}$ roots, obtain M DOAs i. e., $\{\hat{\theta}_m\}_{m=1}^{M}$ using Equation (4.15)

4.4 SIMULATION RESULTS AND DISCUSSION

This section details the simulations for the validation of the estimation performances of the proposed method in terms of reliability, accuracy, angular resolution and computational complexity in comparison with (Zheng *et al.* 2018) method, (He *et al.*2020) method, (Yang *et al.*2019) method and (Huang *et al.*2021) method. To start with, two distinct grating-angle ambiguity cases are considered for the illustration of the estimation results of the proposed method. Case 1: $M = 3$ incoming emitter signals from directions $\theta_1 = 12.37^{\text{o}}, \theta_2 = 37.92^{\text{o}}$ and $\theta_3 = 64.16^{\text{o}}$. Case 2: $M = 5$ incoming emitter signals that are closely spaced in directions $\theta_1 = 12.37^{\text{o}}, \theta_2 = 28.00^{\text{o}}, \theta_3 = 32.00^{\text{o}}$ $\theta_4 = 37.92^{\text{o}}$ and $\theta_5 = 64.16^{\text{o}}$ impinging on a UCLA having $N = 11$ elements $(N_1 = 5, N_2 = 7)$ under SNR of 10 dB and $K = 200$ snapshots.

For case 1 and case 2, the polynomial $f(z)$ in Equation (4.7) results in $2r = 116$ roots as $\{z_p\}_{p=1}^{58}$ and $\{1/z_p^*\}_{p=1}^{58}$. Table 4.2, for case 1, shows $\{z_p\}_{p=1}^{4}$ roots among $\{z_p\}_{p=1}^{58}$ as closer to the unit circle with the largest magnitude ($|z_p| \cong 1$). Table 4.3 shows, for case 2, $\{z_p\}_{p=1}^{6}$ roots among $\{z_p\}_{p=1}^{58}$ as closer to the unit circle with the largest magnitude and it is referred to as RoI (Roots of Interest). Among the RoI, signal roots such as $\{z_m\}_{m=1}^{3}$ and $\{z_m\}_{m=1}^{5}$ of case 1 and case 2 respectively yields a higher value for the maximum signal power function $p(z_p)$ with $\delta\theta = 0.01$. As a result, the DOA of the emitter signals that are obtained using Equation (4.15) shows the proposed method successfully estimating the true DOAs without ambiguity for both the cases taken into consideration.

Table 4.2 The proposed method's DOA estimation result for case 1

Case 1 : $\theta_1 = 12.37^o$, $\theta_2 = 37.92^o$ and $\theta_3 = 64.16^o$					
$\{z_p\}_{p=1}^{58}$	RoI $\{z_p\}_{p=1}^{4}$				Remaining Roots
	$0.7805 - 0.6218i$	$-0.3478 - 0.9368i$	$-0.9503 - 0.3096i$	$-0.0009 - 0.9982i$	$\{z_p\}_{p=5}^{58}$
$\lvert z_p \rvert$	0.9979	0.9993	0.9995	0.9982	< 0.85
$s(z_p)$	0.9963	0.9998	0.6132	0.4504	< 0.4145
$s''(z_p)$	0.9960	0.9602	0.6836	0.4851	< 0.5491
$p(z_p)$	0.9924	0.9601	0.4192	0.2185	< 0.2417
$\{\hat{\theta}_m\}_{m=1}^{3}$	12.36^o	37.81^o	64.12^o	NA*	NA*

Table 4.3 The proposed method's DOA estimation result for case 2

Case 2: $\theta_1 = 12.37^o, \theta_2 = 28.00^o, \theta_3 = 32.00^o,$ $\theta_4 = 37.92^o$ and $\theta_5 = 64.16^o$							
$\{z_p\}_{p=1}^{58}$	RoI $\{z_p\}_{p=1}^{6}$						Remaining Roots
	$0.7782 - 0.6266i$	$0.0947 - 0.9937i$	$0.0082 - 0.9981i$	$-0.0933 - 0.9899i$	$-0.3478 - 0.9368i$	$-0.9446 - 0.3134i$	$\{z_p\}_{p=7}^{58}$
$\lvert z_p \rvert$	0.9991	0.9982	0.9981	0.9943	0.9993	0.9952	< 0.80
$s(z_p)$	0.9739	0.8155	0.6121	0.5772	0.9991	0.8821	< 0.5647
$s''(z_p)$	0.9921	0.7808	0.4917	0.9792	0.9821	0.5951	< 0.6590
$p(z_p)$	0.9663	0.6368	0.3010	0.5652	0.9813	0.5250	< 0.3721
$\{\hat{\theta}_m\}_{m=1}^{5}$	12.46^o	28.01^o	NA*	32.00^o	37.81^o	63.99^o	NA*

* Not applicable

4.4.1 Reliability Comparison

For the demonstration of the reliability of the improved polynomial rooting-based DOA estimation method, 10 unbiased simulation trials were carried out under the consideration of $N = 11$, SNR $= 10$ dB and $K = 200$. For case 1, Figure 4.1 (c) shows the proposed method successfully resolving the ambiguity problem and resulting in a consistent estimate of true DOAs in contrast to the methods suggested by (Zheng *et al.* 2018; He *et al.*2020) which fail to resolve and result in an inconsistent estimate of true DOAs as it can be seen from Figure 4.1 (a) and Figure 4.1 (b). It is noted that the proposed method's results accord with the results of the methods (Yang *et al.*2019; Huang *et al.*2021). However, the methods suggested by (Yang *et al.*2019; Huang *et al.*2021) result in an ambiguous estimate of true DOAs for case 2 as shown in Figure 4.2 (a) and Figure 4.2 (b), whereas the proposed method successfully resolves the closely spaced emitter signal DOAs and results in a

consistent estimate of true DOAs without ambiguity as it can be seen from Figure 4.2 (c).

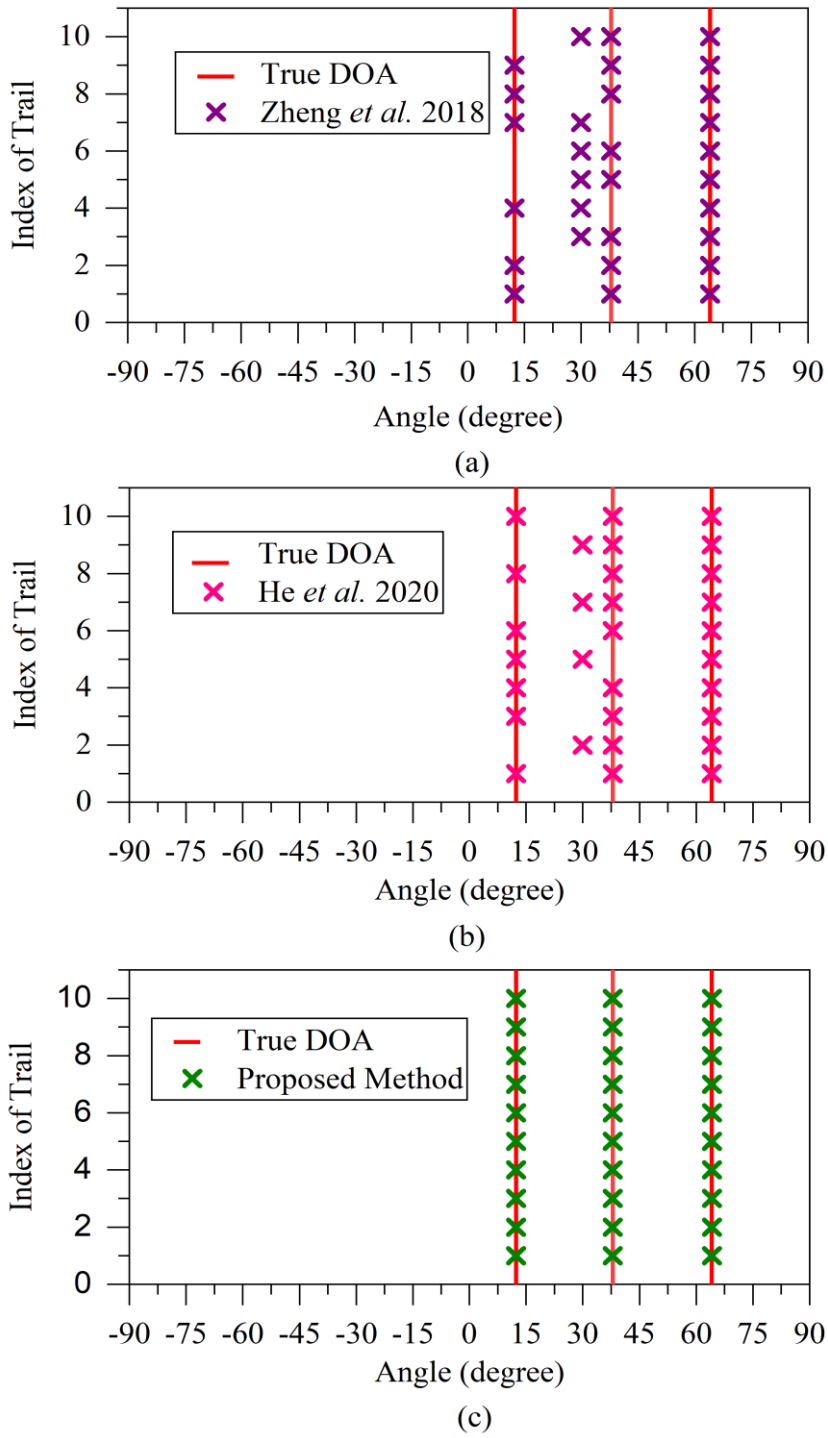

Figure 4.1 Reliability comparison for case 1 : (a) Zheng *et al.*2018 method (b) He *et al.*2020 method (c) Proposed method

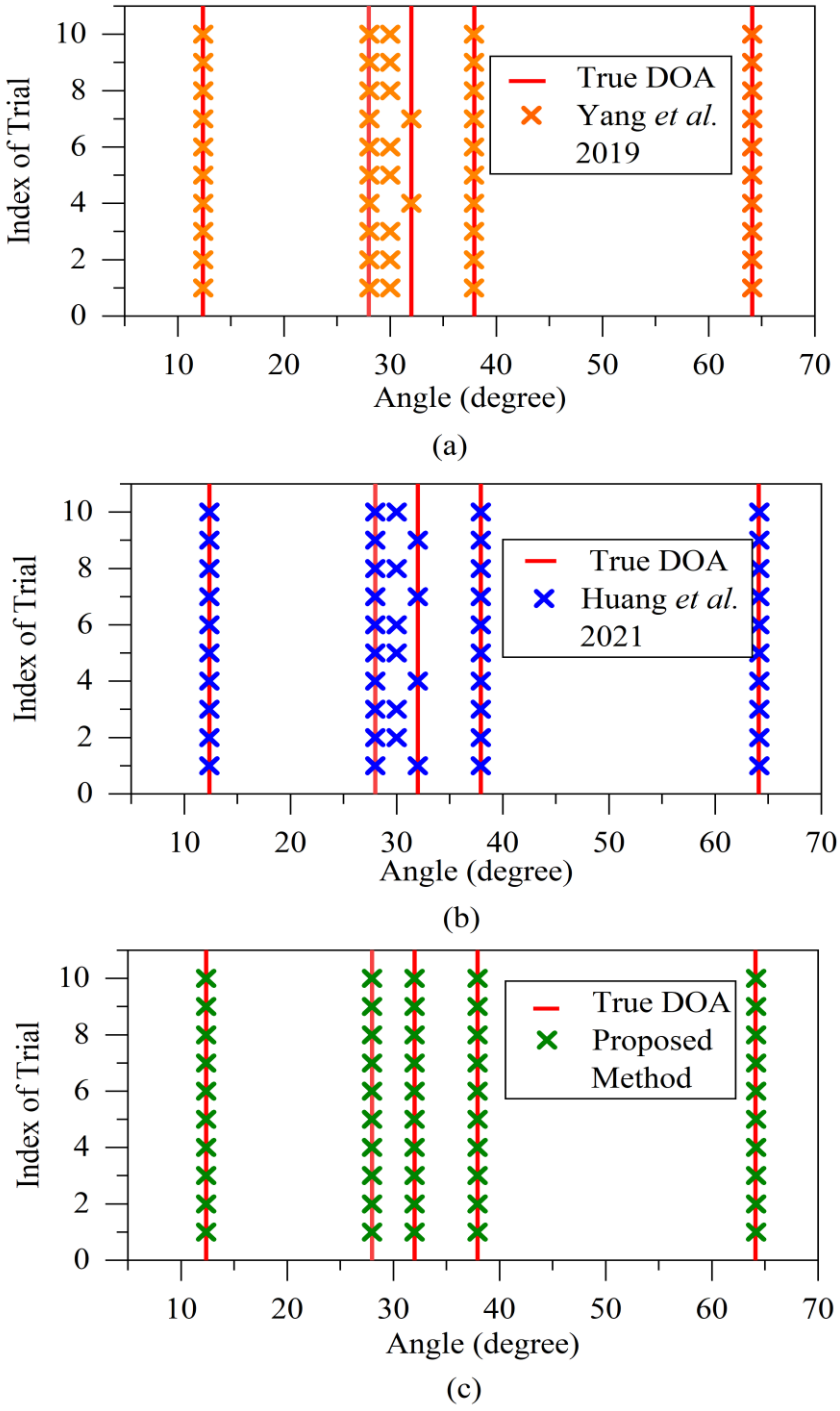

Figure 4.2 Reliability comparison for case 2 : (a) Yang *et al.*2019 method (b) Huang *et al.*2021 method (c) Proposed method

4.4.2 Estimation Accuracy

The estimation accuracy of the proposed method is assessed against the methods in (Zheng *et al.* 2018; He *et al.*2020) and (Yang *et al.*2019;

Huang *et al.*2021) for case 2 using root mean square error (RMSE) under different SNR and number of snapshots variations. For $Q = 500$ Monte-Carlo simulation trails, RMSE is evaluated for different SNR variations i.e., 0 dB $\leq$ SNR$\leq$ 15 dB with $K = 200$ fixed number of snapshots.

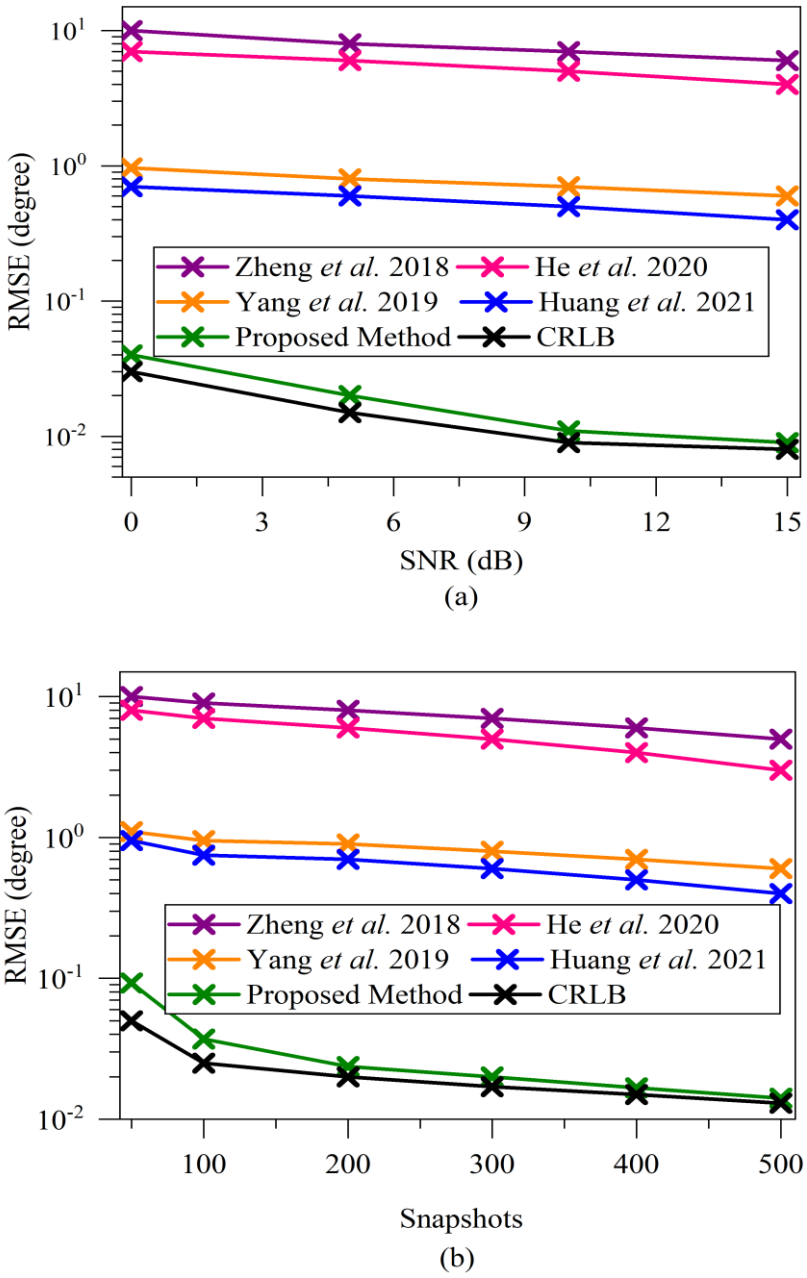

Figure 4.3 (a) RMSE comparison versus SNR (b) RMSE comparison versus the number of snapshots

Figure 4.3 (a) shows the proposed method exhibiting better estimation accuracy compared to the methods (Zheng *et al.* 2018; He *et al.*2020; Yang *et al.*2019; Huang *et al.*2021). It also closely follows the limits of the CRLB even at low SNR. Similarly, RMSE is also evaluated for a different number of snapshot variations i.e., $50 \leq K \leq 500$ with SNR $= 0$ dB fixed. Figure 4.3 (b) shows the proposed method exhibiting better estimation accuracy compared to the methods in (Zheng *et al.* 2018; He *et al.*2020; Yang *et al.*2019; Huang *et al.*2021). Furthermore, it closely follows the limits of the CRLB even at a lower number of snapshots.

4.4.3 Angular Resolution

The angular resolution capability of the proposed method is assessed against the methods suggested by (Yang *et al.*2019; Huang *et al.*2021) using the resolving probability for different angular separations. Considering two closely distributed emitters in case 2 such as $\{12.37^{o}, 30.00^{o} - \Delta\theta, 30.00^{o} + \Delta\theta, 37.92^{o}, 64.16^{o}\}$, where $\Delta\theta$ is the angular separation. The resolving probability is given by Q_s'/Q, where Q_s' is the number of successful detections of true DOAs satisfying the condition given as follows

$$max\left\{\left|\hat{\theta}_1 - \theta_1\right|, \left|\hat{\theta}_2 - \theta_2\right|, \left|\hat{\theta}_3 - \theta_3\right|, \left|\hat{\theta}_4 - \theta_4\right|, \left|\hat{\theta}_5 - \theta_5\right|\right\} < \frac{\Delta\theta}{2} \quad (4.16)$$

where Q is the total number of Monte-Carlo simulation trials. Here, resolving probability is evaluated for angular separation $(\Delta\theta)$ with variations from 0.1^{o} to 3.0^{o} in steps of 0.2^{o}. Figure 4.4 shows the proposed method exhibiting better resolution capability compared to the methods proposed by (Yang *et al.*2019; Huang *et al.*2021) in the range of $0.1^{o} \leq \Delta\theta \leq 1.5^{o}$.

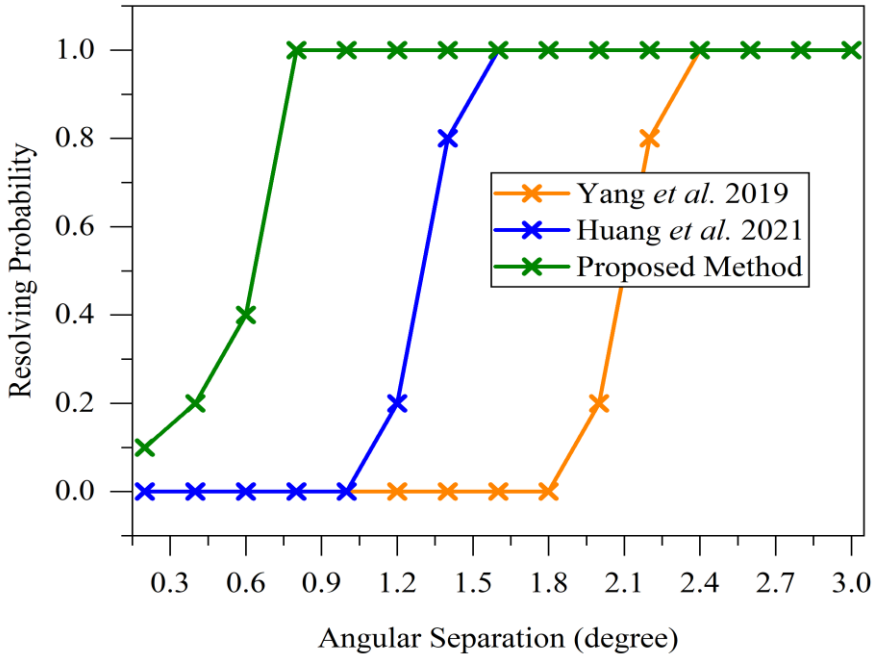

Figure 4.4 Resolving probability comparison versus angular separation

4.4.4 Complexity Analysis

Assessment of the computational complexity has been made using the number of complex multiplications involved. The proposed method involves estimation of the array covariance matrix, eigenvalue decomposition (EVD) and finding signal roots with complexities that are $O(N^2K)$, $O(N^3)$ and $O(rN^2)$ respectively. Details of the computational complexity comparison of the proposed method and the methods proposed by (Yang *et al.*2019; Huang *et al.*2021) are given in Table 4.4. Complexity has been evaluated for a varying number of array elements i. e., $6 \leq N \leq 20$ with fixed $K = 200$ snapshots for the consideration of $M = 3$, search step $sch = 0.01$ and $J = 4$ (Yang *et al.*2019; Huang *et al.*2021). Similarly, complexity has been evaluated for a varying number of snapshots i. e., $20 \leq K \leq 500$ with $N = 11$ fixed number of array elements. Figure 4.5 (a) and Figure 4.5 (b) show the proposed method involving less computational complexity compared to the methods in (Yang *et al.*2019; Huang *et al.*2021).

Table 4.4 Computational complexity comparison

Method	Computational Complexity
Yang *et al.*2019	$O(N^2K + N^3 + \frac{180^{o}}{sch}N(N-M) + JN^2)$
Huang *et al.*2021	$O(N^2K + N^3 + (2N-1)^3 + JN^2)$
Proposed Method	$O(N^2K + N^3 + rN^2)$

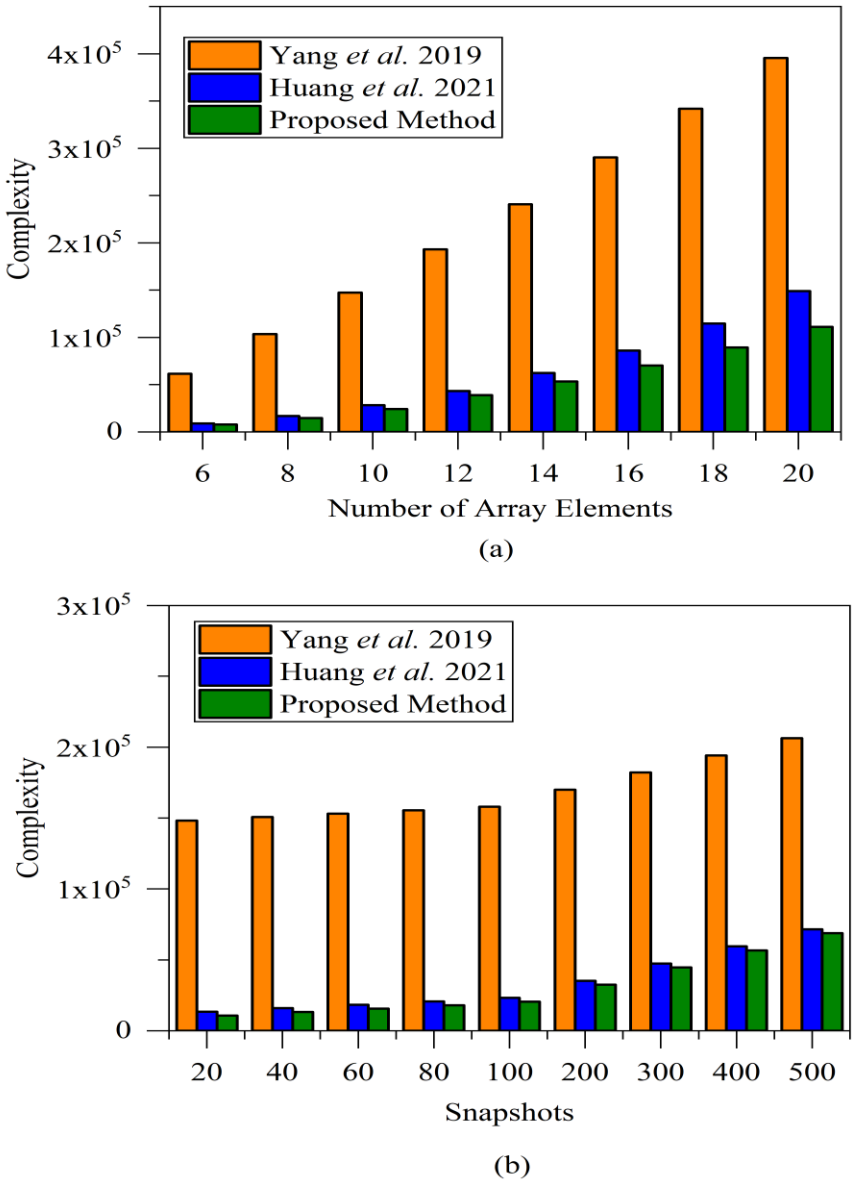

Figure 4.5 (a) Complexity comparison versus the number of array elements (b) Complexity comparison versus the number of snapshots

4.5 SUMMARY

The proposed method aims at providing high-resolution unambiguous DOA estimation with UCLA. The proposed improved polynomial rooting-based method involves a maximum signal power function based on spatial filtering and second-order differential for the selection of the signal roots that are associated with true DOAs over ambiguous roots obtained from the polynomial function. The proposed method overcomes the grating-angle ambiguity and estimates the true DOAs successfully with improved estimation performance. The analysis and simulation findings show the superiority and effectiveness of the proposed method over the existing methods in terms of estimation reliability, estimation accuracy, angular resolution and computational complexity.

CHAPTER 5

COMPUTATIONALLY EFFICIENT UNAMBIGUOUS DOA ESTIMATION BASED ON SUPPORT VECTOR REGRESSION

5.1 INTRODUCTION

In this chapter, a computationally efficient DOA estimation method based on support vector regression (SVR) has been proposed for addressing the ambiguity problem associated with the GCLA and UCLA. As discussed in the previous chapters, the estimation performances in terms of reliability, accuracy and angular resolution of the existing subarray-based methods (Zhou *et al.*2013; Sun *et al.*2015; Zhang *et al.* 2017; Liu *et al.* 2018; Yan *et al.* 2018**)**, adjoined subarray-based methods (Zheng *et al.* 2018; He *et al.*2020) and beamforming-like methods (Yang *et al.*2019; Huang *et al.*2021) degrade in the ambiguity problem situation of GCLA and UCLA. Furthermore, the aforementioned methods entail high computational complexity and execution time.

The problem of DOA estimation can be approached as a non-linear approximation wherein the non-linear function has to be approximated that maps the array output received vector and DOA of the incoming source signals. This can be accomplished effectively through learning-based methods wherein the radial basis-function neural network (RBFNN) (El Zooghby *et al.*2000; Sun *et al.*2018; Liu *et al.*2018) and support vector regression (SVR) (El Gonnouni *et al.*2012; Randazzo *et al.*2007; Tarkowski *et al.*2019; Wu *et*

*al.*2019) performs comparably better than the subspace-based methods with reduced computational complexity. The RBFNN is one of the simplest types of a neural network with only one hidden layer and each neuron in the hidden layer consists of the RBF activation function. It also involves trial-and-error procedures in the determination of the number of hidden neurons (Wu *et al.*2019; Liu 2020). Compared to RBFNN, the SVR-based methods for DOA estimation are relatively simple to implement and have good generalization capabilities that offer better estimation performances with less computational complexity. As a result, the SVR-based methods for DOA estimation are considered as the most promising and well-experimented learning-based method.

In the existing SVR-based formulations, the array covariance matrix mapped to its corresponding DOA of the incoming source signals is approximated using SVR. The foremost limitation of the existing SVR-based methods is that as the number of sources varies, its overall performance severely degrades or even fails to work (Chen *et al.* 2020). It also requires a multiple regression model for the estimation of the DOAs in the case of more than one incoming source signal. This increases the training complexity and makes it cumbersome in considering all possible sources with different angular separations (Elbir 2020). Moreover, the generalization of the existing SVR formulation is not guaranteed in the varying number of incoming source signals. This leads to the failure of the models presented in (El Gonnouni *et al.*2012; Randazzo *et al.*2007; Tarkowski *et al.*2019; Wu *et al.*2019) in the detection and estimation of the true DOAs and imposes constraints on achieving the full DOF.

To overcome the aforementioned limitations of the existing formulations, a modified formulation is proposed which approximates the unknown regression function that maps the signal subspace eigenvectors with

its associated DOA of the incoming source signals using SVR. The proposed formulation uses only one regression model for the estimation of multi-source DOAs without increasing the training complexity. It also offers good generalization in the varying number of source signals situation and results in the achievement of full DOF with reduced complexity compared to the existing SVR-based methods. Numerous simulations are presented in comparison with existing methods to show the superiority and efficacy of the proposed method in terms of estimating reliability, estimation accuracy, DOF, and complexity analysis.

5.2 PROPOSED METHOD FOR DOA ESTIMATION WITH GCLA

Consider, $M\ (M < N)$ far-field source signals from directions $\Theta = \{\theta_m\}_{m=1}^{M}$ impinging on N element GCLA with the field-of-view (FOV) such that $\theta_m \in (-90^o, +90^o)$ as shown in Figure 2.4 of chapter 2. Then, the observed array output received signal vector by i^{th}subarray of GCLA can be expressed as

$$\mathbf{x}_i\ (t) = \mathbf{A}_i\ \mathbf{s}(t) + \mathbf{n}_i(t) \quad ; \quad i = 1,2 \tag{5.1}$$

where $\mathbf{x}_1(t) \in \mathbb{C}^{N_1 \mathrm{x}\ 1}$ and $\mathbf{x}_2(t) \in \mathbb{C}^{N_2 \mathrm{x}\ 1}$ represents the received output vector of subarray 1 and subarray 2 of GCLA. Here, $\mathbf{A}_i$ represents the array directional matrix of i^{th}subarray and for each subarray, it is given by

$$\mathbf{A}_1 = [\mathbf{a}_1(\theta_1)\ \ \mathbf{a}_1(\theta_2) \ldots\ \mathbf{a}_1(\theta_M)\ ] \in \mathbb{C}^{N_1 \mathrm{x}\ M} \tag{5.2}$$

$$\mathbf{A}_2 = [\mathbf{a}_2(\theta_1)\ \ \mathbf{a}_2(\theta_2) \ldots\ \mathbf{a}_2(\theta_M)\ ] \in \mathbb{C}^{N_2 \mathrm{x}\ M} \tag{5.3}$$

where $\mathbf{a}_1(\theta_m)$ and $\mathbf{a}_2(\theta_m)$ represents the array directional vector of subarray 1 and subarray 2 and it is given by

$$\mathbf{a}_1(\theta_m) = \left[1, e^{-j\pi N_2 \sin(\theta_m)}, \ldots, e^{-j\pi N_2 (N_1-1) \sin(\theta_m)}\right]^T \in \mathbb{C}^{N_1 \mathrm{x}\, 1} \quad (5.4)$$

$$\mathbf{a}_2(\theta_m) = \left[1, e^{-j\pi N_1 \sin(\theta_m)}, \ldots, e^{-j\pi N_1 (N_2-1) \sin(\theta_m)}\right]^T \in \mathbb{C}^{N_2 \mathrm{x}\, 1} \quad (5.5)$$

Then, the observed array output received signal vector of GCLA can be expressed as follows

$$\mathbf{x}_1(t) = \begin{bmatrix} 1 & 1 & & 1 \\ e^{-jN_2\pi \sin(\theta_1)} & e^{-jN_2\pi \sin(\theta_2)} & \cdots & e^{-jN_2\pi \sin(\theta_M)} \\ \vdots & \vdots & & \vdots \\ e^{-jN_2(N_1-1)\pi \sin(\theta_1)} & e^{-jN_2(N_1-1)\pi \sin(\theta_2)} & & e^{-jN_2(N_1-1)\pi \sin(\theta_M)} \end{bmatrix} \begin{bmatrix} \mathrm{s}_1(t) \\ \mathrm{s}_2(t) \\ \vdots \\ \mathrm{s}_M(t) \end{bmatrix} + \begin{bmatrix} n_{1,0}(t) \\ n_{1,1}(t) \\ \vdots \\ n_{1,N_1-1}(t) \end{bmatrix} = \mathbf{A}_1\mathbf{s}(t) + \mathbf{n}_1(t) \quad (5.6)$$

$$\mathbf{x}_2(t) = \begin{bmatrix} 1 & 1 & & 1 \\ e^{-jN_1\pi \sin(\theta_1)} & e^{-jN_1\pi \sin(\theta_2)} & \cdots & e^{-jN_1\pi \sin(\theta_M)} \\ \vdots & \vdots & & \vdots \\ e^{-jN_1(N_2-1)\pi \sin(\theta_1)} & e^{-jN_1(N_2-1)\pi \sin(\theta_2)} & & e^{-jN_1(N_2-1)\pi \sin(\theta_M)} \end{bmatrix} \begin{bmatrix} \mathrm{s}_1(t) \\ \mathrm{s}_2(t) \\ \vdots \\ \mathrm{s}_M(t) \end{bmatrix} + \begin{bmatrix} n_{2,0}(t) \\ n_{2,1}(t) \\ \vdots \\ n_{2,N_2-1}(t) \end{bmatrix} = \mathbf{A}_2\mathbf{s}(t) + \mathbf{n}_2(t) \quad (5.7)$$

Here, $\mathbf{s}(t) = \left[s_1(t)\ s_2(t) \ldots\ s_M(t)\right]^T \in \mathbb{C}^{M \mathrm{x}\, 1}$ represents the incoming source signal vector, $\mathbf{n}_1(t) \in \mathbb{C}^{N_1 \mathrm{x}\, 1}$ and $\mathbf{n}_2(t) \in \mathbb{C}^{N_2 \mathrm{x}\, 1}$ represents the zero-mean additive white noise of subarray 1 and subarray 2 with covariance $\mathrm{E}\{\mathbf{n}_i(t)\mathbf{n}_i^H(t)\} = \sigma_{\mathbf{n}_i}^2 \mathbf{I}_i$, $i = 1,2$, where $\sigma_{\mathbf{n}_i}^2$ is the noise power and $\mathbf{I}_i$ is the identity matrix (Vaidyanathan *et al.* 2011). The proposed method aims at the resolution of the ambiguity problem in DOA estimation through

the approximation of the unknown non-linear function that maps the signal subspace eigenvectors with the DOA of the incoming source signals. The co-prime property makes the space spanned by signal subspace eigenvectors and directional vectors associated with true DOAs to be the same. The distinct training pairs comprise signal subspace eigenvectors and its associated DOAs allow the mapping processing feasible. The proposed method involves pre-processing, training, and testing (estimation) phase.

5.2.1 Pre-Processing Phase

In the pre-processing phase, the estimated array covariance matrix of the output signal vector from individual subarrays $\widehat{\mathbf{R}}_{\mathbf{x}_1\mathbf{x}_1}$, $\widehat{\mathbf{R}}_{\mathbf{x}_2\mathbf{x}_2}$ and between the subarrays $\widehat{\mathbf{R}}_{\mathbf{x}_1\mathbf{x}_2}$, $\widehat{\mathbf{R}}_{\mathbf{x}_2\mathbf{x}_1}$ of GCLA with K snapshots can be expressed as

$$\widehat{\mathbf{R}}_{\mathbf{x}_u\mathbf{x}_v} = E\{\mathbf{x}_u(t)\mathbf{x}_v{}^H(t)\} = \frac{1}{K}\sum_{t=1}^{K}\mathbf{x}_u(t)\,\mathbf{x}_v{}^H(t)\,;\;\; u,v \in \{1,2\} \qquad (5.8)$$

Using Equation (5.8), the total estimated array covariance matrix of GCLA can be constructed and it is given by

$$\widehat{\mathbf{R}}_{\mathbf{x}} = \begin{bmatrix} \widehat{\mathbf{R}}_{\mathbf{x}_1\mathbf{x}_1} & \widehat{\mathbf{R}}_{\mathbf{x}_1\mathbf{x}_2} \\ \widehat{\mathbf{R}}_{\mathbf{x}_1\mathbf{x}_2} & \widehat{\mathbf{R}}_{\mathbf{x}_2\mathbf{x}_2} \end{bmatrix} \in \mathbb{C}^{N\,\mathrm{x}\,N} \qquad (5.9)$$

The eigenvalue decomposition (EVD) of $\widehat{\mathbf{R}}_{\mathbf{x}}$ yields $\widehat{\mathbf{R}}_{\mathbf{x}} = \widehat{\mathbf{U}}_s\,\widehat{\mathbf{D}}_s\widehat{\mathbf{U}}_s^H + \widehat{\mathbf{U}}_n\,\widehat{\mathbf{D}}_n\,\widehat{\mathbf{U}}_n^H$ where $\widehat{\mathbf{U}}_s \triangleq [\mathbf{u}_1, \mathbf{u}_2, \ldots, \mathbf{u}_M] \in \mathbb{C}^{N\,\mathrm{x}\,M}$ and $\widehat{\mathbf{U}}_n \triangleq [\mathbf{u}_{M+1}, \mathbf{u}_{M+2}, \ldots, \mathbf{u}_N]\ \mathbb{C}^{N\,\mathrm{x}\,N-M}$ contains the signal- and noise-subspace eigenvectors of $\widehat{\mathbf{R}}_{\mathbf{x}}$ corresponding to the eigenvalues in the diagonal matrix $\widehat{\mathbf{D}}_s \triangleq \mathrm{diag}\{\lambda_1, \lambda_2, \ldots, \lambda_M\}$ and $\widehat{\mathbf{D}}_n \triangleq \mathrm{diag}\{\lambda_{M+1}, \lambda_{M+2}, \ldots, \lambda_N\}$. Alternatively, the signal subspace eigenvectors associated with the DOA of the incoming source signals are computed from the total array covariance

matrix $\widehat{\mathbf{R}}_{\mathbf{x}}$ using a linear operator termed propagator $\mathbf{P}$ (Meng *et al.* 2019)**.**

The total array directional matrix $\mathbf{A} \in \mathbb{C}^{N \times M}$ of GCLA is partitioned into two block matrices $\mathbf{A}_1 \in \mathbb{C}^{M \times M}$ and $\mathbf{A}_2 \in \mathbb{C}^{(N-M) \times M}$ as

$$\mathbf{A} = \begin{bmatrix} \mathbf{A}_1 \\ \mathbf{A}_2 \end{bmatrix} \tag{5.10}$$

Here, the linear relationship exists between $\mathbf{A}_1$ and $\mathbf{A}_2$ can be given by

$$\mathbf{P}\mathbf{A}_1 = \mathbf{A}_2 \tag{5.11}$$

The propagator $\mathbf{P}$ is determined by minimizing the cost function $||\mathbf{A}_2 - \mathbf{A}_1\widehat{\mathbf{P}}||^2$ and the resulting solution is $= (\mathbf{A}_1{}^H\mathbf{A}_1)^{-1}\mathbf{A}_1{}^H\mathbf{A}_2$. However, information relating to the total array directional matrix $\mathbf{A}$ of the incoming source signals is not known. As a result, the propagator $\mathbf{P}$ is estimated from the estimated total array covariance matrix $\widehat{\mathbf{R}}_{\mathbf{x}}$ and it can be represented as $\widehat{\mathbf{R}} = [\mathbf{G} \;\; \mathbf{H}]$ where $\mathbf{G} = \widehat{\mathbf{R}}(:, 1{:}M)$ and $\mathbf{H} = \widehat{\mathbf{R}}(:, M+1{:}N)$. Based on this, the cost function is now reformulated as $||\mathbf{H} - \mathbf{G}\widehat{\mathbf{P}}||^2$, then the propagator $\widehat{\mathbf{P}}$ can be obtained by minimizing the cost function and the resulting solution is given by

$$\widehat{\mathbf{P}} = (\mathbf{G}^H\mathbf{G})^{-1}\mathbf{G}^H\mathbf{H} \tag{5.12}$$

Now, defining a $\mathbf{U}_s \in \mathbb{C}^{N \times M}$ matrix using $\widehat{\mathbf{P}}$ is given by

$$\mathbf{U}_s = \begin{bmatrix} \mathbf{I}_M \\ \widehat{\mathbf{P}}^H \end{bmatrix} \tag{5.13}$$

Combining Equation (5.11) and Equation (5.13) results $\mathbf{U}_s\mathbf{A}_1 = [\mathbf{I}_M \;\; \widehat{\mathbf{P}}^H]^T\mathbf{A}_1 = [\,\mathbf{A_1} \;\; \mathbf{A_2}\,]^T = \mathbf{A}$. Here, the space spanned by $\mathbf{U}_s \in \mathbb{C}^{N \times M}$ and $\mathbf{A} \in \mathbb{C}^{N \times M}$ are same (Wang *et al.*2013). The signal subspace eigenvectors

associated with the source signals are the columns of $\mathbf{U}_s \in \mathbb{C}^{N \times M}$ such that $\mathbf{u}_s \in \mathbb{C}^{N \times 1}$.

5.2.2 Training Phase

The training phase is an offline process in which the DOA estimation model $\hat{F}: \mathbf{u}_s \rightarrow \theta$ is obtained from the available training pairs through the process of learning. The generated L set of training pairs utilized for learning is given by $\{(\mathbf{u}_s^1, \theta_1), (\mathbf{u}_s^2, \theta_2), .., (\mathbf{u}_s^l, \theta_l), .., (\mathbf{u}_s^L, \theta_L)\}$. The total array covariance matrix $\widehat{\mathbf{R}}_{\mathbf{x}}^l$ is computed for each angle θ_l that is uniformly distributed in the range -90^o to $+90^o$ i.e., $\theta_l = -90^o + (l-1)\Delta\theta, l = 1,2,\ldots L$ for the acquisition of the training set, where $\Delta\theta$ is the angular separation. Then, the signal subspace eigenvector $\mathbf{u}_s^l$ for each angle θ_l is computed from the corresponding total array covariance matrix $\widehat{\mathbf{R}}_{\mathbf{x}}^l$ using Equation (5.13). The SVR model learns using the given training set is defined as

$$\hat{F}(\mathbf{u}_s) = \langle \mathbf{w}, \phi(\mathbf{u}_s) \rangle + b \tag{5.14}$$

where $\langle ., . \rangle$ indicates the inner product, $\mathbf{w}$ represents the orientation of the regression, b represents the position of the regression, ϕ is a non-linear transformation function that maps the input vector $\mathbf{u}_s$ from its original space to a higher-dimensional space termed Hilbert space (HS). In the testing (estimation) phase, the generalization capabilities of the model in the estimation of the unknown DOAs (not included in the training phase) are decided by the parameters $\mathbf{w}$ and b. It can be computed by minimizing the regression risk R_{reg} (Smola *et al.*2004) and it is given by

$$min\ R_{reg} = C \sum_{i=1}^{L} l_\varepsilon(\mathbf{u}_s^i, \theta_i) + \frac{1}{2} \parallel \mathbf{w} \parallel^2 \tag{5.15}$$

where C denotes the regularization constant and $l_\varepsilon(\mathbf{u}_s^i, \theta_i)$ denotes the ε-insensitive cost function that specifies the margin of allowable error during the training process (Smola *et al.*2004) and it is given by

$$l_\varepsilon(\mathbf{u}_s^i, \theta_i) = \begin{cases} 0 & ; \quad \left|\theta_i - \hat{F}(\mathbf{u}_s^i)\right| < \varepsilon \\ |\theta_i - \hat{F}(\mathbf{u}_s^i)| - \varepsilon & ; \quad otherwise \end{cases} \tag{5.16}$$

where ε is the limit of allowable error. According to the Vapnik theory (Vapnik *et al.*1997), by introducing Lagrange multipliers, the primal optimization problem (minimization problem) in Equation (5.15) can be recast into a dual optimization problem and the optimal solution can be obtained based on the Karush – Kuhn – Tucker (KKT) conditions. The KKT conditions for the primal optimization problem can be given as follows

$$\frac{\partial R_{reg}}{\partial \mathbf{w}} = \mathbf{w} - \sum_{i=1}^{L} (\alpha_i - \alpha_i') \phi(\mathbf{u}_s^i) = 0 \tag{5.17}$$

$$\frac{\partial R_{reg}}{\partial b} = \sum_{i=1}^{L} (\alpha_i' - \alpha_i) = 0 \tag{5.18}$$

The dual optimization problem can be given by

$$max\left\{-\varepsilon \sum_{i=1}^{L} (\alpha_i' + \alpha_i) + \sum_{i=1}^{L} \theta_i (\alpha_i' - \alpha_i) - \frac{1}{2} \sum_{i=1}^{L} (\alpha_i' + \alpha_i)(\alpha_i' - \alpha_i)\, \mathcal{K}(\mathbf{u}_s^i, \mathbf{u}_s)\right\}$$

Subject to

$$0 \le \alpha_i, \alpha_i' \le C$$

$$\sum_{i=1}^{L} (\alpha_i' - \alpha_i) = 0 \tag{5.19}$$

where $\mathcal{K}(\mathbf{u}_s^i, \mathbf{u}_s)$ represents the kernel trick and α_i, α_i' represents the Lagrange multipliers. The Gaussian radial basis kernel (Randazzo *et al.*2007) is the kernel trick used and defined as $\mathcal{K}(\mathbf{u}_s^i, \mathbf{u}_s) = \exp\left(-\gamma \parallel \mathbf{u}_s^i - \mathbf{u}_s \parallel^2\right)$ where γ is the kernel parameter. The dual optimization problem in Equation (5.19) can be solved and the Lagrange multiplier variable α_i and α_i' can be computed using standard quadratic programming (QP) techniques. Using the KKT condition, the parameter $\mathbf{w}$ can be computed and it is given as follows

$$\mathbf{w} = \sum_{i=1}^{L} (\alpha_i - \alpha_i')\phi(\mathbf{u}_s^i) \tag{5.20}$$

$$b = \sum_{i=1}^{L} \theta_i - \phi(\mathbf{u}_s^i)^T \mathbf{w} + \varepsilon \tag{5.21}$$

By substituting $\mathbf{w}$ and b in Equation (5.14), the function $\hat{F}(\mathbf{u}_s)$ can be re-written as

$$\hat{F}(\mathbf{u}_s) = \sum_{i=1}^{L} (\alpha_i - \alpha_i') \langle \phi(\mathbf{u}_s^i), \phi(\mathbf{u}_s) \rangle + b$$

$$= \sum_{i=1}^{L} (\alpha_i - \alpha_i') \mathcal{K}(\mathbf{u}_s^i, \mathbf{u}_s) + b \tag{5.22}$$

The explicit representation of the nonlinear transformation function of the input vector i. e., $\langle \phi(\mathbf{u}_s^i), \phi(\mathbf{u}_s) \rangle$ present in $\hat{F}(\mathbf{u}_s)$ can be implicitly related to the kernel trick and is given by $\langle \phi(\mathbf{u}_s^i), \phi(\mathbf{u}_s) \rangle = \mathcal{K}(\mathbf{u}_s^i, \mathbf{u}_s)$. It is important to note that the generalization capability of the proposed model depends on the hyper-parameters such as C, ε and γ. As per the rules suggested in (Cherkassky *et al.*2004) and (Randazzo *et al.*2007), the hyper-parameters are given as follows $C = 3\sigma$, $\varepsilon = 3\sigma\sqrt{\frac{\ln L}{L}}$ and $\gamma = 0.5$.

5.2.3 Testing (Estimation) Phase

In the testing (estimation) phase, the trained DOA estimation model $\hat{F}(\mathbf{u}_s)$ is used in the estimation of the unknown M DOAs $\{\hat{\theta}_m\}_{m=1}^{M}$ of the incoming source signals and it is given by

$$\{\hat{\theta}_m\}_{m=1}^{M} = \hat{F}(\mathbf{u}_s^m) \tag{5.23}$$

where $\mathbf{u}_s^m$ being the signal subspace eigenvector of the m^{th} incoming source signal and it is computed from the total array covariance matrix $\widehat{\mathbf{R}}_{\mathbf{x}}$ using Equation (5.13). Table 5.1 summarizes the stepwise processing flow of the proposed method.

Table 5.1 Stepwise processing flow of the proposed method

Training phase	
Step 1	Generate the set of L training pairs $\{(\mathbf{u}_s^1, \theta_1), (\mathbf{u}_s^2, \theta_2), .., (\mathbf{u}_s^l, \theta_l), .., (\mathbf{u}_s^L, \theta_L)\}$ using Equation (5.9)-(5.13).
Step 2	Obtain the DOA estimation model $\hat{F}(\mathbf{u}_s)$ using the set of training pairs.
Testing phase	
Step 3	Estimate the total output covariance matrix $\widehat{\mathbf{R}}_{\mathbf{x}}$ of the received signal using Equation (5.9).
Step 4	Compute the signal subspace eigenvector of the incoming source signals $\{\mathbf{u}_s^m\}_{m=1}^{M}$ from the total output covariance matrix $\widehat{\mathbf{R}}_{\mathbf{x}}$ using Equation (5.13).
Step 5	Estimate the M DOAs using the model $\{\hat{\theta}_m\}_{m=1}^{M} = \hat{F}(\mathbf{u}_s^m)$ defined Equation (5.23).

5.2.4 Simulation Results and Discussion

This section presents various simulations that compare the proposed method with methods (Zhou *et al.*2013; Zheng *et al.* 2018 and Yang *et al.*2019) for the assessment of the estimation performance in terms of reliability and accuracy. In the simulation setup, $L = 1801$ training pairs were obtained from uniformly spaced angles ranging from -90^{o} to $+90^{o}$ with the angular space of 0.1^{o}. It is noted that the DOAs involved in the testing phase are not included in the training phase. According to rules derived in (Cherkassky *et al.*2004; Randazzo *et al.*2007), the hyper-parameters are chosen as $C = 10$ and $\varepsilon = 0.06$.

5.2.4.1 Estimation reliability

Consider the pair-matching ambiguity situation having two sources $M = 2$ from the direction $\theta_1 = 10.00^{o}, \theta_2 = 39.11^{o}$ impinges on GCLA with $N = 11$ $(N_1 = 5, N_2 = 7)$ under SNR of 10 dB and a snapshot of 200. Figure 5.1 (a) shows the failure of the subarray-based method (Zhou *et al.*2013) to estimate the true DOAs consistently. In contrast, the proposed method results in a consistent estimate of true DOAs for all 25 unbiased simulation trials as shown in Figure 5.1 (b). The results of the proposed method accord with the results of the adjoined subarray-based methods (Zheng *et al.* 2018; Yang *et al.*2019) in the case of pair-matching ambiguity situations. However, in the grating-angle ambiguity situation having $M = 6$ sources from the direction $\theta_1 = 10.00^{o}, \theta_2 = 27.35^{o}, \theta_3 = 35.01^{o}, \theta_4 = 39.11^{o}, \theta_5 = 57^{o}, \theta_6 = 62^{o}$ impinges on GCLA with $N = 11$ $(N_1 = 5, N_2 = 7)$ under SNR of 10 dB and a snapshot of 200. It can be seen from Figure 5.2 (a) and Figure 5.2 (b) that the methods (Zheng *et al.* 2018; Yang *et al.*2019) fail to estimate the true DOAs consistently. In contrast, the proposed method results in

a consistent estimate of true DOAs for all the 25 unbiased simulation trails as shown in Figure 5.2 (c) by successfully overcoming the ambiguity problem.

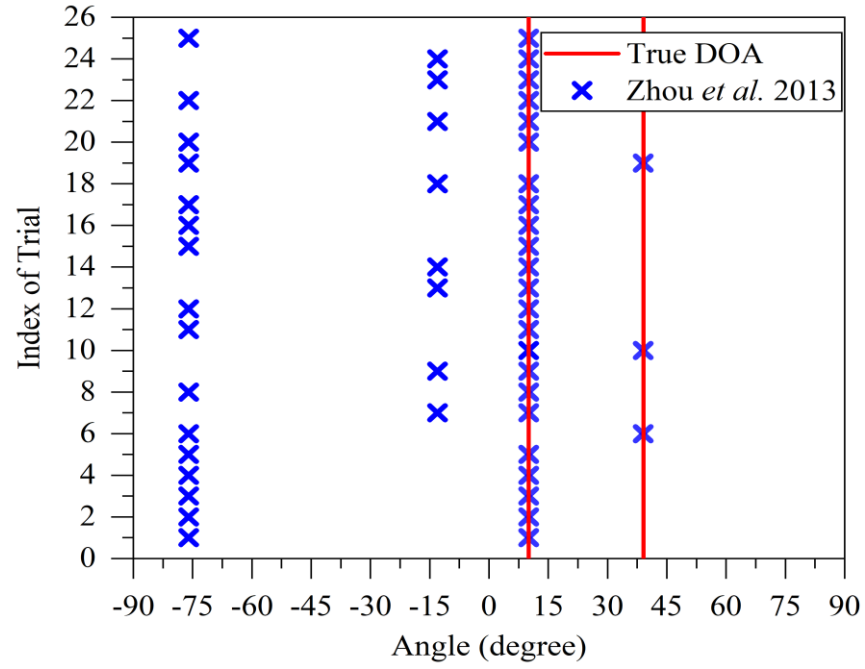

(a)

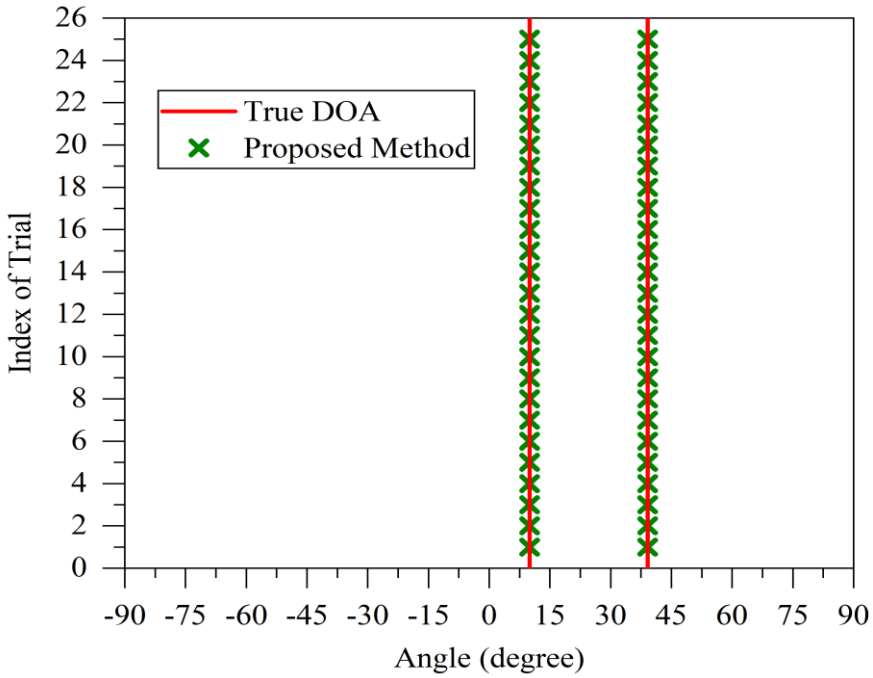

(b)

Figure 5.1 Reliability comparison in pair-matching ambiguity case : (a) Zhou *et al.*2013 method (b) Proposed method

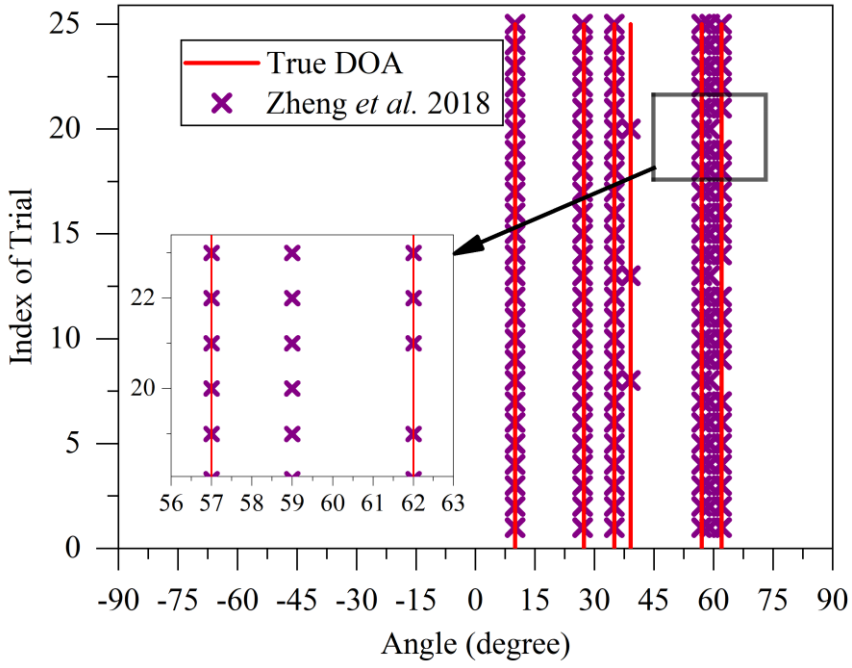

(a)

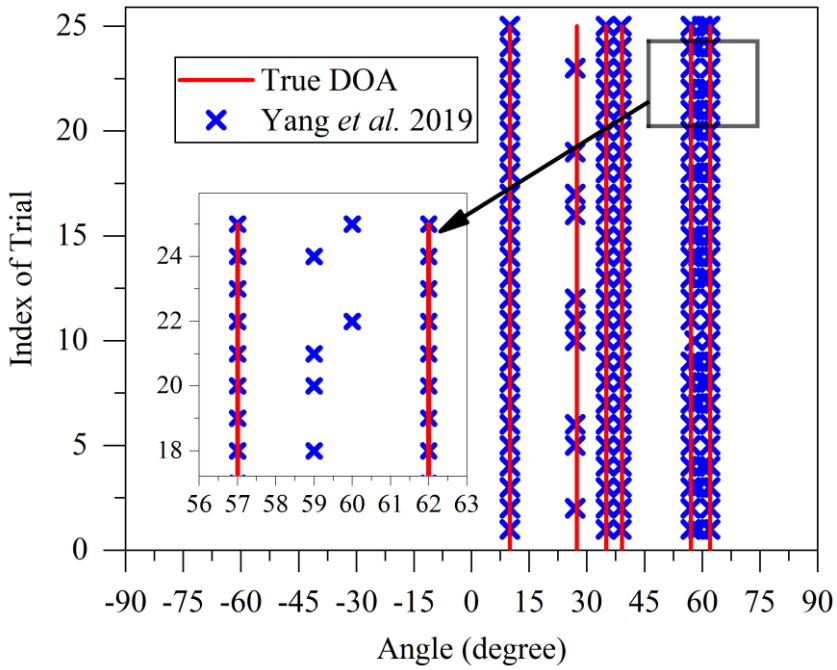

(b)

Figure 5.2 (Continued)

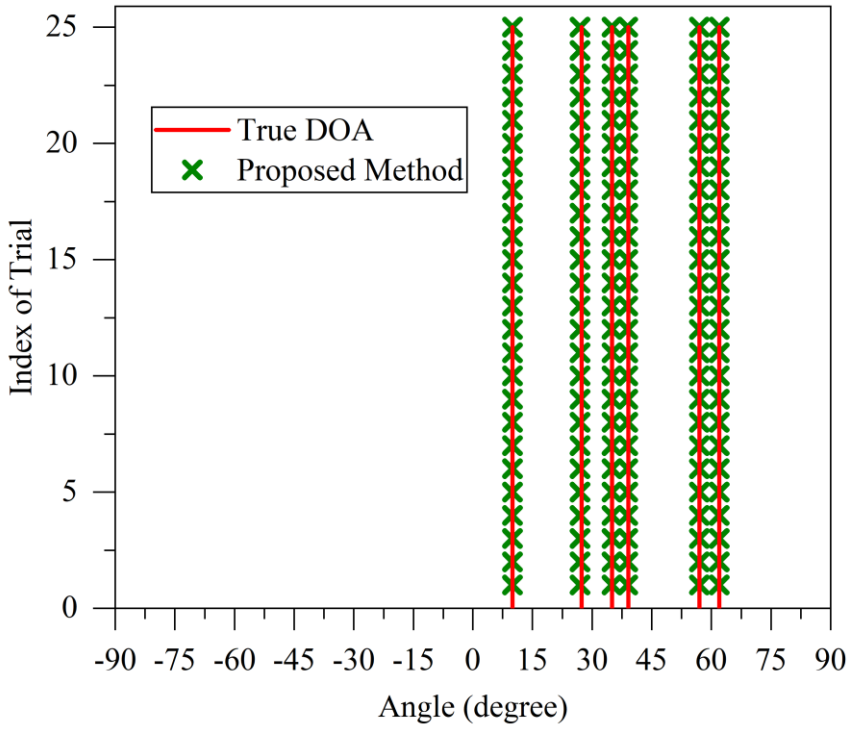

(c)

Figure 5.2 Reliability comparison in grating-angle ambiguity case: (a) Zheng *et al.* 2018 method (b) Yang *et al.*2019 method (c) Proposed method

5.2.4.2 Estimation Accuracy

Assessment of the estimation accuracy of the proposed method is made in both the ambiguity problem situation using an RMSE performance metric. For both the ambiguity situation, RMSE is evaluated for different SNR values ranging from -20 dB to 20 dB with a fixed snapshot of 200 for $Q = 500$ Monte-Carlo simulation trails. Similarly, RMSE is evaluated for varying snapshots ranging from 10 to 500 with a fixed SNR of 10 dB. Figure 5.3 and Figure 5.4 show an increase in the estimation accuracy of the proposed method with an increase in the SNR and snapshots, closely following the limits of the CRLB.

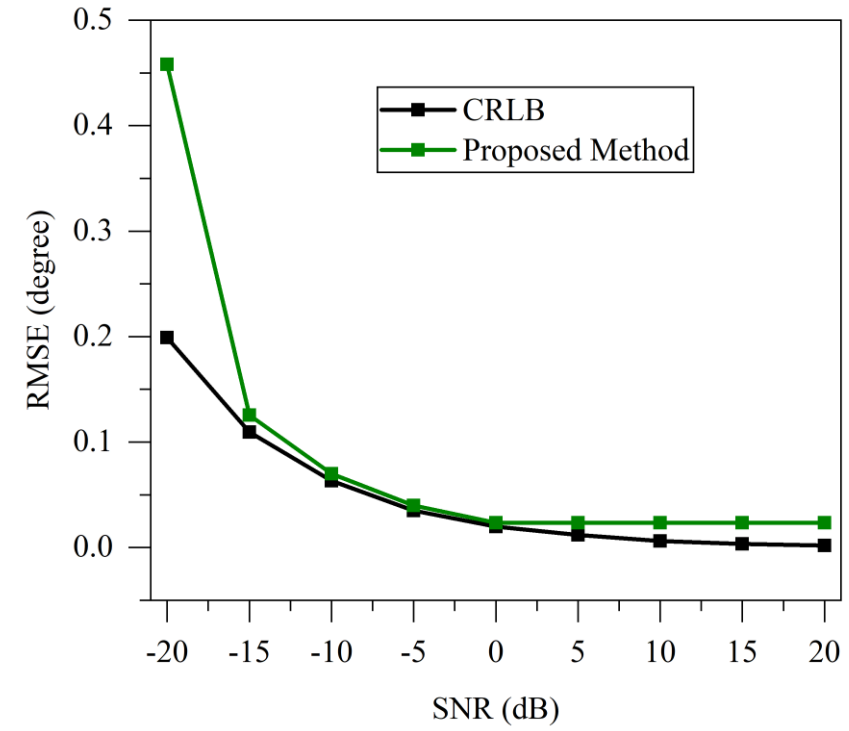

(a)

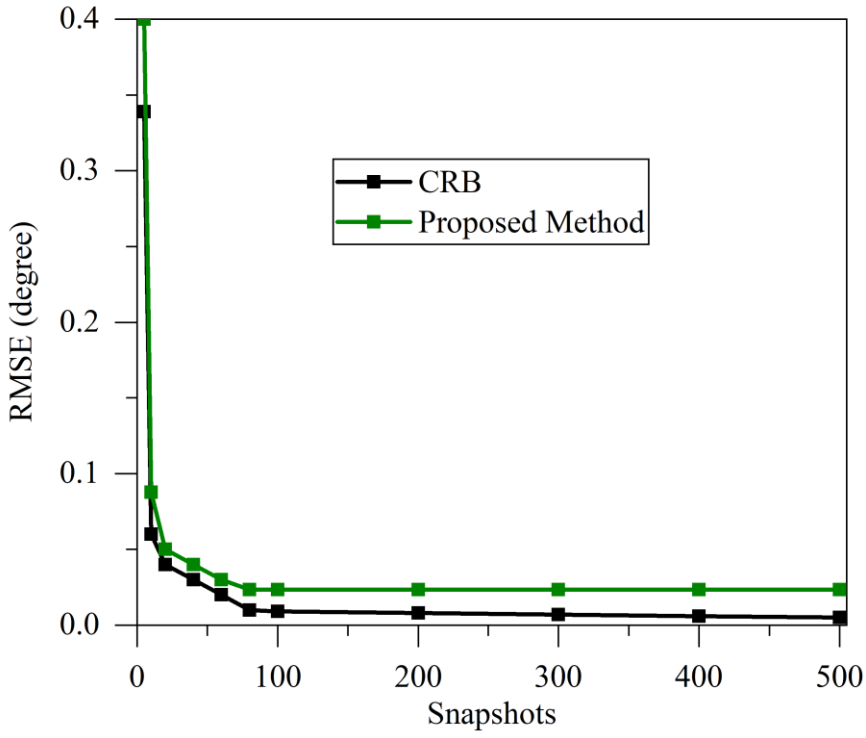

(b)

Figure 5.3 Estimation accuracy in pair-matching ambiguity case: (a) RMSE versus SNR (b) RMSE versus the number of snapshots.

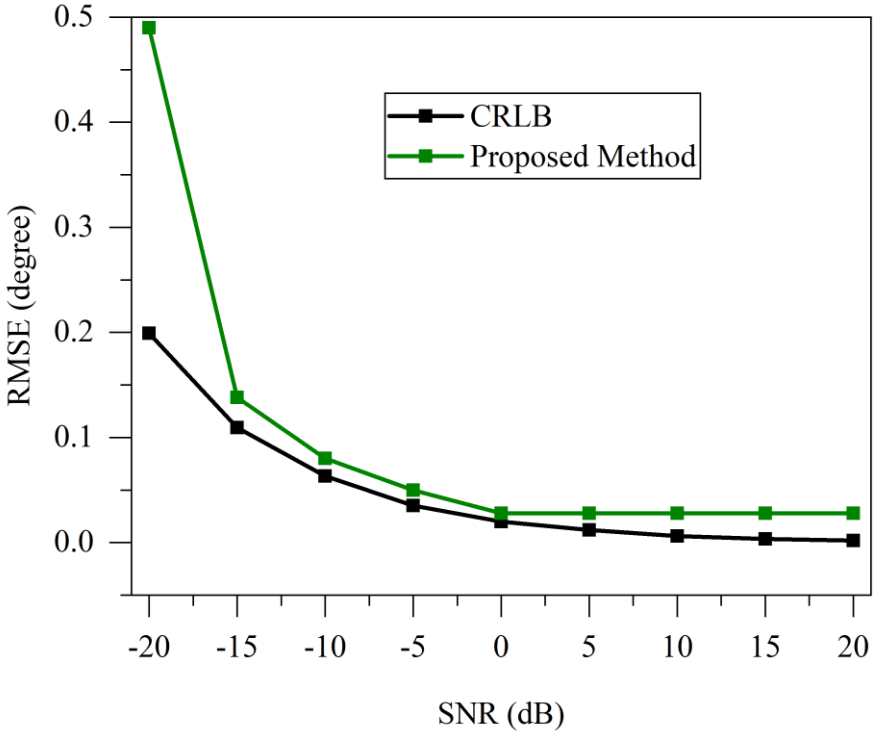

(a)

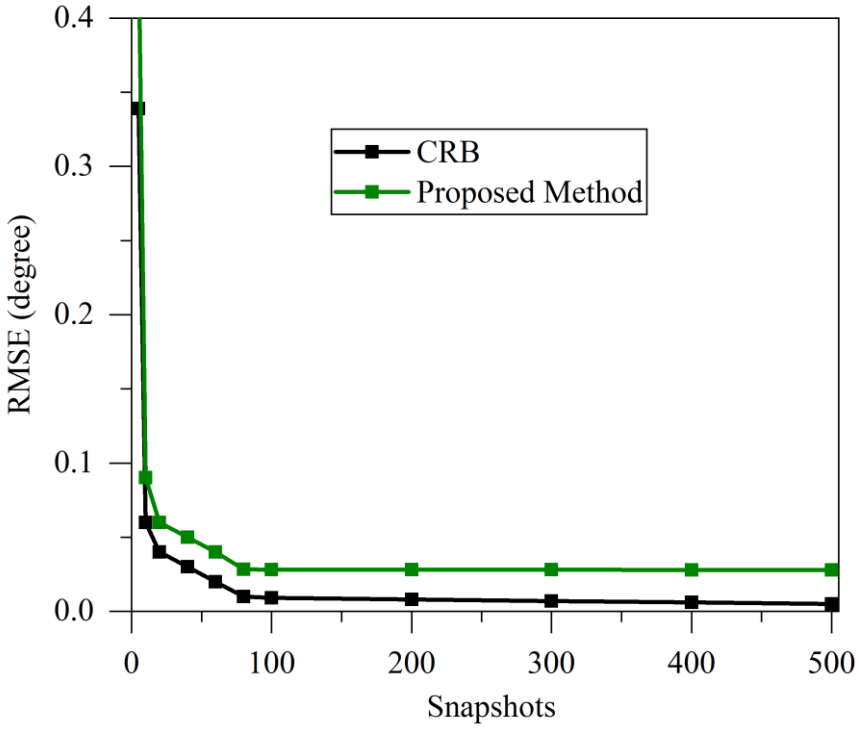

(b)

Figure 5.4 Estimation accuracy in grating angle ambiguity case: (a) RMSE versus SNR (b) RMSE versus the number of snapshots

5.3 PROPOSED METHOD FOR DOA ESTIMATION WITH UCLA

The extension of the proposed method for UCLA is very straightforward. UCLA is a single array configuration, hence $\widehat{\mathbf{R}}_{\mathbf{x}}$ is directly obtained instead from two subarrays separately in the pre-processing phase. Except for the above change, by following the pre-processing, training and testing phase steps described in section 5.2, the DOA of the incoming source signals can be estimated without any ambiguity using UCLA.

5.3.1 Simulation Results and Discussion

This section presents various simulations that compare the proposed method with Yang *et al.* (2019) method for the assessment of the estimation performance in terms of reliability and accuracy. In the simulation setup, $L = 1801$ training pairs were obtained from uniformly spaced angles ranging from -90^{o} to $+90^{o}$ with the angular space of 0.1^{o}. It is noted that the DOAs involved in the testing phase are not included in the training phase. According to rules derived in (Cherkassky *et al.*2004; Randazzo *et al.*2007), the hyper-parameters are chosen as $C = 0.94$ and $\varepsilon = 0.06$.

5.3.1.1 Estimation reliability

Consider the grating-angle ambiguity situation having $M = 5$ sources from the direction $\theta_1 = 10.00^{o}, \theta_2 = 27.35^{o}, \theta_3 = 35.01^{o}, \theta_4 = 57^{o}, \theta_5 = 62^{o}$ impinges on UCLA with $N = 11$ $(N_1 = 5, N_2 = 7)$ under SNR of 10 dB and a snapshot of 200. Figure 5.5 (a) shows the failure of Yang *et al.*(2019) method in the consistent estimation of the true DOAs. In contrast, the proposed method results in a consistent estimate of true DOAs for all 25 unbiased simulation trials by successfully overcoming the grating-angle ambiguity problem as shown in Figure 5.5(b).

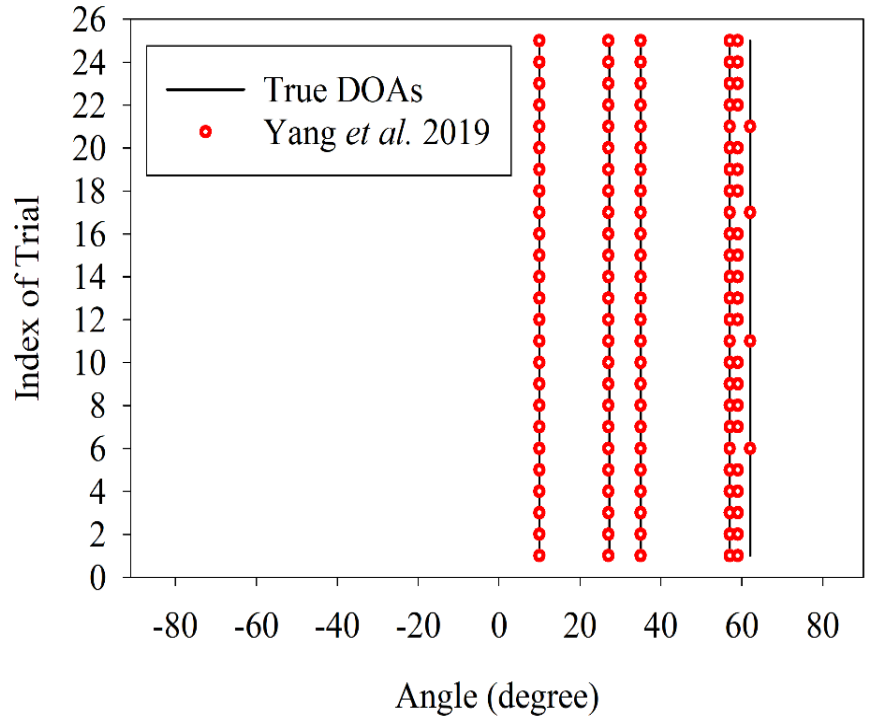

(a)

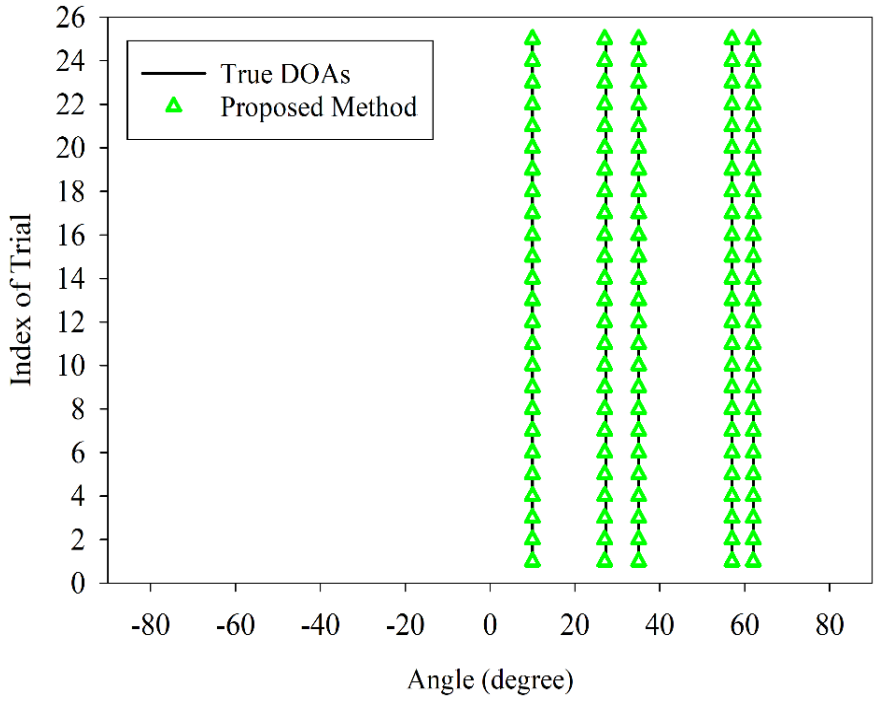

(b)

Figure 5.5 Reliability comparison in grating-angle ambiguity case : (a) Yang *et al.*2019 method (b) Proposed method

5.3.1.2 Estimation accuracy

Assessment of the estimation accuracy of the proposed method is made in a grating-angle ambiguity problem situation using an RMSE performance metric. The RMSE is evaluated for different SNR values ranging from -20 dB to 20 dB with a fixed snapshot of 200 for $Q = 500$ Monte-Carlo simulation trails. Similarly, RMSE is evaluated for varying snapshots ranging from 10 to 500 with a fixed SNR of 10 dB. Figure 5.6 (a) Figure 5.6 (b) shows an increase in the estimation accuracy of the proposed method with an increase in the SNR and snapshots, closely following the limits of the CRLB.

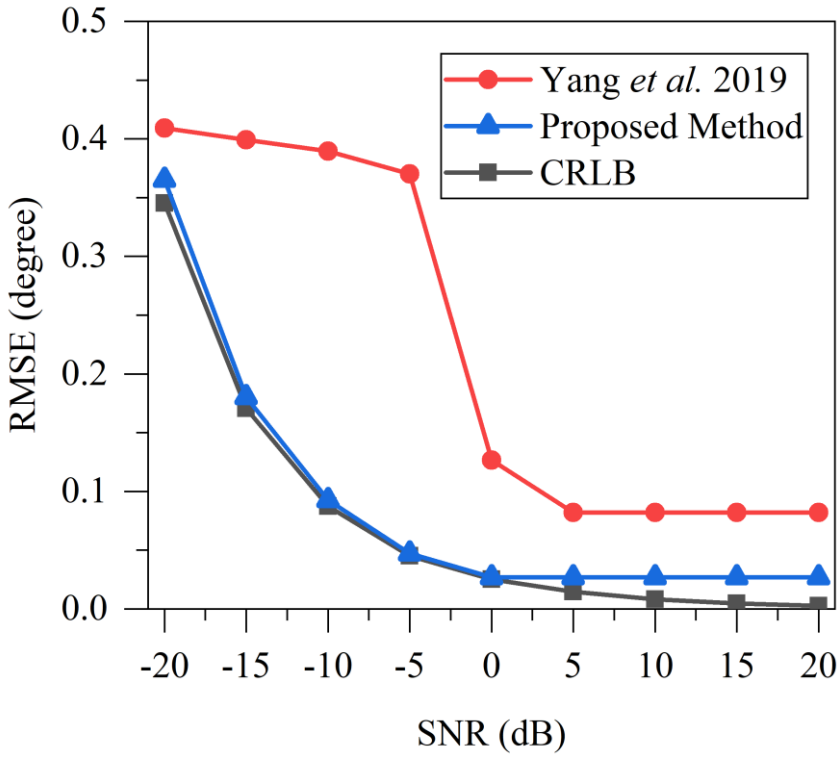

(a)

Figure 5.6 (Continued)

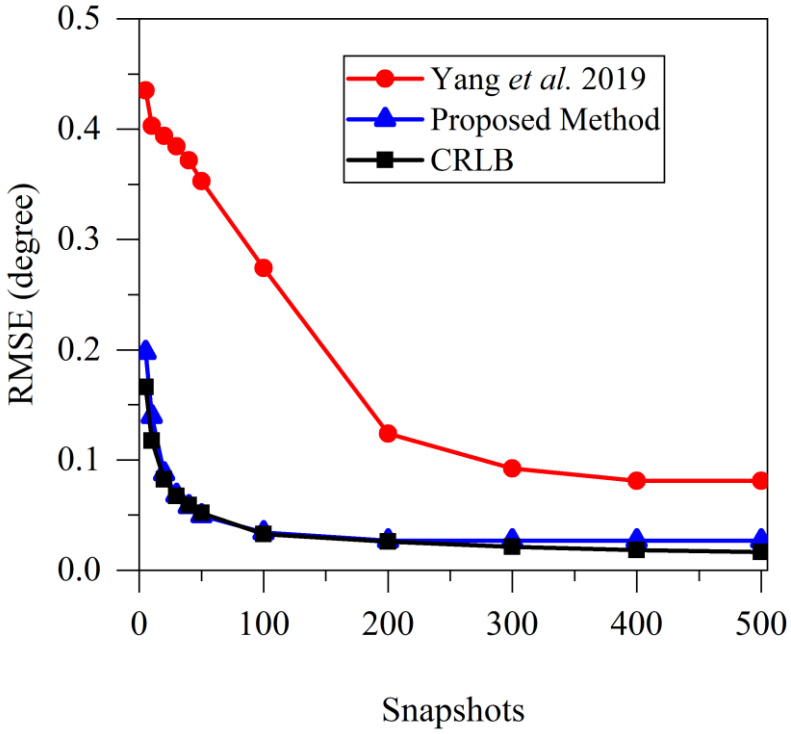

(b)

Figure 5.6 Estimation accuracy in grating-angle ambiguity case: (a) RMSE versus SNR (b) RMSE versus the number of snapshots

5.4 PERFORMANCE ANALYSIS

This section details the performance analysis of the proposed method in terms of complexity and DOF for both GCLA and UCLA.

5.4.1 Complexity Analysis

Assessment of the complexity is made in terms of the number of complex multiplications and execution time required. In the existing SVR formulation (El Gonnouni *et al.*2012; Randazzo *et al.*2007; Tarkowski *et al.*2019; Wu *et al.*2019**)**, the length of the training data set increases in the order of L^M, where L is the number of grid points in the angular region and M is the number of sources. According to (Dass *et al.* 2019), the training complexity is given by $O(L^{2M})$. However, in the proposed method, the length

of the training data set is independent of the number of sources, and its training complexity is given by $O(L^2)$. As a result, the proposed method can estimate multi-source DOAs without increasing the training complexity.

In the testing phase, the computational complexity of the proposed method is given by $O(N^2K + N^2M + n_{sv}\,M)$, where $O(N^2K)$ is the array covariance matrix complexity, $O(N^2M)$ is the propagator complexity, $O(n_{sv}\,M)$ is the SVR complexity where n_{sv} is the number of support vectors. Table 5.2 summarizes the computational complexity of the proposed method and methods (Zhou *et al.*2013; Zheng *et al.* 2018 and Yang *et al.*2019).

Table 5.2 Computational complexity comparison

Methods	Computational Complexity
Zhou *et al.*2013	$O((N_1{}^2 + N_2{}^2)K + N_1{}^3 + N_2{}^3 + \frac{180^{\circ}}{sch}N_1(N_1 - M)) + \frac{180^{\circ}}{sch}N_2(N_2 - M))$
Zheng *et al.* 2018	$O(N^2K + N^3 + \frac{180^{\circ}}{sch}N(N - M))$
Yang *et al.*2019	$O(N^2K + N^3 + \frac{180^{\circ}}{sch}N(N - M) + JN^2)$
Proposed Method	$O(N^2K + N^2M + n_{sv}\,M)$

The execution time is evaluated for $M = 5$ sources under $N = 11$, $K = 200$ snapshots and $n_{sv} = 2$ on a PC equipped with 1.8 GHz and 8 GB of RAM. Table 5.3 shows the proposed method involving less execution time compared to the existing methods (Zhou *et al.*2013; Zheng *et al.* 2018 and Yang *et al.*2019). Also, the computational complexity is evaluated for a varying number of array elements i.e., $12 \leq N \leq 30$ with fixed $K = 200$ snapshots for the consideration of $M = 5$, search step $sch = 0.01$ and $J = 6$.

Similarly, computational complexity is evaluated for a varying number of snapshots i.e., $10 \leq K \leq 500$ with $N = 11$ fixed number of array elements. Figure 5.7 (a) and Figure 5.7 (b) show the proposed method involving less computational complexity compared to the method in (Zhou *et al.*2013; Zheng *et al.* 2018 and Yang *et al.*2019).

Table 5.3 Comparison of Execution time

Methods	Execution Time (*ms*)
Zhou *et al.*2013	141.86
Zheng *et al.* 2018	134.06
Yang *et al.*2019	135.20
Proposed Method	8.48

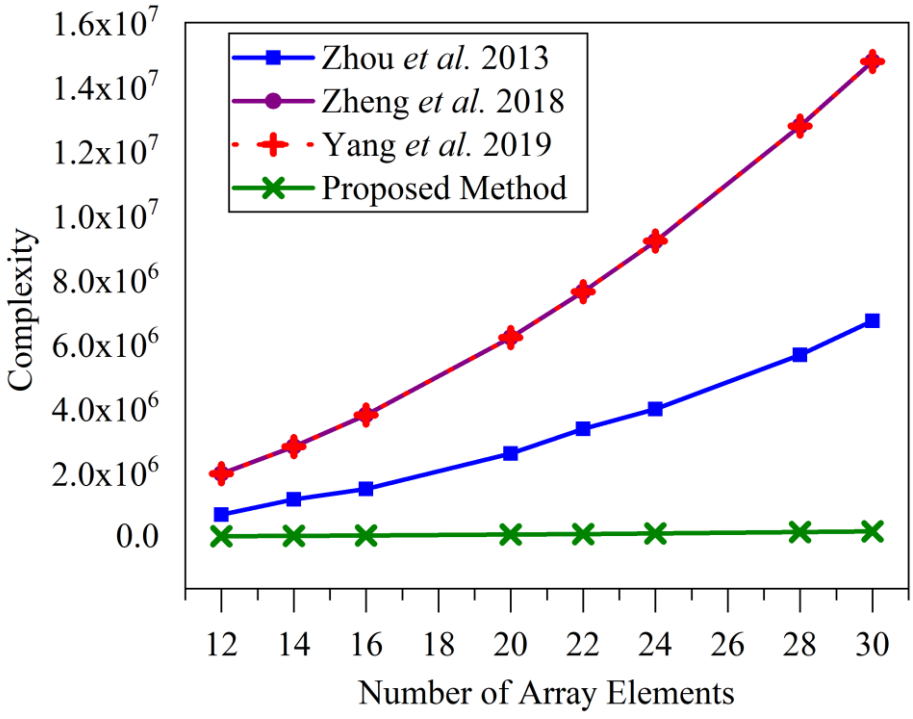

(a)

Figure 5.7 (Continued)

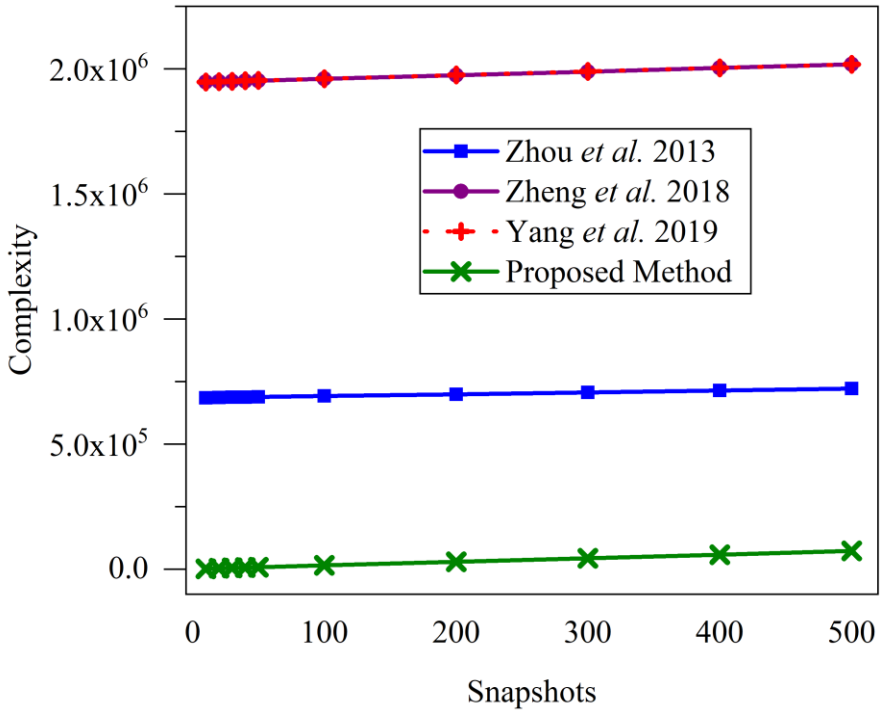

(b)

Figure 5.7 Computational complexity comparison: (a) Number of complex multiplications versus the number of array elements (b) Number of complex multiplications versus the number of snapshots

5.4.2 Degrees-of-Freedom (DOF) Analysis

The DOF expresses the capability of the given method in detecting the maximum number of sources. The method (Zhou *et al.*2013) decomposes the N element GCLA into two separate subarrays as N_1 and N_2 sensor array elements and performs DOA estimation on them individually. Thus, the DOF of (Zhou *et al.*2013) is given by $min(N_1, N_2) - 1$ for an N element GCLA ($N = N_1 + N_2 - 1$). On the other hand, the methods (Zheng *et al.* 2018 and Yang *et al.*2019) consider the GCLA and UCLA as a single array with the ability to achieve DOF of $N - 1$. However, the method proposed for UCLA estimates multi-source DOAs by using a regression model that relates the signal subspace eigenvectors and the DOA of the incoming source signals. In the case of $M = N$ incoming source signal situation, the output array

covariance matrix $\widehat{\mathbf{R}} \in \mathbb{C}^{N \times N}$ of the received signal vector can yield a signal eigenvector matrix $\mathbf{U}_s \in \mathbb{C}^{N \times N}$ whose columns are signal eigenvector $\mathbf{u}_s^m \in \mathbb{C}^{N \times 1}$, $m = 1,2,..,N$ corresponding to the N incoming source signals. As a result, the proposed method can estimate N DOAs $\{\hat{\theta}_m\}_{m=1}^{N}$ given the $\mathbf{u}_s^m$ and thereby achieves the full N DOF for an N element UCLA.

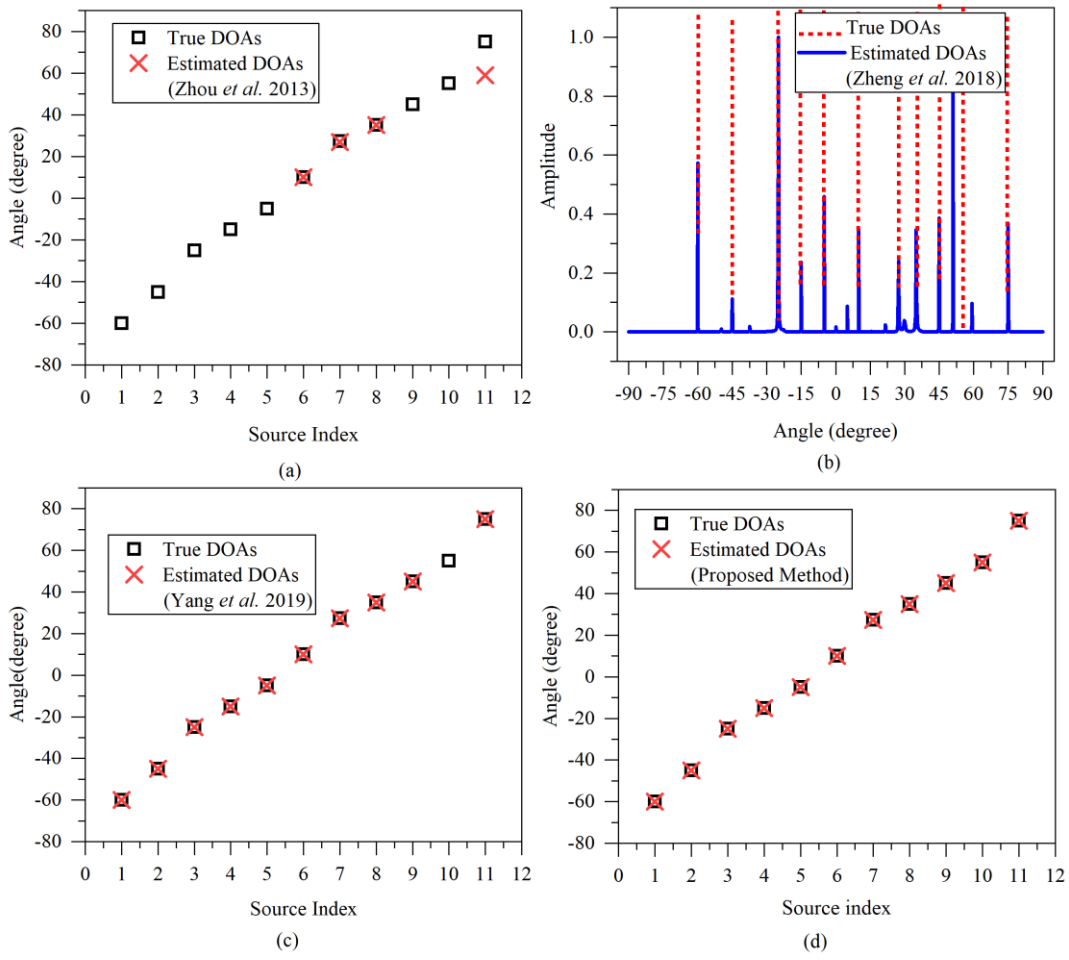

Figure 5.8 Degrees-of-Freedom (DOF) comparison: (a) Zhou *et al.*2013 method (b) Zheng *et al.* 2018 method (c) Yang *et al.*2019 method (d) Proposed method

Simulations have been carried out with $M = 11$ random sources (including grating-angle case) from -90^o to $+90^o$ impinging on $N = 11$ $(N_1 = 5, N_2 = 7)$ element UCLA under SNR of 10 dB and a snapshot of 200 for the demonstration of the DOF achieved by the proposed method and the

methods proposed by (Zhou *et al.*2013; Zheng *et al.* 2018 and Yang *et al.*2019). Figure 5.8 shows the proposed method outperforming the methods (Zhou *et al.*2013; Zheng *et al.* 2018 and Yang *et al.*2019) by estimating $M = 11$ true DOAs without any ambiguity thereby achieving full N DOF.

5.5 SUMMARY

This chapter presents a computationally efficient DOA estimation method based on support vector regression (SVR) for addressing the ambiguity problem associated with GCLA and UCLA. The ambiguity problem is resolved by treating DOA estimation as approximating the unknown regression function that maps the signal subspace eigenvectors with the DOA of the incoming source signals. The proposed formulation uses only one regression model for the detection of multiple DOAs whereas the other SVR formulation requires a multiple regression model. This provides computational efficiency for the proposed method. The proposed formulation estimates the multi-source DOAs involving full DOF without any increase in the training complexity. Furthermore, it offers good generalization for a varying number of sources and robustness in estimating the multi-source DOAs successfully without ambiguity. The analysis and simulation findings show the proposed method outperforms the existing methods in terms of estimation reliability, estimation accuracy, computational complexity, execution time and DOF.

CHAPTER 6

CONCLUSION AND FUTURE PERSPECTIVES

6.1 CONCLUSION OF CONTRIBUTIONS

The problem of estimating the DOA of the incoming source signal with general co-prime linear array (GCLA) and unfolded co-prime linear (UCLA) have been the subjects of this research work. A comprehensive investigation of the ambiguity issues such as pair-matching ambiguity and grating-angle ambiguity in DOA estimation associated with GCLA and UCLA has been presented. The focus of the research work is on the resolution of the ambiguity issues associated with GCLA and UCLA. Towards this, different methods have been proposed that offer the following advantages (i) superior estimation performances in terms of reliability, accuracy and angular resolution (ii) good generalization and robustness in estimation performances with less complexity in terms of computational complexity and execution time (iii) full degrees-of-freedom (DOF). The superiority and effectiveness of the proposed methods in comparison with the existing methods have been validated with several standard simulations and analysis. The main contributions are summarized as follows.

First, the proposed unambiguous DOA estimation method incorporates an initial estimation of DOAs through UCLA-MUSIC. The true DOAs are distinguished from ambiguous estimates obtained from UCLA-MUSIC using the estimated power of the transmitted source signals. The source power function derived is based on the signal subspace eigenvalues

and its associated eigenvectors for the estimation of the power of the source signals transmitted. The proposed approach distinguishes and detects the true DOAs successfully without ambiguity. The simulation results guarantee the superiority of the proposed method over the existing methods in terms of reliability and accuracy.

In the second solution, an improved polynomial rooting-based method for high-resolution unambiguous DOA estimation is proposed. Based on the orthogonality between the noise subspace eigenvectors and array directional vectors, a polynomial function is derived. Then, a maximum signal power function based on spatial filtering and second-order differential has been proposed for the selection of the signal roots that are associated with true DOAs over ambiguous roots obtained from the polynomial function. The proposed method overcomes grating-angle ambiguity and estimates the true DOAs successfully with improved estimation performances. Simulations have been performed to show the effectiveness and superiority of the proposed method in terms of reliability, accuracy and angular resolution involving low computational complexity.

Finally, a computationally efficient DOA estimation method based on support vector regression (SVR) has been proposed for addressing the ambiguity problem associated with GCLA and UCLA. The ambiguity problem is resolved by treating DOA estimation as approximating the unknown regression function that maps the signal subspace eigenvectors with the DOA of the incoming source signals. The proposed formulation uses only one regression model for the detection of multiple DOAs whereas the other existing SVR formulation requires a multiple regression model. This provides computational efficiency for the proposed method. The proposed formulation estimates the DOAs involving full DOF without increasing the training complexity. It also offers good generalization for a varying number of sources

and robustness in estimating the DOAs successfully without ambiguity. The analysis and simulation findings show the proposed method outperforms the existing methods in terms of estimation reliability, estimation accuracy, computational complexity, execution time and DOF.

6.2 PERSPECTIVES OF FUTURE WORK

In this research work, the co-prime arrays considered are linear (1-Dimensional) arrays. The investigations on the problem of ambiguity in DOA estimation for planar 2-D and 3-D co-prime arrays would be one of the subjects for significant future research. The focus of the proposed work is on the second-order statistics-based DOA estimation, the investigations on the problem of ambiguity in higher-order statistics-based DOA estimation using GCLA and UCLA would be another orientation of future research. In contrast to the subarray domain processing, the investigations of ambiguity problems in difference-coarray domain processing of GCLA and UCLA would be another topic of future research. The orientation of extending the presented work for massive sparse arrays would be an interesting area of future research.

Developing optimal sparse array configurations is an important research direction. This includes determining the optimal placement of sensors in the array to achieve higher spatial resolution and better DOA estimation performance. Various optimization techniques, such as convex optimization, compressive sensing, and sparse reconstruction, can be explored to design sparse arrays. Research can focus on developing data-driven approaches including deep learning and neural network that exploit the rich information captured by sparse arrays to improve the accuracy and robustness of DOA estimation.

The proposed formulations can be extended to other general practical cases such as mixed far-field and near-field source signals, wideband signal sources, moving sources, correlated noise environments and multi-path scenarios, etc. The future of DOA estimation using sparse arrays holds great potential for real-time applications. The implementation of the proposed algorithms in DSP-based hardware systems would be of great interest for evaluation of the performance in real-time applications. Sparse arrays can be deployed in various scenarios, such as wireless communication systems, radar systems, sonar systems, and autonomous vehicles. Real-time DOA estimation using sparse arrays can enable accurate localization, beamforming, and tracking of signal sources, leading to improved performance in applications like wireless communication, radar-based target detection, and navigation. DOA estimation using sparse arrays can be integrated into beamforming algorithms for adaptive and efficient transmission and reception in dynamic wireless environments.

APPENDIX 1

Table A1.1 Pair-matching ambiguity in GCLA - Case 1: $\theta_1 = 10.00^{o}$ and $\theta_2 = 39.11^{o}$; $N = 11$ $(N_1 = 5, N_2 = 7)$; SNR = 10 dB; $K = 200$

	Method	DOA Estimation Result					Ambiguity exists or not	DOF	Complexity
Subarray-based Methods	Zhou *et al.*2013	Common angle pairs in $\hat{f}_1(\theta)$ and $\hat{f}_2(\theta)$	$\hat{\theta}_1 = 9.99^{o}$	$\hat{\theta}_2 = 39.11^{o}$	$\hat{\theta}_3 = -13.08^{o}$	$\hat{\theta}_4 = -75.74^{o}$	Pair-matching Ambiguity exists	$\min(N_1, N_2 - 1)$	$O((N_1{}^2 + N_2{}^2)K + N_1{}^3 + N_2{}^3 + \frac{180^{o}}{\Delta\theta} N_1(N_1 - M) + \frac{180^{o}}{\Delta\theta} N_2(N_2 - M))$
		True or Ambiguous	True	True	Ambiguous	Ambiguous			
	Sun *et al.*2015	Common angle pairs in transformed domain	$\hat{\theta}_1 = 10.00^{o}$	$\hat{\theta}_2 = 39.11^{o}$	$\hat{\theta}_3 = -13.07^{o}$	$\hat{\theta}_4 = -75.77^{o}$	Pair-matching Ambiguity exists	$\min(N_1, N_2) - 1$	$O((N_1{}^2 + N_2{}^2)K + N_1{}^3 + N_2{}^3 + \frac{180^{o}}{\Delta\theta}(N_1{}^2/N_2) + \frac{180^{o}}{\Delta\theta}(N_2{}^2/N_1))$
		True or Ambiguous	True	True	Ambiguous	Ambiguous			
	Zhang *et al.* 2017	RoI (Roots of Interest)	$0.8533 - 0.5183i$	$-0.3985 - 0.916i$	$0.7565 + 0.6524i$	$-0.9935 + 0.09662i$	Pair-matching Ambiguity exists	$\min(N_1, N_2) - 1$	$O((N_1{}^2 + N_2{}^2)K + N_1{}^3 + N_2{}^3)$
		Magnitude of RoI	0.9989	0.9984	0.9990	0.9982			
		$\hat{\theta}$	$\hat{\theta}_1 = 10.00^{o}$	$\hat{\theta}_2 = 39.09^{o}$	$\hat{\theta}_3 = -13.09^{o}$	$\hat{\theta}_4 = -75.72^{o}$			
		True or Ambiguous	True	True	Ambiguous	Ambiguous			

Table A1.1 (Continued)

	Liu *et al.* 2018	RoI (Roots of Interest)	$0.8518 - 0.5186i$	$-0.3987 - 0.9161i$	$0.7567 + 0.6524i$	$-0.9927 + 0.09684i$	Pair-matching Ambiguity exists	$\min(N_1, N_2)$	$O((N_1{}^2 + N_2{}^2)K + N_1{}^3 + N_2{}^3)$
		Magnitude of RoI	0.9973	0.9991	0.9991	0.9974			
		$\hat{\theta}$	$\hat{\theta}_1 = 10.02^o$	$\hat{\theta}_2 = 39.09^o$	$\hat{\theta}_3 = -13.09^o$	$\hat{\theta}_4 = -75.70^o$			
		True or Ambiguous	True	True	Ambiguous	Ambiguous			
	Yan *et al.* 2018	RoI (Roots of Interest)	$0.8536 - 0.5177i$	$-0.3983 - 0.9148i$	$0.7557 + 0.6514i$	$-0.9937 + 0.09609i$	Pair-matching Ambiguity exists	$\min(N_1, N_2) - 1$	$O((N_1{}^2 + N_2{}^2)K + N_1{}^3 + N_2{}^3)$
		Magnitude of RoI	0.9983	0.9977	0.9977	0.9983			
		$\hat{\theta}$	$\hat{\theta}_1 = 9.99^o$	$\hat{\theta}_2 = 39.10^o$	$\hat{\theta}_3 = -13.08^o$	$\hat{\theta}_4 = -75.76^o$			
		True or Ambiguous	True	True	Ambiguous	Ambiguous			
Adjoined Subarray-based methods	Zheng *et al.* 2018	Angles associated with the highest peaks of $\hat{f}_{AdS-MUSIC}(\theta)$	$\hat{\theta}_1 = 9.99^o$	$\hat{\theta}_2 = 39.10^o$	-	-	Pair-matching Ambiguity does not exist	$N - 1$	$O(N^2K + N^3 + \frac{180^o}{\Delta\theta}N(N - M))$
		True or Ambiguous	True	True	-	-			
	He *et al.*2020	RoI (Roots of Interest)	$0.852 - 0.5199i$	$-0.3989 - 0.9162i$	-	-	Pair-matching Ambiguity does not exist	$N - 1$	$O(N^2K + N^3 + (2N - 1)^3)$
		Magnitude of RoI	0.9981	0.9993	-	-			
		$\hat{\theta}$	$\hat{\theta}_1 = 10.04^o$	$\hat{\theta}_2 = 39.10^o$	-	-			
		True or Ambiguous	True	True	-	-			

Table A1.2 Grating-angle ambiguity in GCLA - Case 1: $\boldsymbol{\theta_1 = 10.00^{o}, \theta_2 = 27.35^{o}}$ and $\boldsymbol{\theta_3 = 35.01^{o}}$; $\boldsymbol{N = 11}$ $\boldsymbol{(N_1 = 5, N_2 = 7)}$; SNR = 10 dB; $\boldsymbol{K = 200}$

	Method	DOA Estimation Result					Ambiguity exists or not	DOF	Complexity
Subarray-based Methods	Zhou *et al.*2013	Common angle pairs in $\hat{f}_1(\theta)$ and $\hat{f}_2(\theta)$	$\hat{\theta}_1 = 10.00^{o}$	$\hat{\theta}_2 = 27.40^{o}$	$\hat{\theta}_3 = 35.00^{o}$	$\hat{\theta}_4 = 59.20^{o}$	Grating-angle Ambiguity exists	$\min(N_1, N_2) - 1$	$O((N_1{}^2 + N_2{}^2)K + N_1{}^3 + N_2{}^3 + \frac{180^{o}}{\Delta\theta} N_1(N_1 - M) + \frac{180^{o}}{\Delta\theta} N_2(N_2 - M))$
		True or Ambiguous	True	True	True	Ambiguous			
	Sun *et al.*2015	Common angle pairs in transformed domain	$\hat{\theta}_1 = 10.00^{o}$	$\hat{\theta}_2 = 27.33^{o}$	$\hat{\theta}_3 = 35.01^{o}$	$\hat{\theta}_4 = 59.23^{o}$	Grating-angle Ambiguity exists	$\min(N_1, N_2) - 1$	$O((N_1{}^2 + N_2{}^2)K + N_1{}^3 + N_2{}^3 + \frac{180^{o}}{\Delta\theta}(N_1{}^2/N_2) + \frac{180^{o}}{\Delta\theta}(N_2{}^2/N_1))$
		True or Ambiguous	True	True	True	Ambiguous			
	Zhang *et al.* 2017	RoI (Roots of Interest)	$0.8536 - 0.5189i$	$0.1266 - 0.9909i$	$-0.2236 - 0.9734i$	$-0.9031 - 0.4272$	Grating-angle Ambiguity exists	$\min(N_1, N_2) - 1$	$O((N_1{}^2 + N_2{}^2)K + N_1{}^3 + N_2{}^3)$
		Magnitude of RoI	0.9989	0.9990	0.9985	0.9990			
		$\hat{\theta}$	$\hat{\theta}_1 = 10.01^{o}$	$\hat{\theta}_2 = 27.35^{o}$	$\hat{\theta}_3 = 34.88^{o}$	$\hat{\theta}_4 = 59.24^{o}$			
		True or Ambiguous	True	True	True	Ambiguous			
	Liu *et al.* 2018	RoI (Roots of Interest)	$0.8543 - 0.5188i$	$0.127 - 0.9914i$	$-0.229 - 0.9718i$	$-0.9026 + 0.4268i$	Grating-angle Ambiguity exists	$\min(N_1, N_2) - 1$	$O((N_1{}^2 + N_2{}^2)K + N_1{}^3 + N_2{}^3)$
		Magnitude of RoI	0.9995	0.9995	0.9984	0.9984			
		$\hat{\theta}$	$\hat{\theta}_1 = 10.01^{o}$	$\hat{\theta}_2 = 27.35^{o}$	$\hat{\theta}_3 = 35.00^{o}$	$\hat{\theta}_4 = 59.24^{o}$			
		True or Ambiguous	True	True	True	Ambiguous			

Table A1.2 (Continued)

	Yan *et al.* 2018	RoI (Roots of Interest)	$0.8524 - 0.5193i$	$0.1254 - 0.9902i$	$-0.2308 - 0.9724i$	$-0.9041 + 0.4258i$	Grating-angle Ambiguity exists	$\min(N_1, N_2) - 1$	$O((N_1{}^2 + N_2{}^2)K + N_1{}^3 + N_2{}^3)$
		Magnitude of RoI	0.9981	0.9981	0.9994	0.9994			
		$\hat{\theta}$	$\hat{\theta}_1 = 10.03^o$	$\hat{\theta}_2 = 27.38^o$	$\hat{\theta}_3 = 35.04^o$	$\hat{\theta}_4 = 59.30^o$			
		True or Ambiguous	True	True	True	Ambiguous			
Adjoined Subarray-based methods	Zheng *et al.* 2018	Angles associated with the highest peaks of $\hat{f}_{Ads-MUSIC}(\theta)$	$\hat{\theta}_1 = 9.99^o$	$\hat{\theta}_2 = 27.34^o$	$\hat{\theta}_3 = 35.01^o$	$\hat{\theta}_4 = 59.29^o$	Grating-angle Ambiguity exists	$N - 1$	$O(N^2K + N^3 + \frac{180^o}{\Delta\theta}N(N-M))$
		True or Ambiguous	True	True	True	Ambiguous			
	He *et al.*2020	RoI (Roots of Interest)	$0.8534 - 0.5182i$	$0.1269 - 0.9903i$	$-0.2304 - 0.9718i$	$-0.9035 - 0.4258i$	Grating-angle Ambiguity exists	$N - 1$	$O(N^2K + N^3 + (2N-1)^3)$
		Magnitude of RoI	0.9984	0.9984	0.9987	0.9988			
		$\hat{\theta}$	$\hat{\theta}_1 = 10.03^o$	$\hat{\theta}_2 = 27.35^o$	$\hat{\theta}_3 = 35.03^o$	$\hat{\theta}_4 = 59.29^o$			
		True or Ambiguous	True	True	True	Ambiguous			

Note: In addition to case 1, all the aforementioned methods for GCLA suffer from the existence of grating-angle ambiguity for any three angles from the following case 2: $\{20.00^o, 38.88^o, 47.90^o, -76.47^o\}$; case 3: $\{12.37^o, 30.00^o, 37.92^o, 64.16^o\}$ under $N = 11$ $(N_1 = 5, N_2 = 7)$; SNR = 10 dB; $K = 200$.

Table A1.3 Grating-angle ambiguity in UCLA - Case 1: $\boldsymbol{\theta_1 = 10.00^{o}, \theta_2 = 27.35^{o}}$ and $\boldsymbol{\theta_3 = 35.01^{o}}$; $\boldsymbol{N = 11}$ $\boldsymbol{(N_1 = 5, N_2 = 7)}$; SNR = 10 dB; $\boldsymbol{K = 200}$

	Method	DOA Estimation Result					Ambiguity exists or not	DOF	Complexity
Adjoined Subarray-based methods	Zheng *et al.* 2018	Angles associated with the highest peaks of $\hat{f}_{UCLA-MUSIC}(\theta)$	$\hat{\theta}_1 = 10.00^{o}$	$\hat{\theta}_2 = 27.33^{o}$	$\hat{\theta}_3 = 35.03^{o}$	$\hat{\theta}_4 = 59.26^{o}$	Grating-angle Ambiguity exists	$N-1$	$O(N^2K + N^3 + \frac{180^{o}}{\Delta\theta}N(N-M))$
		True or Ambiguous	True	True	True	Ambiguous			
	He *et al.*2020	RoI (Roots of Interest)	$0.8536 - 0.518i$	$0.1273 - 0.9903i$	$-0.229 - 0.9721i$	$-0.9028 - 0.427i$	Grating-angle Ambiguity exists	$N-1$	$O(N^2K + N^3 + (2N-1)^3)$
		Magnitude of RoI	0.9985	0.9984	0.9987	0.9987			
		$\hat{\theta}$	$\hat{\theta}_1 = 9.99^{o}$	$\hat{\theta}_2 = 27.34^{o}$	$\hat{\theta}_3 = 35.00^{o}$	$\hat{\theta}_4 = 59.24^{o}$			
		True or Ambiguous	True	True	True	Ambiguous			
Beamforming-like methods	Yang *et al.*2019	Angles associated to highest peaks of $\hat{f}_{UCLA-MUSIC}(\theta)$	$\hat{\theta}_1 = 10.00^{o}$	$\hat{\theta}_2 = 27.33^{o}$	$\hat{\theta}_3 = 35.03^{o}$	$\hat{\theta}_4 = 59.26^{o}$	Grating-angle Ambiguity resolved	$N-1$	$O(N^2K + N^3 + \frac{180^{o}}{\Delta\theta}N(N-M) + JN^2)$
		$\hat{P}_{CBF}$ (normalized)	0.9415	0.4585	0.7778	0.1672			
		$\hat{\theta}$	$\hat{\theta}_1 = 10.00^{o}$	$\hat{\theta}_2 = 27.33^{o}$	$\hat{\theta}_3 = 35.03^{o}$	-			
		True or Ambiguous	True	True	True	-			

Table A1.3 (Continued)

	Huang *et al.*2021	RoI (Roots of Interest)	$0.8536 - 0.518i$	$0.1273 - 0.9903i$	$-0.229 - 0.9721i$	$-0.9028 - 0.427i$	Grating-angle Ambiguity resolved	$N-1$	$O(N^2K + N^3 + (2N-1)^3 + JN^2)$
		Magnitude of RoI	0.9985	0.9984	0.9987	0.9987			
		$\hat{\theta}$	$\hat{\theta}_1 = 9.99^o$	$\hat{\theta}_2 = 27.34^o$	$\hat{\theta}_3 = 35.00^o$	$\hat{\theta}_4 = 59.24^o$			
		$\hat{P}_{CBF}$ (normalized)	0.9435	0.5088	0.9123	0.1785			
		$\hat{\theta}$	$\hat{\theta}_1 = 9.99^o$	$\hat{\theta}_2 = 27.34^o$	$\hat{\theta}_3 = 35.00^o$	-			
		True or Ambiguous	True	True	True	-			

Note: **In addition to case 1, the aforementioned methods for UCLA exhibit a similar performance for any three angles from the following case 2:** $\{\mathbf{20.00^o}, \mathbf{38.88^o}, \mathbf{47.90^o}, \mathbf{-76.47^o}\}$**; case 3:** $\{\mathbf{12.37^o}, \mathbf{30.00^o}, \mathbf{37.92^o}, \mathbf{64.16^o}\}$ **under** $\boldsymbol{N = 11}$ $(\boldsymbol{N_1 = 5, N_2 = 7})$ **; SNR** $= \mathbf{10}$ **dB;** $\boldsymbol{K = 200}$.

Table A1.4 Grating-angle ambiguity in UCLA under closely distributed sources - Case 1: $\boldsymbol{\theta_1 = 10.00^{o}, \theta_2 = 27.35^{o}, \theta_3 = 35.01^{o}, \theta_4 = 57^{o}, \theta_5 = 62^{o}; N = 11\ (N_1 = 5, N_2 = 7)}$; SNR = 10 dB; $\boldsymbol{K = 200}$

	Method	DOA Estimation Result							Ambiguity exists or not	DOF	Complexity
Beamforming-like methods	Yang *et al.*2019	Angles associated to highest peaks of $\hat{f}_{UCLA-MUSIC}(\theta)$	$\hat{\theta}_1 = 10.00^{o}$	$\hat{\theta}_2 = 27.35^{o}$	$\hat{\theta}_3 = 35.01^{o}$	$\hat{\theta}_4 = 57^{o}$	$\hat{\theta}_5 = 62^{o}$	$\hat{\theta}_6 = 59.25^{o}$	Grating-angle Ambiguity not resolved	$N-1$	$O(N^2K + N^3 + \frac{180^{o}}{\Delta\theta}N(N-M) + JN^2)$
		$\widehat{\boldsymbol{P}}_{\boldsymbol{CBF}}$ (normalized)	0.6805	0.8611	0.4930	0.5277	0.4444	0.5486			
		$\hat{\theta}$	$\hat{\theta}_1 = 10.00^{o}$	$\hat{\theta}_2 = 27.35^{o}$	$\hat{\theta}_3 = 35.01^{o}$	$\hat{\theta}_4 = 57^{o}$	-	$\hat{\theta}_5 = 59.25^{o}$			
		True or Ambiguous	True	True	True	True	-	Ambiguous			
	Huang *et al.*2021	RoI (Roots of Interest)	$0.8537-0.5174i$	$0.1266-0.9912i$	$-0.2293-0.9704i$	$-0.8719-0.4867i$	$-0.9317-0.3592i$	$-0.9017-0.4258i$	Grating-angle Ambiguity not resolved	$N-1$	$O(N^2K + N^3 + (2N-1)^3 + JN^2)$
		Magnitude of RoI	0.9983	0.9993	0.9971	0.9985	0.9985	0.9972			
		$\hat{\theta}$	$\hat{\theta}_1 = 9.98^{o}$	$\hat{\theta}_2 = 27.35^{o}$	$\hat{\theta}_3 = 35.01^{o}$	$\hat{\theta}_4 = 57.92^{o}$	$\hat{\theta}_5 = 61.99^{o}$	$\hat{\theta}_6 = 59.26^{o}$			
		$\widehat{\boldsymbol{P}}_{\boldsymbol{CBF}}$ (normalized)	0.7905	0.6512	0.5390	0.4727	0.3414	0.6686			
		$\hat{\theta}$	$\hat{\theta}_1 = 9.98^{o}$	$\hat{\theta}_2 = 27.35^{o}$	$\hat{\theta}_3 = 35.01^{o}$	$\hat{\theta}_4 = 57.92^{o}$	-	$\hat{\theta}_6 = 59.26^{o}$			
		True or Ambiguous	True	True	True	True	-	Ambiguous			

Table A 1.5 Grating-angle ambiguity in UCLA under closely distributed sources - Case 2: $\boldsymbol{\theta_1 = 12.37^o, \theta_2 = 28.00^o, \theta_3 = 32.00^o, \theta_4 = 37.92^o, \theta_5 = 64.16^o}$; $\boldsymbol{N = 11\ (N_1 = 5, N_2 = 7)}$; SNR $\boldsymbol{= 10}$ dB; $\boldsymbol{K = 200}$

	Method	DOA Estimation Result							Ambiguity exists or not	DOF	Complexity
Beamforming-like methods	Yang *et al.*2019	Angles associated with the highest peaks of $\hat{f}_{UCLA-MUSIC}(\theta)$	$\hat{\theta}_1 = 12.47^o$	$\hat{\theta}_2 = 28.02^o$	$\hat{\theta}_3 = 32.00^o$	$\hat{\theta}_4 = 37.91^o$	$\hat{\theta}_5 = 64.00^o$	$\hat{\theta}_6 = 30.00^o$	Grating-angle Ambiguity not resolved	$N-1$	$O(N^2K + N^3 + \frac{180^o}{\Delta\theta}N(N-M) + JN^2)$
		$\widehat{\boldsymbol{P}}_{\boldsymbol{CBF}}$ (normalized)	0.8369	0.7515	0.5277	0.8999	0.8281	0.7212			
		$\hat{\theta}$	$\hat{\theta}_1 = 12.46^o$	$\hat{\theta}_2 = 28.01^o$	-	$\hat{\theta}_4 = 37.81^o$	$\hat{\theta}_5 = 63.99^o$	$\hat{\theta}_6 = 30.00^o$			
		True or Ambiguous	True	True	-	True	True	Ambiguous			
	Huang *et al.*2021	RoI (Roots of Interest)	$0.7782 - 0.6266i$	$0.0947 - 0.9937i$	$-0.0933 - 0.9899i$	$-0.3478 - 0.9368i$	$-0.9446 - 0.3134i$	$0.0082 - 0.9981$	Grating-angle Ambiguity not resolved	$N-1$	$O(N^2K + N^3 + (2N-1)^3 + JN^2)$
		Magnitude of RoI	0.9991	0.9982	0.9943	0.9993	0.9952	0.9981			
		$\hat{\theta}$	$\hat{\theta}_1 = 12.46^o$	$\hat{\theta}_2 = 28.01^o$	$\hat{\theta}_3 = 32.00^o$	$\hat{\theta}_4 = 37.81^o$	$\hat{\theta}_5 = 63.99^o$	$\hat{\theta}_6 = 30.00^o$			
		$\widehat{\boldsymbol{P}}_{\boldsymbol{CBF}}$ (normalized)	0.9739	0.8155	0.5772	0.9991	0.8821	0.6121			
		$\hat{\theta}$	$\hat{\theta}_1 = 12.46^o$	$\hat{\theta}_2 = 28.01^o$	-	$\hat{\theta}_4 = 37.81^o$	$\hat{\theta}_5 = 63.99^o$	$\hat{\theta}_6 = 30.00^o$			
		True or Ambiguous	True	True	-	True	True	Ambiguous			

Note : In addition to case 1 and case 2, the aforementioned methods for UCLA exhibit a similar performance for the following $\boldsymbol{M = 6}$ case 3: $\boldsymbol{\theta_1 = 10.00^o, \theta_2 = 27.35^o, \theta_3 = 35.01^o, \theta_4 = 39.11^o, \theta_5 = 57^o, \theta_6 = 62^o}$ under $\boldsymbol{N = 11\ (N_1 = 5, N_2 = 7)}$; SNR $\boldsymbol{= 10}$ dB; $\boldsymbol{K = 200}$.

REFERENCES

1. Aboumahmoud, I, Muqaibel, A, Alhassoun, M & Alawsh, S 2021, 'A Review of Sparse Sensor Arrays for Two-Dimensional Direction-of-Arrival Estimation', IEEE Access, vol. 9, pp. 92999-93017.

2. Albera, L, Ferreol,A, Cosandier-Rimele, D, Merlet, I & Wendling, F 2008, 'Brain source localization using a fourth-order deflation scheme', IEEE Transactions on Biomedical Engineering, vol. 55, no. 2, pp. 490-501.

3. Balanis, CA & Ioannides, PI 2007, 'Introduction to Smart Antennas', Morgan & Claypool, San Rafael, United States of America.

4. Barabell, A 1983, 'Improving the resolution performance of eigenstructure-based direction-finding algorithms', ICASSP'83 IEEE International Conference on Acoustics, Speech, and Signal Processing, pp. 336-339.

5. Bartlett, M 1961, 'An Introduction to Stochastic Processes with Special References to Methods and Applications', Cambridge University Press, New York.

6. Bartlett, M.S 1948, 'Smoothing Periodograms from Time Series with Continuous Spectra,', Nature, vol. 161, pp. 686-687.

7. Bellofiore, S, Balanis, CA, Foutz, J & Spanias, AS 2002, 'Smart-antenna systems for mobile communication networks. Part 2: Beamforming and network throughput', IEEE Antennas and Propagation Magazine, vol. 44, no. 4, pp. 106-114.

8. Belloni, F, Richter, A & Koivunen, V 2007, 'DOA estimation via manifold separation for arbitrary array structures', IEEE Transactions on Signal Processing, vol. 55, no. 10, pp. 4800-4810.

9. Bronez, T.P, 1988, 'Sector interpolation of non-uniform arrays for efficient high-resolution bearing estimation', International Conference on Acoustics, Speech, and Signal Processing, vol.5,pp. 2885–2888.

10. Burg, JP1972, 'The Relationship Between Maximum Entropy Spectra and Maximum Likelihood Spectra', Geophysics, vol. 37, pp. 375–376.

11. Capon, J 1969, 'High-Resolution Frequency-Wavenumber Spectrum Analysis', Proceedings of the IEEE, vol. 57, no. 8, pp. 1408–1418.

12. Chandran, S 2005, 'Advances in Direction-of-Arrival Estimation', Artech House, Norwood.

13. Chen, M, Gong, Y & Mao, X 2020, 'Deep neural network for estimation of direction of arrival with antenna array', IEEE Access, vol.8, pp. 140688-140698.

14. Chen, Z, Gokeda, G & Yu, Y 2010, 'Introduction to Direction-of-Arrival Estimation', Artech House, Boston, London.

15. Cherkassky, V & Ma, Y 2004, 'Practical selection of SVM parameters and noise estimation for SVM regression', Neural Networks, vol.17, no.1, pp.113–126.

16. Chevalier, P, Albera, L, Ferreol, A & Comon, P 2005, 'On the virtual array concept for higher order array processing', IEEE Transactions on Signal Processing, vol. 53, no.4, pp.1254–1271.

17. Cramer, H 1951, 'Mathematical methods of statistics', Princeton University Press.

18. Dandekar, KR, Ling, H & Xu, G 2000, 'Smart antenna array calibration procedure including amplitude and phase mismatch and mutual coupling effects', IEEE International Conference on Personal Wireless Communications. pp. 293-297.

19. Dass, J, Sarin, V & Mahapatra, RN 2019, 'Fast and communication efficient algorithm for distributed support vector machine training', IEEE Transactions on Parallel and Distributed Systems, vol. 30, no. 5, pp. 1065-1076.

20. Davies, DEN 1965, 'A transformation between the phasing techniques required for linear and circular aerial arrays', Proceedings of IEEE, vol. 112, no.11, pp. 2041–2045.

21. Dehghan Firoozabadi, A, Irarrazaval, P, Adasme, P, Zabala-Blanco, D & Azurdia-Meza, C 2020, 'A novel method for estimating the number of speakers based on generalized eigenvalue–vector decomposition and adaptive wavelet transform by using K-means clustering',Signal Image Video Processing, vol.14, pp. 1017–1025.

22. El Gonnouni, A, Martinez-Ramon, M, Rojo-Alvarez, J, Camps-Valls, G, Figueiras-Vidal, A & Christodoulou, C 2012, 'A Support Vector Machine MUSIC Algorithm', IEEE Transactions on Antennas and Propagation, vol. 60, no. 10, pp. 4901-4910.

23. El Zooghby, AH, Christodoulou, CG & Georgiopoulos, M 2000, 'A neural network-based smart antenna for multiple source tracking', IEEE Transactions on Antennas and Propagation, vol. 48, no. 5, pp. 768-776.

24. Elbir, AM 2020, 'DeepMUSIC: Multiple signal classification via deep learning', IEEE Sensors Letters, vol. 4, no. 4, pp. 1-4.

25. Ermolaev, V, & Gershman, A 1994, 'Fast Algorithm for Minimum-Norm Direction-of-Arrival Estimation', IEEE Transactions on Signal Processing, vol. 42, no. 9, pp. 2389-2394.

26. Evers, C, Habets, EAP, Gannot, S & Naylor, PA 2018, 'DOA reliability for distributed acoustic tracking,' IEEE Signal Processing Letters, vol. 25, no. 9, pp.1320-1324.

27. Federal Communications Commission 2022, http://www.fcc.gov/e911/.

28. Foutz, J, Spanias, A & Banavar, MK 2008, 'Narrowband direction of arrival estimation of antenna arrays', Synthesis Lectures on Antennas, Morgan and Claypool Publishers, San Rafael, United States of America.

29. Friedlander, B & Weiss, AJ 1992, 'Direction finding using spatial smoothing with interpolated arrays', IEEE Transactions on Aerospace and Electronic Systems, vol. 28, no. 2, pp. 574-587.

30. Fu, H, Abeywickrama, S, Yuen, C & Zhang, M 2019, 'A Robust Phase-Ambiguity-Immune DOA Estimation Scheme for Antenna Array', IEEE Transactions on Vehicular Technology, vol. 68, no. 7, pp. 6686-6696.

31. Gao, F & Gershman, AB 2005, 'A generalized ESPRIT approach to direction-of-arrival estimation', IEEE Signal Processing Letters, vol.12, no.3, pp. 254–257.

32. Gardner, WA 1988, 'Simplification of MUSIC and ESPRIT by Exploitation of Cyclostationarity', Proceedings of the IEEE, vol. 76, no. 7, pp. 845-847.

33. Grenier, D, Elahian, B & Blanchard-Lapierre, A 2016, ' Joint delay and direction of arrivals estimation in mobile communication', Signal Image Video Processing, vol. 10, no. 1,pp. 45-54.

34. Gross, F 2005, 'Smart Antennas for Wireless Communications', McGraw-Hill , New York.

35. Gupta, I, Baxter, J, Ellingson, S, Park, H-G, Oh, H & Kyeong, M 2003, 'An experimental study of antenna array calibration', IEEE Transactions on Antennas and Propagation, vol. 51, no. 3, pp. 664-667.

36. He, W, Yang, X & Wang, Y 2020, 'A High-Resolution and Low-Complexity DOA Estimation Method with Unfolded Coprime Linear Arrays', Sensors, vol. 20, no.1, pp. 218.

37. He, Z, Zhao, Z, Nie, Z, Ma, P & Liu, QH 2012, 'Resolving manifold ambiguities for sparse array using planar substrates', IEEE Transactions on Antennas and Propagation, vol. 60, no. 5, pp. 2558-2562.

38. Huang, X, Yang,X, Cao, L & Lu, W 2021, 'Pseudo Noise Subspace Based DOA Estimation for Unfolded Coprime Linear Arrays', IEEE Wireless Communications Letters, vol. 10, no. 11, pp. 2335-2339.

39. Ifeachor, EC & Jervis, BW 2022, 'Digital Signal Processing: a practical approach', Pearson Education.

40. Ishiguro, M 1980, 'Minimum redundancy linear arrays for a large number of antennas', Radio Science, vol. 15, no. 6, pp. 1163–1170.

41. Johnson, D 1982 'The Application of Spectral Estimation Methods to Bearing Estimation Problems', Proceedings of the IEEE, Vol. 70, No. 9, pp. 1018–1028.

42. Joshi, SK, Baumgartner, SV, Da Silva, ABC & Krieger G 2022, 'Direction-of-Arrival Angle and Position Estimation for Extended Targets using Multichannel Airborne Radar Data', IEEE Geoscience and Remote Sensing Letters, vol. 19, pp. 1-5.

43. Kiang, JF & Wu, CW 2004, 'Introduction to Smart Antenna Systems. In: Novel Technologies for Microwave and Millimeter — Wave Applications', Springer, Boston.

44. Krim, H & Viberg, M 1996, 'Two decades of array signal processing research: The parametric approach', IEEE Signal Processing Magazine, vol. 13, no. 4, pp. 67–94.

45. Kumaresan, R, & Tufts, D 1983, 'Estimating the Angles of Arrival of Multiple Plane Waves', IEEE Transactions on Aerospace and Electronic Systems, vol. 19, no. 1, pp. 134-139.

46. Lan, H, Lv, Y,Jin, J, Li, J, Sun, D & Yang, Z 2021, 'Acoustical Observation With Multiple Wave Gliders for Internet of Underwater Things', IEEE Internet of Things Journal, vol. 8, no. 4, pp. 2814-2825.

47. Levi, M & Messer, H 1990, 'Sufficient conditions for array calibration using sources of mixed types', International Conference on Acoustics, Speech, and Signal Processing, vol.5, pp. 2943-2946.

48. Li, Q, Gan, L & Ye, Z, 2003 'An overview of self-calibration in sensor array processing', 6th International Symposium on Antennas, Propagation and EM Theory, Beijing, pp. 279-282.

49. Liao, B, Madanayake, A & Agathaklis, P 2018, 'Array signal processing and systems', Multidimensional Systems and Signal Processing, vol. 29, no.2, pp. 467–473.

50. Liberti, JC, & Rappaport, TS 1999, 'Smart Antennas for Wireless Communications: IS-95 and Third Generation CDMA Applications', Prentice Hall PTR, Upper Saddle River, New Jersey.

51. Liu, A, Yang, Q, Zhang, X & Deng, W 2018, 'Modified root MUSIC for co-prime linear arrays', Electronic Letters, vol. 54, no.15, pp.949-951.

52. Liu, CL & Vaidyanathan, PP 2015, 'Remarks on the spatial smoothing step in coarray MUSIC', IEEE Signal Processing Letters, vol.22, no.9, pp.1438–1442.

53. Liu, CL & Vaidyanathan, PP 2016, 'Super nested arrays with less mutual coupling than nested arrays', in Proceedings of IEEE International Conference on Acoustics, Speech,and Signal Processing, pp. 2976 -2980.

54. Liu, J, Zhao, Z, He, Z, Nie, Z & Liu, Q 2013, 'Resolving manifold ambiguities for direction-of-arrival estimation of sparse array using semi-circular substrates', IET Microwaves, Antennas and Propagation, vol.7, no.12, pp. 1016-1020.

55. Liu, W 2020, 'Super resolution DOA estimation based on deep neural network', Scientific Reports, vol.10. pp. 19859.

56. Liu, ZM, Zhang, C & Yu, PS 2018, 'Direction-of-arrival estimation based on deep neural networks with robustness to array imperfections', IEEE Transactions on Antennas and Propagation, vol. 66, no. 12, pp. 7315–7327.

57. Manikas, A 2004, 'Differential Geometry in Array Processing', Imperial College Press, London, U.K.

58. McCowan, I 2001, 'Microphone arrays: A tutorial', Queensland University, Australia, pp.1-38.

59. Meng, X, Xue, J, Yan, F & Yan, X 2019, 'Real-valued propagator method for fast DOA estimation via polynomial rooting', The Journal of Engineering, vol. 19, no. 21, pp.7792-7795.

60. Moffet, AT 1968, 'Minimum-redundancy linear arrays', IEEE Transactions on Antennas and Propagation, vol.16, no.2, pp.172–175.

61. Muhamed, R & Rappaport, TS 1996, 'Comparison of Conventional Subspace Based DOA Estimation Algorithms with those Employing Property-Restoral Techniques: Simulation and Measurements', 5th IEEE International Conference on Universal Personal Communications, vol. 2, pp. 1004–1008.

62. Nannuru, S, Gemba, KL, Gerstoft, P, Hodgkiss, WS & Mecklenbrauker, CF 2017, 'Multi-frequency sparse Bayesian learning with uncertainty models', arXiv:1704.00436.

63. Pal, P & Vaidyanathan, PP 2010, 'Nested arrays: A novel approach to array processing with enhanced degrees of freedom', IEEE Transactions on Signal Processing, vol. 58, no. 8, pp. 4167-4181.

64. Pal, P & Vaidyanathan, PP 2011, 'Coprime sampling and the music algorithm," Digital Signal Processing and Signal Processing Education Meeting (DSP/SPE), pp. 289-294.

65. Parra, I, Xu, G & Liu, H 1995, 'A Least Squares Projective Constant Modulus Approach', 6th International Symposium on Personal, Indoor and Mobile Radio Communications, vol. 2, pp. 673–676.

66. Pesavento, M, Gershman, AB & Wong, KM 2002, 'Direction finding using partly calibrated sensor arrays composed of multiple subarrays', IEEE Transaction on Signal Processing, vol.50, no. 9, pp. 2103–2115.

67. Pettersson, L & Grahn, P 2003, 'Experiences using DOA methods with a small digital beamforming antenna', IEEE International Symposium on Phased Array Systems and Technology, pp. 164-169.

68. Pierre, J & Kaveh, M 1995, 'Experimental evaluation of high-resolution direction-finding algorithms using a calibrated sensor array testbed', Digital Signal Processing, vol. 5, no.4, pp. 243–254.

69. Pillai, SU & Kwon, BH 1989, 'Forward/Backward Spatial Smoothing Techniques for Coherent Signal Identification', IEEE Transactions on Acoustics, Speech, and Signal Processing, vol. 37, no. 1, pp. 8-15.

70. Pisarenko, VF 1973, 'The Retrieval of Harmonics from a Covariance Function', Geophysical Journal of the Royal Astronomical Society, vol. 33, pp. 347–366.

71. Pöhlmann, R, Zhang, S, Staudinger, E, Dammann, A, & Hoeher, P. A 2022, 'Simultaneous Localization and Calibration for Cooperative Radio Navigation', IEEE Transactions on Wireless Communications, vol. 21, no. 8, pp. 6195-6210.

72. Qin, S, Zhang, Y & Amin, M 2015, 'Generalized coprime array configurations for direction-of-arrival estimation', IEEE Transaction on Signal Processing, vol. 63,no.6, pp. 1377–1390.

73. Randazzo, A, Abou-Khousa, MA, Pastorino, M & Zoughi, R 2007, 'Direction of arrival estimation based on support vector regression: Experimental validation and comparison with MUSIC', IEEE Antennas and Wireless Propagation Letters, vol. 6, pp. 379-382.

74. Razavizadeh, SM, Ahn, M & Lee, I 2014, 'Three-dimensional beamforming: A new enabling technology for 5G wireless networks,' IEEE Signal Processing Magazine, vol. 31, no. 6, pp. 94-101.

75. Rockah, Y & Schultheiss, PM 1987, 'Array shape calibration using sources in unknown locations—part I: far-field sources', IEEE Transactions on Acoustics, Speech, and Signal Processing, vol. 35, no. 3, pp. 286-299.

76. Roy, R & Kailath, T 1989, 'ESPRIT-Estimation of signal parameters via rotational invariance techniques', IEEE Transactions on Acoustics, Speech, and Signal Processing, vol. 37, pp. 984–995.

77. Rübsamen, M & Gershman, AB 2008, 'Root-MUSIC based direction-of-arrival estimation methods for arbitrary non-uniform arrays', IEEE International Conference on Acoustics, Speech and Signal Processing, pp. 2317-2320.

78. Rübsamen, M & Gershman,AB 2009, 'Direction-of-arrival estimation for non-uniform sensor arrays: From manifold separation to Fourier domain MUSIC methods', IEEE Transaction on Signal Processing, vol.57, no.2, pp. 588–599.

79. Sakaguchi, K, Kuroda, K, Takada, JI & Araki, K 2002, 'Comprehensive calibration for MIMO systems', 5th International Symposium on Wireless Personal Multimedia Communications, vol.2, pp. 440-443.

80. Schmidt, R 1986, 'Multiple Emitter Location and Signal Parameter Estimation', IEEE Transactions on Antennas and Propagation, vol. 34, no. 3, pp. 276-280.

81. Shan, TJ, Wax, M & Kailath, T 1985, 'On Spatial Smoothing for Directions of Arrival Estimation of Coherent Signals', IEEE Transactions on Acoustics, Speech, and Signal Processing, vol. 33, no. 4, pp. 806-811.

82. Shu, F, Qin, Y, Liu, T, Gui, L, Zhang, Y, Li, J & Han, Z 2018, 'Low-Complexity and High-Resolution DOA Estimation for Hybrid Analog and Digital Massive MIMO Receive Array', IEEE Transactions on Communications, vol. 66, no. 6, pp. 2487-2501.

83. Shu, F, Shen, T, Xu, L, Qin, Y, Wan, S, Jin, S, You, X & Wang, J 2020, ' Directional modulation: A physical-layer security solution to B5G and future wireless networks' IEEE Network, vol. 34, no. 2, pp. 210-216.

84. Smola AJ & Schölkopf, B 2004, 'A tutorial on support vector regression', Statistics and Computing, vol.14, no.3, pp. 199–222.

85. Stansfield, RG 1947, 'Statistical Theory of D.F. fixing', Journal of IEE (London), vol. 94 (k), no. 3A, pp. 762-770.

86. Stoica, P & Nehorai, A 1990, 'Performance study of conditional and unconditional direction-of-arrival estimation', IEEE Transactions on Acoustics, Speech, and Signal Processing, vol. 38, no. 10, pp. 1783-1795.

87. Strobach, P 1998, 'Fast recursive subspace adaptive ESPRIT algorithms', IEEE Transactions on Signal Processing, vol. 46, no. 9, pp. 2413-2430.

88. Strobach, P 2000, 'Equirotational Stack Parameterization in Subspace Estimation and Fitting', IEEE Transaction on Signal Processing, vol. 48, pp. 713–722.

89. Sun, F, Lan, P & Gao, B 2015, 'Partial spectral search-based DOA estimation method for co-prime linear arrays', Electronic Letters, vol. 51, no. 24, pp. 2053–2055.

90. Sun, Y, Chen, J, Yuen, C & Rahardja, S 2018, 'Indoor sound source localization with probabilistic neural network', IEEE Transactions on Industrial Electronics, vol. 65, no. 8, pp. 6403-6413.

91. Swindlehurst, AL, Ottersten, B, Xu, G, Roy, R & Kailath, T 1992, 'Multiple invariance ESPRIT', IEEE Transactions on Signal Processing, vol. 40, pp. 867–881.

92. Tan, CM, Foo, SE, Beach, MA, & Nix, AR 2002, 'Ambiguity in MUSIC and ESPRIT for direction of arrival estimation', Electronic Letters, vol. 38, no. 24, pp. 1598–1600.

93. Tan, Z, Eldar, Y & Nehorai, A 2014, 'Direction of arrival estimation using co-prime arrays: A super-resolution viewpoint', IEEE Transaction on Signal Processing, vol. 62, no. 21, pp. 5565–5576.

94. Tarkowski, M & Kulas, L 2019, 'RSS-based DoA estimation for ESPAR antennas using support vector machine', IEEE Antennas and Wireless Propagation Letters, vol. 18, no. 4, pp. 561-565.

95. Tokgoz, S & Panahi, I M. S 2021, 'Robust Three-Microphone Speech Source Localization Using Randomized Singular Value Decomposition', IEEE Access, 9, pp. 157800-157811.

96. Torrieri, DL,1984, 'Statistical Theory of Passive Location Systems', IEEE Transactions on Aerospace and Electronic Systems, vol. AES-20, no. 2, pp. 183-198.

97. Tuncer, T, Kaya Yasar, T & Friedlander, B 2007, 'DOA estimation for nonuniform linear arrays by using array interpolation', Radio Science, vol. 42 no. 4, pp. 4002-I–4002-II.

98. Tuncer, TE & Friedlander, B 2009, 'Classical and Modern Direction-of-Arrival Estimation', Elsevier Science, United States of America.

99. Vaidyanathan, PP & Pal, P 2011, 'Sparse sensing with co-prime samplers and arrays', IEEE Transactions on Signal Processing, vol. 59, no. 2, pp. 573-586.

100. Van Trees, HL 2022, 'Detection, Estimation, and Modulation Theory, Part IV: Optimum Array Processing', John Wiley & Sons, New York.

101. Vapnik, V, Golowich, S & Smola, AJ 1997, 'Support vector method for function approximation, regression estimation, and signal processing' NIPS'96: Proceedings of the 9th International Conference on Neural Information Processing Systems, pp.281–287.

102. Vertatschitsch, E & Haykin, S 1986, 'Nonredundant arrays', Proceedings of the IEEE, vol. 74, no. 1, pp. 217-217.

103. Wang, A, Yin, R & Zhong, C 2020, 'PCA-Based Channel Estimation and Tracking for Massive MIMO Systems with Uniform Rectangular Arrays,' IEEE Transactions on Wireless Communications, vol. 19, no. 10, pp. 6786-6797.

104. Wang, W, Wang, X & Li, X 2013, 'Propagator method for angle estimation of non-circular sources in bistatic MIMO radar', IEEE Radar Conference (RadarCon13), pp. 1-5.

105. Wax, M 1995, 'Model-Based Processing in Sensor Arrays', Advances in Spectrum Analysis and Array Processing, Vol. III, S. Haykin, (ed.), Prentice Hall, Englewood Cliffs, New Jersey.

106. Wu, L & Huang, Z 2019, 'Coherent SVR learning for wideband direction-of-arrival estimation', IEEE Signal Processing Letters, vol. 26, no. 4, pp. 642-646.

107. Xiao, Y, Wang, Y, Chargé, P & Ding, Y 2019, 'An efficient DOA estimation method for co-prime linear arrays', IEEE Access, vol.7, pp. 90874-90881.

108. Xie, Q, Pan, X & Xiao. S 2019, 'Enhance degrees of freedom for coprime array using optspace algorithm', IEEE Access, vol.7, pp. 32672–32680.

109. Xu, F, Morency, MW & Vorobyov, SA 2022, 'DOA Estimation for Transmit Beamspace MIMO Radar via Tensor Decomposition With Vandermonde Factor Matrix', IEEE Transactions on Signal Processing, vol. 70, pp. 2901-2917.

110. Xu, G & Kailath, T 1994, 'Fast Subspace Decomposition', IEEE Transactions on Signal Processing, vol. 42, no. 3, pp. 539-551.

111. Xu, G & Liu, H 1995, 'An Effective Transmission Beamforming Scheme for Frequency-Division-Duplex Digital Wireless Communication Systems', International Conference on Acoustics, Speech, and Signal Processing, vol. 3, pp. 1729–1732.

112. Xu, G, Silverstein, SD, Roy, RH & Kailath, T 1994, 'Beamspace ESPRIT', IEEE Transactions on Signal Processing, vol. 42, no. 2, pp. 349-356.

113. Yan, FG, Liu, S, Wang, J, Jin, M & Shen, Y 2018, 'Fast DOA estimation using co-prime array', Electronic Letters, vol. 54, no. 7, pp. 409–410.

114. Yang, X, Wang, Y & Chargé, P 2019, 'Modified DOA estimation with an unfolded co-prime linear array', IEEE Communications Letters, vol. 23, no. 5, pp. 859-862.

115. Zhang, D, Zhang, Y, Zheng, G, Feng, C & Tang, J 2017, 'Improved DOA estimation algorithm for co-prime linear arrays using root-MUSIC algorithm', Electronic Letters, vol.53, no.18, pp.1277–1279.

116. Zheng, W, Zhang, X, Gong, P & Zhai, H 2018, 'DOA estimation for coprime linear arrays: An ambiguity-free method involving full DOFs', IEEE Communications Letters, vol. 22, no. 3, pp. 562–565.

117. Zhou, C, Shi, Z, Gu, Y & Shen,X 2013, 'DECOM: DOA estimation with combined MUSIC for coprime array', International Conference on Wireless Communications and Signal Processing, pp. 1–5.

118. Ziskind, I & Wax, M 1990, 'Maximum Likelihood Localization of Diversely Polarized Sources by Simulated Annealing', IEEE Transactions on Antennas and Propagation, vol. 38, no. 7, pp. 1111-1114.

119. Ziskind, I, & Wax, M 1988, 'Maximum Likelihood Localization of Multiple Sources by Alternating Projection', IEEE Transactions on Acoustics, Speech, and Signal Processing, vol. 36, no. 10, pp. 1553-1560.

120. Zoltowski, MD, Haardt, M & Mathews, CP 1996, 'Closed-Form 2-D Angle Estimation with Rectangular Arrays in Element Space or Beam Space via Unitary ESPRIT', IEEE Transactions on Signal Processing, vol. 44, pp.316–328.

LIST OF PUBLICATIONS

International Journals

1. **Ashok C** & Venkateswaran N 2021, 'Manifold Ambiguity-Free Low Complexity DOA Estimation Method for Unfolded Co-Prime Arrays', IEEE Communications Letters, vol. 25, no. 6, pp. 1886-1890, ISSN: 1089-7798. **Impact Factor: 3.553.**

2. **Ashok C** & Venkateswaran N 2022, 'An Efficient Method for Resolving Ambiguity in DOA Estimation with Coprime Linear Array', Circuits Systems and Signal Processing, vol. 41, pp.2411-2427, ISSN: 0278-081X. **Impact Factor: 2.311.**

3. **Ashok C** & Venkateswaran N 2022, 'An Improved Polynomial Rooting-based Method for Solving Non-Trivial Ambiguity in Direction-Finding using an Unfolded Co-prime Linear Array', Signal, Image and Video Processing, doi.org/10.1007/s11760-022-02224-0, ISSN: 1863-1703. **Impact Factor: 2.157.**

4. **Ashok, C**, Venkateswaran, N, Vaddi Lakshmi Satya Sai Sarojini & Sneha Rajan 2022, **'**An Unambiguous DOA Estimation Method for Coprime Array with Displaced Subarrays', Applied Acoustics, vol. 195, pp. 108818, ISSN: 0003-682X. **Impact Factor: 3.614.**